AN INVESTIGATION INTO THE EFFECT OF INTERFACE DYNAMICS ON THE RESPONSE OF COUPLED SYSTEMS

ALLAN ROBERT CLARK

A thesis submitted for the degree of PhD

The University of Aston in Birmingham

June 1982

AN INVESTIGATION INTO THE EFFECT OF INTERFACE DYNAMICS ON THE RESPONSE OF COUPLED SYSTEMS

ALLAN ROBERT CLARK

Submitted for the degree of Doctor of Philosophy
of the University of Aston in Birmingham

June 1982

SUMMARY

An experimental and theoretical investigation into the effect of interface dynamic properties on the overall response of coupled complex structures has been successfully completed. Experiments were carried out on an idealised laboratory model comprising two cantilevers coupled at two positions via simple connectors which allowed only axial forces to be transmitted from one cantilever to the other. Data was collected from frequency response tests on the uncoupled cantilevers and combined with theoretical connector data by the 'Impedance Coupling Technique' in order to predict the coupled system response.

It has been shown that the behaviour of complex coupled systems can be predicted to an acceptable degree of accuracy up to frequencies of 500 Hz. Further, the results show quite clearly that in certain cases a considerable reduction in energy transmission between two coupled structures can be effected within a narrow frequency band by optimising on the dynamic characteristics of the interface mechanism. In particular adjusting the stiffness of the interface was found to be very effective in this detuning process where relatively high coupling stiffness could be utilised without appreciably altering the overall dynamic response of the system.

This thesis reflects the effort expended in developing the required experimental technique, instrumentation and computing software necessary to obtain and manipulate the experimental results.

Key Words

Mechanical Impedance
Frequency Response
Beam Vibrations
Interface Dynamics

ACKNOWLEDGEMENTS

I wish to thank my supervisors, Professor E Downham and Dr J E T Penny for their guidance and support during this work.

I also want to acknowledge the assistance given by the technician staff of the Department of Mechanical Engineering. In particular, thanks to Brian, Barry and Malcolm.

I would also like to thank Anne for typing this thesis.

Special thanks are also due to Pam and my wife Mary-Rose for their most valuable assistance in the preparation of this thesis.

Financial support for the project was provided by the Science Research Council, and the Royal Aircraft Establishment, Farnborough, (MOD).

CONTENTS

CONTENTS

LIST OF FIGURES

LIST OF FIGURES

LIST OF TABLES

TABLE NUMBER

NOMENCLATURE

NOMENCLATURE

$[a]$	flexibility matrix
$[\bar{a}]$	flexibility sub-matrix including only translational elements
A	apparent mass, force/acceleration ratio; $[A]$ apparent mass matrix
A	area
c	damping co-efficient
C	Coulomb, unit of electrical charge
dB	decibel, logarithmic ratio
E	Young's modulus of elasticity
F	force; $\{F\}$, force vector
g	gravitational unit of acceleration, normally 9.81 m/s^2
H_n	complex magnification factor for nth mode of vibration
Hz	Hertz, unit of frequency, ie cycle per second
i	tensor parameter
I	Inertance, acceleration/force ratio ; $[I]$ inertance matrix
I	2nd moments of area; mass moments of inertia
j	imaginary number $\sqrt{1}$; tensor parameter
k	stiffness co-efficient; $[k]$, stiffness matrix; kilo, ie $\times 10^3$
$[\bar{k}]$	stiffness matrix including only translational elements
l	length
m	mass; metre, unit of length; milli, ie $\times 10^{-3}$
M	mega, ie $\times 10^6$
n	nth mode of vibration
N	Newton, unit of force
p	pico, ie $\times 10^{-12}$
p_n	nth principal co-ordinate, displacement; $\dot{p}_n$, velocity; $\ddot{p}_n$, acceleration
P_n	forces associated with principal co-ordinates

q	generalised co-ordinate, displacement; $\dot{q}$, velocity; $\ddot{q}$, acceleration; $\{q\}$, displacement vector etc
Q	generalised force; $\{Q\}$, generalised force vector
r_n	ratio of exciting frequency to nth natural frequency, ie Ω/ω_n
s	second, unit of time
t	time
V	volts, unit of electrical potential
x	co-ordinate, ie in x direction; displacement
y	co-ordinate, ie in y direction; displacement; $\dot{y}$, velocity; $\ddot{y}$, acceleration; $\{y\}$, displacement vector etc

δ	Loss factor
ζ	damping ratio
ρ	mass density
τ	moment; $\{\tau\}$, moment vector
ϕ	rotation co-ordinate; angular displacement; $\{\phi\}$, angular displacement vector
ϕ_n	characteristic shape function - nth mode
ω	frequency
ω_n	nth natural frequency
Ω	exciting frequency
σ	stress, ie load/area

CHAPTER ONE

INTRODUCTION

CHAPTER ONE

INTRODUCTION

Recent years have witnessed an unprecedented increase in quantity and sophistication of dynamic based problems in engineering which by necessity has required the Engineer to look deeper into this subject area and to use up-to-date technology as an aid to rationalise these problems. This activity has evolved not only because of the increased awareness of noise pollution but also due to the fact that engineering structures are becoming lighter (more flexible) in the Engineer's quest for increasing power to weight ratios.

The problems with which the Engineer is confronted are usually categorised into noise radiation and vibration of structures though are very often linked together in some cause and effect situation. Nevertheless, the Engineer may find this division useful when quantifying or choosing a possible solution. For example, does the solution require sound-proofing or an adjustment in structural flexibility? This division though, which is usually made on the basis of frequency range, may not always be quite clear, so then the Engineer may find himself in a 'grey area'. Such an area is in the lower audio range of frequencies where either or both methods of approach may be helpful.

The research program outlined in this report was instigated by the Helicopter Cabin Acoustic Group based at RAE studying the problem of cabin noise in a helicopter. The problem has many of the ingredients previously mentioned. In particular, the modern helicopter has a much improved power to weight ratio over its forerunners but inevitably its noise problem has become severe, especially in the lower audio range.

The Helicopter Cabin Acoustic Group has co-ordinated research and development in various directions with a view to alleviate this problem. The main areas of activity are: noise/vibration absorption, reduction of exciting forces generated within the gear box and reduction of vibration transmitted from the source (gear box) to the receiver (airframe). The investigation outlined in this thesis is confined to the latter area.

From previous noise and vibration experiments on a helicopter carried out by Westland Helicopters Limited[1] it was observed that a prominent peak of vibration and noise occurred at a gear meshing frequency; this frequency is confined to a narrow frequency range which is dependent on flying conditions. The initial hypothesis was, that if the helicopter could be considered as a coupled complex system involving the airframe and gear box/rotor as the two major sub-systems coupled via an interface mechanism, then the interface might be designed such as to optimise the helicopter response at the meshing frequency and, consequently, the noise might be significantly reduced. Because of the high modal densities of these sub-systems, this de-tuning procedure is likely to be effective over only a narrow frequency bandwidth.

The sub-systems to be joined are of such complexity it is unlikely that a purely theoretical analysis would be of sufficient accuracy to define the response of these systems to vibratory forces at relatively high frequencies. Thus it is necessary to obtain the dynamic characteristics of each sub-system by experiment. Having gained confidence in the accuracy with which the sub-systems can be measured, this data can be used in a theoretical examination to establish the effect of a particular spring/mass/damper interface on the overall energy flow from one sub-system to another on the assumption that vibratory forces are generated within one such sub-system and are transmitted to the other.

This method of combining sub-systems has become very popular in recent years and is referred to as the 'Impedance Coupling Technique' or the 'Building Block Approach'. [2,3,4] The technique requires the measurement or theoretical prediction of the mechanical impedance of each sub-system at all the points where they are connected in the assembled structure. The response of the connected structure is then predicted by combining vectorily, since mechanical impedance has magnitude and phase, the impedance data at all the connecting points.

Mechanical Impedance was first introduced as an engineering quantity by Professor A.G.Webster of Clark University in 1918 when he presented a paper entitled 'A Mechanically Blown Wind Instrument' at the Baltimore meeting of the American Physical Society. However, it is only since World War II that this quantity has been used extensively in the mechanical vibration of structures[5]. Two significant text books on this topic were published in this period: Bishop and Johnson's 'The Mechanics of Vibration' and Salter's 'Stead State Vibration' (references 6 and 7 respectively). In addition numerous articles and research papers have been presented. One of the earliest significant papers was by Kennedy and Pancu[8] in which they outline the use of mechanical impedance measurements in the vibration analysis of complex structures. In 1958 the ASME held a colloquium on mechanical impedance methods[9] and by the mid 1960's Schloss reported on the accurate measurement of mechanical impedance[10,11] whilst Remmers and Belsheim[12] presented the results of a 'Round Robin' test which demonstrated the difficulty of attaining reliable and repeatable impedance data. This 'Round Robin' test involved 19 organisations, each one measureing the same set of three test structures. Experimental skill and ability to select optimum measuring and force generating equipment was shown to vary considerably between each organisation. An envelope of these results showed calibration errors of 6 dB's, a spread of 25 to 35 dB's in magnitude measurement and large errors in resonant frequencies which were, in some cases, not even detected. The report ends with a useful 10 point recommendation for reliable measurements.

During the past decade one of the most prolific researchers in this field has been Ewins of Imperial College, London, who together with research papers and reports, has produced a comprehensive bibliography of Mechanical Impedance[13] in which he has listed and categorised some 284 references.

The general term 'Mechanical Impedance' is used to describe a group of frequence response functions. These functions are derived, for an elastic system, by comparing the exciting force (or moment) with the resulting response at some point in the system. This comparison is made at all frequencies in the range of interest and is expressed as a complex ratio i.e. a quantity having both magnitude and phase or, if preferred, having real and imaginary components. This ratio may be expressed as the exciting force per unit response or vice versa and, furthermore, the response may be expressed in terms of displacement, velocity or acceleration. Thus the frequency response function can be expressed in any of six different forms. The terminology used to describe these ratios is only now in the process of being standardised and Table I shows the most widely used terms and particularly those recommended by BS 3015: 1976. When the response is measured at the point of application of the force then the measurement is referred to as a direct or driving point measurement; for example driving point impedance. If the force is applied to one point in the system and the response is measured at another then the measurement is called a transfer measurement; for example transfer mobility.

Ratio \ Response	Displacement	Velocity	Acceleration
Response/force	**Receptance**	Mechnical mobility*	Inertance
Force/response	Dynamic stiffness*	Mechnical impedance*	Apparent mass*

* Recommended for use by BS3015: 1976.

Table I

Which one of the six frequency response functions should be used is entirely a matter of personal preference since each function contains the same information but in a slightly different form. Response is usually measured by accelerometers and so inertance and apparent mass have the advantage of being expressed directly in terms of the measured quantities. However, mobility and impedance are extensively used.

The most recent work on the 'Impedance Coupling Technique' was successfully completed by Ewins and Silva [14] where they predicted major structural resonances, within a 3-30 Hz frequency range, of a helicopter structure with an externally coupled store carrier and store.

This practical application proved to be a difficult and laborious operation involving several procedures which are summarised as follows

The carrier assembly, which had several coupled sub-structures, was coupled to the helicopter airframe at four points, each point having a possible six degrees of freedom. Both the airframe and the carrier required the experimental formulation of an impedance matrix of order 24. This required a total of 1152 impedance measurements at each frequency increment, although this figure was significantly reduced due to experience, judgement and the use of reciprocity relationships to a total of 29 measurements for each structure, see Chapter 2, reference 14. Raw data taken directly from measurements of these complex structures proved not only to be inconsistent in terms of modal parameters but was of such quantity as to prevent their use directly in the 'Impedance Coupling Technique .' The researchers elected to proceed by a lengthy and detailed method of rationalising and regenerating the raw data via modal analysis. This process not only refines the raw data but also provides a more efficient means of storing it [15].

Clearly this work has many features which may be directly applicable in the de-tuning exercise outlined earlier in this chapter. To avoid repeating this work it was decided to concentrate on the effect of interface characteristics on the coupled system response and to implement this procedure in a higher frequency range. The work described in this report was performed on a simplified model in order to reduce the quantity of 'Impedance'* data as compared with that measured by Ewins and Silva and to allow the use of unrefined

* 'Impedance' is used as a generic term for frequency response type measurements.

experimental data since the inaccuracies are not likely to be so significant. The research, therefore, proceeded initially on a two plate system with four connection points, but due to measurement difficulties was completed on a two cantilever system with two connection points. Hence this thesis is concerned for the main part with the two cantilever system especially in the theoretical study since this system is more easily solved by classical analytical methods.

CHAPTER TWO

THEORETICAL STUDY

CHAPTER TWO

THEORETICAL STUDY

2.1 INTRODUCTION

The first part of this chapter is a review of the 'Impedance Coupling Technique'* applied to a two cantilever system coupled at two positions by connectors which have dynamic properties. The resulting system matrix equation shows how the sub-systems are theoretically coupled by manipulating their individual 'Impedance'* matrices. These matrices may be obtained theoretically or from experiments on the sub-systems. Since, from a theoretical point of view, each element within these matrices has mass, stiffness and damping coefficients, then readily available models of cantilever systems may be built up using the stiffness influence coefficients and mass properties of beams. A study on a very simple two cantilever system is shown to be a valuable aid in demonstrating and quantifying the effect of rotational intertia/stiffness of the connectors on the coupled system. Finally, frequency response functions are theoretically generated for cantilevers of differing specifications by using classical forced response theory. This approach has the advantage over the stiffness influence coefficient techniques in that it is relatively easy to include the higher modes thus producing a more accurate frequency response function. These results are then combined, together with various connector configurations, by the use of the 'Impedance Coupling Equation',* in order to compute the coupled system responses. This part of the study gives a more detailed representation of system behaviour and is complemented by a discussion.

* 'Impedance' is a general term comprising all frequency response type data involving motion and force ratios. See Chapter 1.

2.2 'IMPEDANCE COUPLING TECHNIQUE'*

The 'Impedance Coupling Technique' used in this work is described in detail in references 2, 3, 4, 16 and only a brief review of this theory as applied to two coupled cantilevers is given.

When two cantilevers are coupled by two connectors as shown in Fig 2.1, 24 co-ordinates are necessary to completely describe the system frequency response at the four connecting points, six co-ordinates per point allowing for translation and rotation in three planes. However, if we assume that translation and rotation in two planes are not excited, then the number of co-ordinates is reduced to 8, i.e. one vertical translation and one rotation at each point.

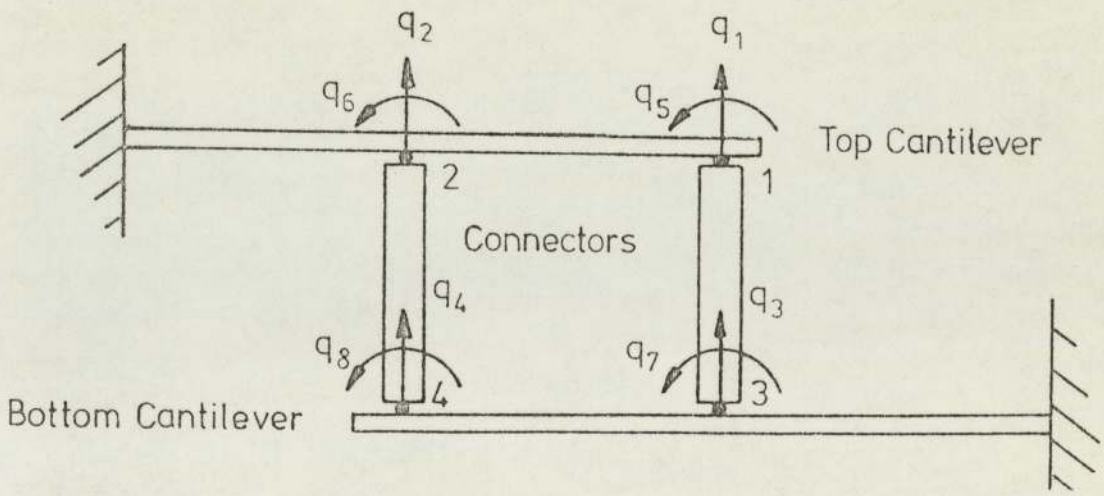

FIG 2.1 TWO CANTILEVER SYSTEM COUPLED AT TWO POSITIONS

Assuming a linear elastic system then the apparent mass matrix, $[A]$, is defined thus:-

$$[A]\ \{\ddot{q}\} = \{Q\} \qquad \text{. . . eq 2.1}$$

where $\{\ddot{q}\}$ is a vector of translational and rotational accelerations.

$\{Q\}$ is a vector of forces and moments.

The inertance matrix, $[I]$, is defined as:-

$$[I]\ \{Q\} = \{\ddot{q}\} \qquad \text{. . . eq 2.2}$$

* This coupling technique is applied using apparent mass since acceleration was measured in the experimental work.

so that

$$[I] = [A]^{-1} \qquad \text{. . . eq 2.3}$$

Two other sets of related matrix equations may be formulated in terms of displacement and velocity as explained in Chapter 1.

The dynamic behaviour of each sub-system, when considered in isolation, may be described by its own matrix equation. In particular, the two cantilever system of Fig 2.1 may be considered to be composed of three sub-systems; the top cantilever, the coupling system and the bottom cantilever. The independent behaviour of each sub-system is described by the following equations:-

$$\left.\begin{aligned} [A]_T \{\ddot{q}\}_T &= \{Q\}_T \\ [A]_C \{\ddot{q}\}_C &= \{Q\}_C \\ [A]_B \{\ddot{q}\}_B &= \{Q\}_B \end{aligned}\right\} \qquad \text{. . . eq 2.4}$$

where the subscripts have the following meaning:-

T - top cantilever

B - bottom cantilever

C - coupling system

S - coupled system

For convenience let the coupling system matrix equation and the coupled system matrix equation be partitioned such that those co-ordinates associated with coupling points 1 and 2 are together and those of points 3 and 4 are together.

<u>ie</u>

$$\begin{bmatrix} [A_{11}] & [A_{12}] \\ [A_{21}] & [A_{22}] \end{bmatrix} \begin{bmatrix} \{\ddot{q}\}^{1,2} \\ \{\ddot{q}\}^{3,4} \end{bmatrix} = \begin{bmatrix} \{Q\}^{1,2} \\ \{Q\}^{3,4} \end{bmatrix}$$

Then, if the system is to be coupled at these four connecting points, the forces at the points must be equal to the algebraic sum of the forces in the sub-systems

$$\left.\begin{array}{ll} & \{Q\}_T + \{Q\}_C^{1,2} = \{Q\}_S^{1,2} \\ \text{and} & \{Q\}_B + \{Q\}_C^{3,4} = \{Q\}_S^{3,4} \end{array}\right\} \quad . . . \quad \text{eq } 2.5$$

and the accelerations must be compatible such that

$$\left.\begin{array}{ll} & \{\ddot{q}\}_T = \{\ddot{q}\}_C^{1,2} = \{\ddot{q}\}_S^{1,2} \\ \text{and} & \{\ddot{q}\}_B = \{\ddot{q}\}_C^{3,4} = \{\ddot{q}\}_S^{3,4} \end{array}\right\} \quad . . . \quad \text{eq } 2.6$$

Using equations 2.4, 2.5 and 2.6 the coupled system **apparent mass** matrix becomes

$$[A]_S = \begin{bmatrix} [A]_T + [A_{11}]_C & [A_{12}]_C \\ [A_{21}]_C & [A]_B + [A_{22}]_C \end{bmatrix} \quad . . . \quad \text{eq } 2.7$$

Since this matrix equation will be of order eight the amount of experimental data required for each sub-system matrix will be quite substantial. For example, the top cantilever matrix will require 16 frequency response measurements at each frequency. These measurements will have a mixture of translation and angular responses due to transmitted forces and moments. This clearly would add complications to this initial experimental demonstration and it can be seen that the amount of data would be significantly reduced if the transmission of moments could be neglected, ie from 16 to 4 measurements at each frequency for the top cantilever. In order to investigate this possibility a model of this coupled system was set up using stiffness influence coefficients and mass properties of beams.

2.3 DYNAMIC ANALYSIS OF A TWO CANTILEVER SYSTEM

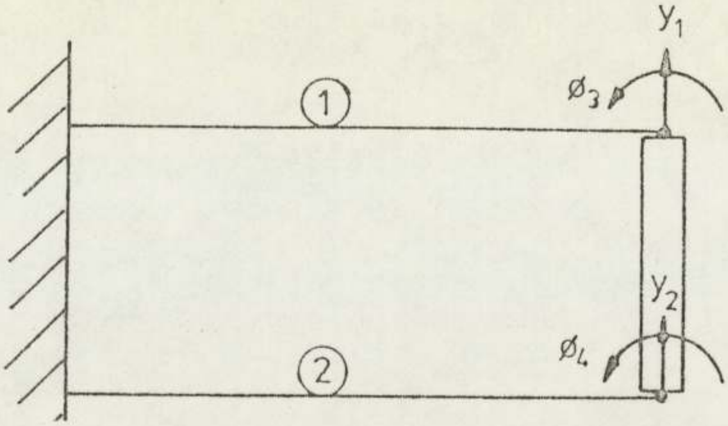

FIG 2.2 SIMPLE REPRESENTATION OF A TWO CANTILEVER SYSTEM COUPLED AT THE END POSITION ALLOWING 4 DEGREES OF FREEDOM

A mathematical model may be obtained for the simplified representation of the two cantilever system shown in Fig 2,2 to demonstrate the effect of coupling the cantilevers at their free ends. The connector is allowed both linear and rotational stiffness together with mass and inertia.

If we assume small oscillations then each cantilever may be represented by a single dynamic element which utilises the consistent mass matrix, see references 17 and 18.

For cantilever 1

$$\left\{ \frac{EI}{\ell^3}\begin{bmatrix} 12 & -6\ell \\ -6\ell & 4\ell^2 \end{bmatrix} - \frac{\omega^2\rho A}{420}\begin{bmatrix} 156\ell & -22\ell^2 \\ -22\ell^2 & 4\ell^3 \end{bmatrix} \right\} \begin{bmatrix} y_1 \\ \phi_3 \end{bmatrix} = \begin{bmatrix} F_1 \\ \tau_3 \end{bmatrix} \quad \text{. . . eq 2.8}$$

A simple connector having four degrees of freedom may be represented by:-

$$\left\{ \begin{bmatrix} k & -k & 0 & 0 \\ -k & k & 0 & 0 \\ 0 & 0 & k_r & -k_r \\ 0 & 0 & -k_r & k_r \end{bmatrix} - \omega^2 \begin{bmatrix} m & 0 & 0 & 0 \\ 0 & m & 0 & 0 \\ 0 & 0 & I & 0 \\ 0 & 0 & 0 & I \end{bmatrix} \right\} \begin{bmatrix} y_1 \\ y_2 \\ \phi_3 \\ \phi_4 \end{bmatrix} = \begin{bmatrix} F_1 \\ F_2 \\ \tau_3 \\ \tau_4 \end{bmatrix} \quad \text{. . . eq 2.9}$$

The coupled system matrix equation then becomes:-

$$\left\{ \frac{EI}{\ell^3}\begin{bmatrix} 12+K & -K & -6\ell & 0 \\ -K & 12+K & 0 & -6\ell \\ -6\ell & 0 & 4\ell^2+K_r & -K_r \\ 0 & -6\ell & -K_r & 4\ell^2+K_r \end{bmatrix} - \frac{\omega^2\rho A}{420}\begin{bmatrix} 156+M & 0 & -22\ell^2 & 0 \\ 0 & 156+M & 0 & -22\ell^2 \\ -22\ell^2 & 0 & 4\ell^3+I' & 0 \\ 0 & -22\ell^2 & 0 & 4\ell^3+I' \end{bmatrix} \right\} \begin{bmatrix} y_1 \\ y_2 \\ \phi_3 \\ \phi_4 \end{bmatrix} = \begin{bmatrix} F_1 \\ F_2 \\ \tau_3 \\ \tau_4 \end{bmatrix} \quad \text{. . . eq 2.10}$$

where

$$K = \frac{k\ell^3}{EI} \qquad M = \frac{m.420}{\rho A}$$

$$K_r = \frac{k_r\ell^3}{EI} \qquad I' = \frac{I.420}{\rho A}$$

If k_r is small then the connector will offer negligible torsional restraint to the cantilevers. So, if there are no externally applied moments then the rotations will be dependent on the deflections which will reduce this 4th order matrix equation to an order of 2. For example when a rotational stiffness element is connected to the tip of a cantilever the rotation at the tip can be assumed to be dependent on the deflection to within 1% when the ratio of rotational stiffness to cantilever rotational stiffness ($k_r\ell/EI$) is less than 1%*

To investigate this concept more thoroughly a static model of a two cantilever system was constructed which was coupled at two positions by pure linear stiffnesses. This was a valid exercise since it can be seen from eq 2.10 that the inclusion of the mass matrix does not change the fundamental nature of the analysis, only the complexity.

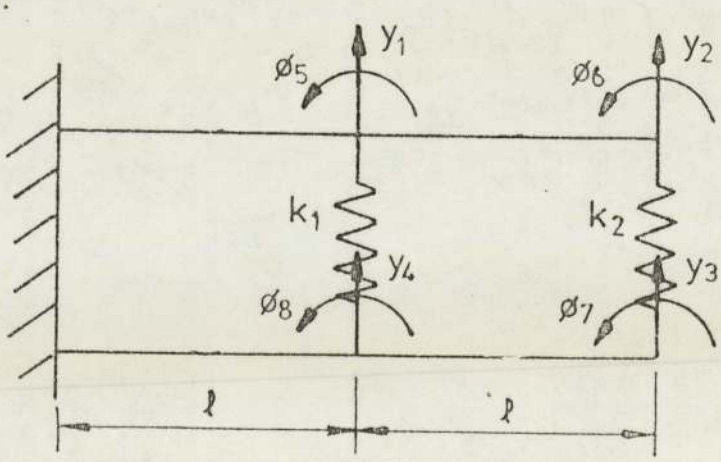

FIG 2.3 STATIC MODEL OF TWO CANTILEVER SYSTEM COUPLED AT TWO POSITIONS WITH PURE STIFFNESSES

* The effect of end restraint on the natural frequencies of cantilevers is discussed in section 6.2 of this thesis.

Each cantilever is allowed 4 degrees of freedom and has a stiffness matrix equation of the form

$$[k]\ \{y\} = \{F\} \qquad \text{. . . eq 2.11}$$

which includes rotations.

The overall system stiffness matrix equation is obtained and is of similar form to eq 2.11. It may be partitioned such that the rotational elements are separated as shown:-

$$\begin{bmatrix} [k_{11}] & [k_{12}] \\ [k_{21}] & [k_{22}] \end{bmatrix} \begin{bmatrix} \{y\} \\ \{\phi\} \end{bmatrix} = \begin{bmatrix} \{F\} \\ \{\tau\} \end{bmatrix} \qquad \text{. . . eq 2.12}$$

If there are no externally applied moments then:-

$$\{\tau\} = \{0\} \qquad \text{. . . eq 2.13}$$

The partitioning of equation 2.12 gives two matrix equations:-

$$[k_{11}]\ \{y\} + [k_{12}]\ \{\phi\} = \{F\} \qquad \text{. . . eq 2.14}$$

$$[k_{21}]\ \{y\} + [k_{22}]\ \{\phi\} = \{0\} \qquad \text{. . . eq 2.15}$$

Equation 2.15 gives

$$\{\phi\} = -\ [k_{22}]^{-1}\ [k_{21}]\ \{y\} \qquad \text{. . . eq 2.16}$$

and by substituting eq 2.16 into 2.14

$$([k_{11}] - [k_{12}]\ [k_{22}]^{-1}\ [k_{21}])\ \ \{y\} = \{F\} \qquad \text{. eq 2.17}$$

or $$[\bar{k}]\ \{y\} = \{F\} \qquad \text{. . . eq 2.18}$$

where $$[\bar{k}] = ([k_{11}] - [k_{12}]\ [k_{22}]^{-1}\ [k_{21}]) \qquad \text{. . . eq 2.19}$$

Equation 2.17 reduces the stiffness equation to a 4th order since the angular deflections are dependent on the translational deflections.

Further, the inversion of eq 2.18 yields:-

$$[\bar{a}]\ \{F\} = \{y\} \qquad \text{. . . eq 2.20}$$

where $$[\bar{a}] = [\bar{k}]^{-1} = ([k_{11}] - [k_{12}]\ [k_{22}]^{-1}\ [k_{21}])^{-1} \text{eq 2.21}$$

$[\bar{a}]$ is the sub-matrix of the system flexibility matrix which consists of only the translational elements. This sub-matrix, defined by eq 2.21, may be easily proved by matrix inversion via partitioning, see Chapter 1, reference 18.

Equation 2.20 is particularly useful since in statics it is experimentally more practical to measure the flexibility matrix and then invert to obtain the stiffness matrix. This is also true for the dynamic case where the mobility* matrix is measured and inverted to give the impedance** matrix. Indeed this is logical since, for example, each element in the dynamic stiffness matrix follows the form

$$k_{ab} + jC_{ab}\Omega - m_{ab}\Omega^2 = S_{ab}$$

where the damping (C) is assumed to be viscous. The static case is when $\Omega = 0$ and so the dynamic stiffness coefficients disappear leaving the stiffness coefficients.

A numerical example on the use of equations 2.18 and 2.20 using simple beam theory is shown in Appendix 1. The example demonstrates the implementation of the static equivalent to the 'Impedance Coupling Technique' where the translational elements of the flexibility matrices are measured, inverted, then coupled together to formulate the system stiffness matrix.

2.4 FREQUENCY RESPONSE OF CANTILEVER BEAMS

The dynamic and static analyses of section 2.3 demonstrated that, providing the connectors offer little angular constraint, the rotational motions are dependent on the flexual motions in the system shown in Fig 2.1. Therefore, only the vertical translational elements are required in the cantilever matrices of the 'Impedance Coupling Equation.' It is theoretically and experimentally$^+$ easier to obtain the inertance matrix of the cantilever shown in fig 2.4 which may then be inverted as in eq 2.3, to obtain the required apparent mass matrix used in the 'Impedance Coupling Equation' eq 2.7.

* or **receptance** or inertance
** or dynamic stiffness or apparent mass
\+ see section 4.2

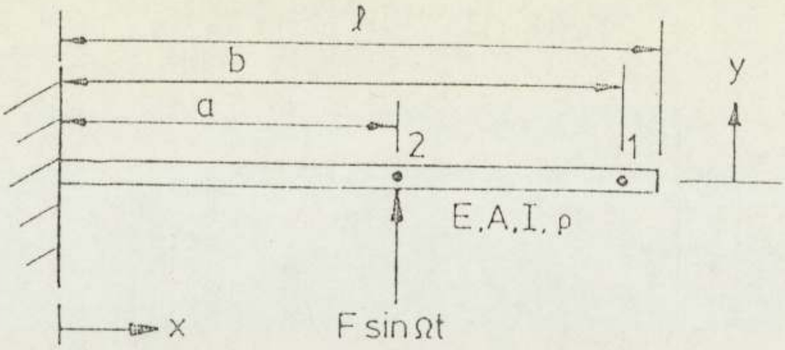

FIG 2.4 CANTILEVER BEAM

Equation 2.2 for the cantilever shown in Fig 2.4 is:-

$$\begin{bmatrix} I_{11} & I_{12} \\ I_{21} & I_{22} \end{bmatrix} \begin{bmatrix} F_1 \\ F_2 \end{bmatrix} = \begin{bmatrix} \ddot{y}_1 \\ \ddot{y}_2 \end{bmatrix} \qquad \text{. . . eq 2.22}$$

Providing there is only one input force, then:-

$$I_{ij} = \frac{\ddot{y}_i}{F_j} \qquad i,j = 1,2 \qquad \text{. . . eq 2.23}$$

The inertance elements defined by eq 2.23 may be found by classical forced response of beam theory[20]. A summary of this theory is as follows:

The free vibration solution is obtained in order to find the natural frequencies and mode shape functions. Reference 21 gives these functions together with the solutions to the frequency equation for the first five modes of vibration and formulae for obtaining an estimate for the higher modes. The forced response is then solved by using energy methods and transforming into principal co-ordinates such that

$$y = \sum_{n=1}^{\infty} \phi_n \, p_n \qquad \text{. . . eq 2.24}$$

where y is the displacement response

n is the nth mode of vibration

ϕ_n is the characteristic function of the beam (mode shape) in its nth mode

and p_n are the principal co-ordinates.

Then by using Lagrange equation the equations of motion become:-

$$\left\{ \rho A \int_0^{\ell} \phi_n^2 \, dx \right\} \ddot{p}_n + \left\{ c \int_0^{\ell} \phi_n^2 \, dx \right\} \dot{p}_n + \left\{ EI \int_0^{\ell} \phi_n''^2 \, dx \right\} p_n = P_n \quad \ldots \text{ eq 2.25}$$

where P_n are the external forces associated with the principal co-ordinate system.

The integrals of eq 2.25 are readily obtained from reference 22 for all possible boundary conditions. Therefore, using the solutions to the integrals for a cantilever and transforming back into the x,y co-ordinate system assuming harmonic motion:-

$$y(\Omega) = \frac{F\sin\Omega t}{\rho A \ell} \sum_{n=1}^{\infty} \frac{\phi_n(a)\phi_n(b).H_n}{\omega_n^2} \quad \ldots \text{ eq 2.26}$$

where H_n is the complex magnification factor and if $\Omega/\omega_n = r_n$

$$H_n = \frac{(1 - r_n^2) - j2\zeta r_n}{(1 - r_n^2)^2 + (2\zeta r_n)^2} \quad \ldots \text{ eq 2.27}$$

Acceleration response is:-

$$\ddot{y}(\Omega) = -\frac{\Omega^2 F\sin\Omega t}{\rho A \ell} \sum_{n=1}^{\infty} \frac{\phi_n(a)\phi_n(b).H_n}{\omega_n^2} \quad \ldots \text{ eq 2.28}$$

For peak inertance, I_{12}

$$I_{12}(\Omega) = \frac{\ddot{y}_1}{F_2} = -\frac{\Omega^2}{\rho A \ell} \sum_{n=1}^{m} \frac{\phi_n(a)\phi_n(b).H_n}{\omega_n^2} \quad \ldots \text{ eq 2.29}$$

In practice equation 2.29 is only summed over the first m modes as shown and is a good approximation when $\Omega << \omega_m$. The inertances shown in section 2.6 were obtained by summing over the first 15 modes.

2.5 FREQUENCY RESPONSE OF CONNECTORS

In order to complete the theoretical model of the cantilever system, it was necessary to obtain theoretical frequency responses of suitable connectors. Initially, the connectors were represented by simple stiffness elements and as such it was not necessary to obtain their frequency response since they could be added to the system matrix as demonstrated in equation 2.10. However, in addition to stiffness, the experimental work utilised connectors with mass and damping properties which were distributed along the length of the connector. In particular, a rubber connector was used to demonstrate low stiffness coupling and this connector was shown to have complex dynamic properties. Although both connectors used in the experimental work could be idealised to a 2 degrees of freedom model, since only the first mode was excited in the frequency range, it was first necessary to investigate this assumption by comparing the experimental frequency response of the connectors together with theoretical data obtained by a 2 degrees of freedom model and a more accurate model using the classical theory of longitudinal vibration of rods.

Only two translational coordinates were required to describe the frequency response of each connector* and these coordinates were positioned at the boundaries of the connectors. Therefore, the analysis is simplified to computing four elements in the apparent mass matrix as shown in eq 2.30.

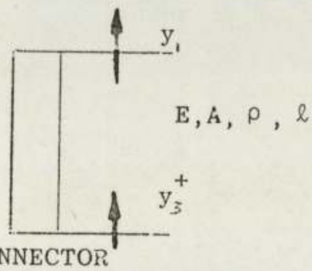

$$\begin{bmatrix} A_{11} & A_{13} \\ A_{31} & A_{33} \end{bmatrix} \begin{bmatrix} \ddot{y}_1 \\ \ddot{y}_3^+ \end{bmatrix} = \begin{bmatrix} F_1 \\ F_3 \end{bmatrix}$$

...eq 2.30

Each element in the apparent mass matrix is computed or measured by 'grounding' or 'blocking'** each coordinate in turn giving the following relationships.

* The connectors were designed to satisfy the conditions discussed in section 2.3

\+ Coordinate y_3 was selected to conform to the coupled system coordinates

** See section 4.7 for a detailed description of a 'blocked Impedance' test.

$$\left.\begin{aligned} A_{i3} &= \frac{F_i}{\ddot{y}_3} \qquad i = 1,3 \quad \text{when} \quad \ddot{y}_1 = 0 \\ A_{i1} &= \frac{F_i}{\ddot{y}_1} \qquad i = 1,3 \quad \text{when} \quad \ddot{y}_3 = 0 \end{aligned}\right\} \quad \text{... eq 2.31}$$

<u>To find A_{ij}</u> $i,\ j = 1,3$

(i) <u>Two Degrees of Freedom Model</u>

The connector may be discretised by concentrating its mass at each end and by connecting these rigid masses by massless stiffness and damping elements. The resulting apparent mass equation has the form:

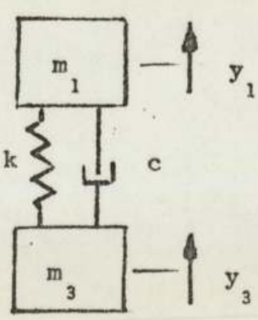

$$\begin{bmatrix} \left(m_1 - \frac{k}{\Omega^2}\right) - j\,\frac{C}{\Omega} & \frac{k}{\Omega^2} + j\,\frac{C}{\Omega} \\ \frac{k}{\Omega^2} + j\,\frac{C}{\Omega} & \left(m_3 - \frac{k}{\Omega^2}\right) - j\,\frac{C}{\Omega} \end{bmatrix} \begin{bmatrix} \ddot{y}_1 \\ \ddot{y}_3 \end{bmatrix} = \begin{bmatrix} F_1 \\ F_3 \end{bmatrix} \quad \text{. eq 2.32}$$

(ii) Forced Response of Rods in Longitudinal Vibration

The apparent mass elements defined by equations 2.31 may be obtained by the classical theory of forced response of rods in longitudinal vibration[23]. A summary of this theory is as follows:

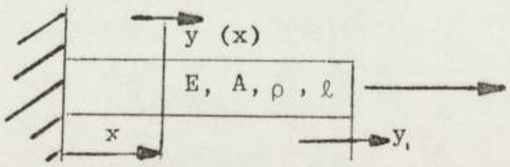

GROUNDED ROD IN LONGITUDINAL VIBRATION

The wave equation for the rod shown above is:

$$\frac{d^2 y(x)}{dx^2} + \beta^2 y(x) = 0 \qquad \text{...eq 2.33}$$

where $\beta^2 = \frac{\Omega^2 \rho}{E}$

The boundary conditions are -

$$\left.\begin{array}{ll} \text{(i)} & y(o) = 0 \\ \text{(ii)} & \sigma(\ell) = E\,\frac{dy_1}{dx} = \frac{F_1}{A} \end{array}\right\} \text{... eq 2.34}$$

which gives the following solution to the wave equation when $x = \ell$

$$\frac{F_1}{\ddot{y}_1} = \frac{-\,m_R \cos\beta\ell}{\beta\ell\,\sin\beta\ell} \qquad \text{... eq 2.35}$$

where m_R is the mass of the rod.

Equation 3.5 may be modified to allow for

(a) a concentrated mass at the free boundary

(b) the internal damping of the rod.

a) Concentrated Mass at the Free Boundary

Equation 2.35 may be modified to allow for concentrated masses at the ends of the rod by the use of the 'Impedance Coupling Technique' as follows:-

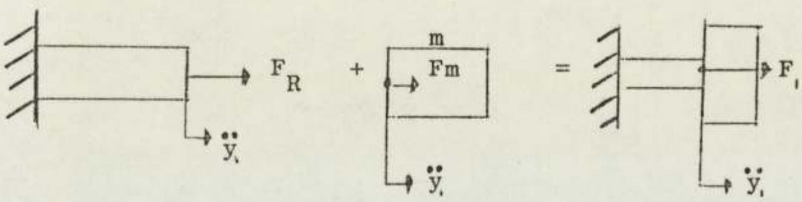

The apparent mass equation of the rod and end mass is:-

$$A_S = A_R + A_m \qquad \text{... eq 2.36}$$

Since for the mass

$$A_m = m$$

Therefore

$$\frac{F_1}{\ddot{y}_1} = \frac{- m_R \cos \beta \ell}{\beta \ell \sin \beta \ell} + m \qquad \text{... eq 2.37}$$

b) Internal Damping of the Rod

Equations 2.35 and 2.37 may be further modified by introducing internal damping which may be taken into account by expressing Young's Modulus of elasticity as a complex quantity such that -

$$E^{*}(\Omega) = E(\Omega)(1+j\delta(\Omega)) \qquad \text{... eq 2.38}$$

where δ is the loss factor. In general the complex modulus varies with exciting frequency as shown. Equations 2.35 and 2.37 are modified by replacing β with β^{*} which is complex and is related to E* by

$$\beta^{*} = \sqrt{\frac{\Omega^{2}\rho}{E^{*}}}$$

Therefore

$$\frac{F_1}{\ddot{y}_1} = \frac{-m_R \cos\beta^{*}\ell}{\beta^{*}\ell \sin\beta^{*}\ell} + m \qquad \text{... eq 2.39}$$

The complex trigonometric functions in eq 2.39 are manipulated by the following identities -

$$\left.\begin{aligned} \cos(p+jq) &= \cos p \cosh q - j \sin p \sinh q \\ \sin(p+jq) &= \sin p \cosh q + j \cos p \sinh q \end{aligned}\right\} \text{... eq 2.40}$$

To obtain E* from Experimental Results

It was found during the 'blocked Impedance' tests on the rubber connector that the complex modulus varied significantly over the frequency range. It was therefore necessary to obtain values of E* at selected frequencies in order to improve the theoretical model. The apparent mass $F_1/\ddot{y}_1$ of the rod together with an end mass was measured and an estimate of E* was computed via Newton's iteration formula. From eqs 2.36 and 2.37 the apparent mass of the rubber rod is -

$$A_R = \left(\frac{F_1}{\ddot{y}_1} - m \right) = \frac{-m_R \cos \beta^* \ell}{\beta^* \ell \sin \beta^* \ell} \qquad \text{....eq 2.41}$$

Let $b = \beta^* \ell$ then eq 2.41 becomes

$$A_R = \frac{-m_R \cos b}{b \sin b}$$

Let

$$g(b) = \frac{m_R \cos b}{b \sin b} + A_R$$

then by using Newton's iteration formula:

$$b_{n+1} = b_n - \frac{g(b_n)}{g'(b_n)} \qquad \text{...eq2.42}$$

where

$$\frac{g(b)}{g'(b)} = \frac{-m_R b \cos b \sin b + A_R b^2 \sin^2 b}{m_R (\cos b \sin b + b)} \qquad \text{...eq 2.43}$$

Hence a value of b and therefore E* may be computed at a selected frequency.

2.6 APPLICATION OF 'IMPEDANCE COUPLING TECHNIQUE' TO THE TWO CANTILEVER SYSTEM

The 'Impedance Coupling Equation'. eq 2.7 has been simplfied to a 4th order equation as shown in Fig 2.5. The cantilever inertance matrices may now be generated by experiment or from classical theory and the connectors may be modelled by a simple two degree of freedom system with 2 masses, a spring and a damper. Various computer programs were written to generate cantilever and connector apparent mass data using equations 2.29 and 2.32 and to manipulate this data according to equation 2.7 in order to compute the coupled system response and the effect of dynamic characteristics of connectors on the system response. These programs are discussed in section 3.6 of this thesis.

2.7 THEORETICAL RESULTS OF TWO CANTILEVER SYSTEMS

A selection of frequency response curves were theoretically generated for some cantilevers. The dimensions of these cantilevers are tabulated in Table 2.1 and were taken from existing cantilevers in order that this study might follow as closely as possible the experimental work. This data was coupled with theoretically generated coupling data in various system configurations as shown in Table 2.2. Some of the coupling dynamic characteristics were also purposely chosen to represent previously manufactured connectors.

It was necessary to provide a small amount of damping in the generation of inertance data for the cantilevers in order to avoid infinite values of inertance at natural frequencies. A damping ratio (ζ) of 0.05% was selected for this purpose and was considered constant for all the modes.

CANTILEVER IDENTIFICATION	LENGTH mm	WIDTH mm	THICKNESS mm
a	973	63.5	6.35
b	930	50.8	6.35
c	963	63.5	12.7
d	930	50.8	6.35

TABLE 2.1 CANTILEVER DIMENSIONS

Description of Theoretical Results

Figures 2.6 - 2.9 show the theoretically generated frequency response curves for the four cantilevers obtained by equation 2.29. The graphs show inertance magnitude within the frequency range 30 - 500 Hz at discrete frequency intervals of 0.5 Hz. The inertance magnitude is expressed as:-

$$|I| = |I.I*|^{\frac{1}{2}} \qquad \text{. . . eq 2.44}$$

where $I*$ is the complex conjugate of I. The phase is not shown on any of these graphs since it predictably changes from in-phase to out-of-phase at resonances and antiresonances and is not of direct significance in this study.

Figures 2.10 - 2.14 show the coupled system inertance magnitudes as described in Table 2.2 The curves shown represent a quarter of the possible system matrix and these were selected to show coupling effects. Since reciprocity was assumed then these matrices are symmetric and so:-

$$I_{ij} = I_{ji} \qquad \text{. . . eq 2.45}$$

Figures 2.15 - 2.18 show the effect of varying the coupling stiffness on frequency response of the system at selected frequencies. In each of the examples neighbouring frequencies are overlaid to give an indication how these contours vary with frequency. This effect would be more ideally represented in three dimensions.

2.8 DISCUSSION OF THEORETICAL RESULTS

The frequency range of these results was purposely chosen to be 30-500 H_z such that direct comparisons could be made with the experimental results. Very low frequency response was of no particular interest to this investigation. Also the equipment was not ideally suited to operate at frequencies less than $30H_z$. Therefore the frequency response in the range $0-30H_z$ is omitted with the consequence that the first peak in the plots are the cantilever's second natural frequency.

The curves for cantilever d (Fig 2.9) show that position 3 is very close to a node position for the third and fifth modes of vibration. The frequency responses of the system indicate an increase in modal density which is due to the coupling of the two cantilever sub-systems. Some of these additional modes are very sensitive to the coupling stiffness. In particular, the curves of system 1 and 2 are quite different, system 1 being fairly rigidly coupled,whereas system 2 has a flexible coupling. However, both curves show the presence of modes that are of similar frequency to the individual cantilever modes and these modes do not seem to be so sensitive to coupling stiffness. This is also true in system 3 where the two cantilevers have significantly different cross-sections, although some of their natural frequencies almost coincide, eg cantilever c has its third mode around 200 Hz whereas cantilever d has its fourth mode at this same frequency. These effects are shown more clearly in the graphs of inertance against coupling stiffness at selected frequencies. For example, Fig 2.15 shows the effect of coupling stiffness on inertance I_{13} for system 1. It is seen that at stiffnesses of about 500 kN/m and 1500 kN/m the system will have a resonance at 400 Hz, but will have an antiresonance at this frequency if the coupling stiffness is 800 kN/m. Therefore, if this system needs to be detuned at 400 Hz, coupling stiffnesses of 800 kN/m will be selected. Conversely other resonant frequencies are not so easily detuned and this is seen in Fig 2.16 where the coupling stiffness does not have much effect on inertance above 400 kN/m. Below this stiffness the coupling is fairly soft. The overlaying curves in this graph are the contours of a resonant frequency which is near to the top cantilever's fourth natural frequency.

Figures 2.17 and 2.18 show similar characteristics for system 3. In this case the contours of Fig 2.17 show that this system is particularly sensitive to changes in frequency around 140 Hz. However, detuning is still possible at 1000 kN/m.

Figures 2.13 and 2.14 show the effect of coupling two identical cantilevers. In Fig 2.13 the extra coupling modes are just evident even though the stiffness of the coupling is quite rigid. Figure 2.14 is the same system with a much higher coupling stiffness. These curves have similar characteristics of cantilever a, but with a general fall in inertance level of 6 dB's. This is due to the combined system behaving effectively as a single cantilever with twice the mass and stiffness of cantilever a.

In order to clarify this difference in the behaviour of coupled system modes, that are either sensitive or non-sensitive to coupling stiffness, further coupled system models were theoretically generated using a series of concentrated rigid masses linked together with massless stiffness elements. These models allowed a quick but comprehensive representation of coupled systems which clearly show the effect of coupling stiffness on mode shapes and natural frequencies.

Three examples of coupled systems are shown in Fig 2.19 to 2.22 together with their mode shapes and natural frequencies. In all three examples the coupled system is represented by eight masses linked by nine stiffness elements. Each of the two sub-systems within the coupled system model is represented by four masses together with three stiffness elements and a further stiffness element at one end which is used to ground the system, the other end being free. The sub-systems are coupled at their free ends by a stiffness element which is situated in the middle of the model diagram. The three examples were selected to represent three combinations of coupled systems with sub-systems of differing dynamic properties. These are, coupled systems with

(i) sub-systems of similar dynamic properties such that their natural frequencies occur in the same frequency range (as Fig 2.19)

(ii) sub-systems in which their range of natural frequencies overlap each other (as Fig 2.20)

(iii) sub-systems in which their ranges of natural frequencies do not overlap (as Fig 2.21).

The natural frequencies and mode shapes of the 2 sub-systems and the coupled system are shown throughout. Two system characteristics are presented for each example and these represent both low and high stiffness coupling.

The first example shown in Fig 2.19 offers the most representative model of the cantilever systems investigated in the preceding paragraphs since the cantilevers were of similar dimensions and as such exhibited similar dynamic properties. In this example the system coupled with a low and a high stiffness shows how the modes are affected by the coupling stiffness. When the coupling stiffness is low the modes occur in pairs with the natural frequencies of each pair near to the corresponding sub-system natural frequency. The mode shape within each pair also corresponds to the sub-system mode shape the only difference being that the coupling stiffness element becomes active in the second mode of each pair which allows a 180 degree phase shift across the coupling element but with each sub-system retaining its individual shape. Increasing the coupling stiffness has, therefore, a significant effect on these particular modes. In contrast, the first mode of each pair is not affected by the coupling stiffness in mode shape or natural frequency. In this example the low coupling stiffness is 10% of a typical sub-system stiffness and as such becomes active at the second mode. The high coupling stiffness is one thousand times greater than a typical sub-system stiffness and this does not become active until the eighth mode. In consequence, the second mode in each pair is moved up the frequency range.

The second and third examples shown in Figs 2.20 and 2.21 both indicate that the coupling stiffness has an effect on all the natural frequencies and mode shapes. In general, an increase in coupling stiffness increases all the natural frequencies and causes a change in the mode shapes.

When the coupling stiffness is very high the natural frequencies and mode shapes are changed to such an extent that each mode resembles the next higher mode of the low stiffness coupled system. The exception to this is the highest frequency mode where the mode shape is dominated by the activity of the stiffness element and its natural frequency is very high. When this coupling stiffness becomes infinite, such that the two middle masses are rigidly connected, the number of generalised coordinates for the coupled system will be reduced to seven, thereby giving seven natral frequencies and so the 8th mode will not be present.

The effect on natural frequencies and mode shapes can be clearly seen in Fig 2.22 where the 4th, 5th and 6th modes of the second coupled system (of Fig 2.20) are shown with intermediate coupling stiffnesses. The biggest change occurs when the coupling stiffness element becomes active.

Comparing the results of the cantilever systems with these models indicate that the first example is the most representative of the cantilever systems and this is because the cantilevers also had similar dynamic properties. Therefore it follows that a stiffness element connecting two cantilevers will not affect the cantilever modes that do not require any activity of the stiffness element. For example if two cantilevers are connected at their free ends, then increasing or removing the stiffness will not affect the cantilever modes in which the ends vibrate in phase to each other. Conversely the modes in which the ends vibrate out of phase to each other will be greatly affected by the coupling stiffness. Introducing extra restraints at other coordinates is therefore likely to have an increasing effect on all the modes since, for example, a rotational stiffness element connecting the free ends would need to become active at all the cantilever modes.

In conclusion, the theoretical study has shown that it is possible to detune a coupled system which comprises two complex structures connected at two positions. This is accomplished by optimising on coupling characteristics at selected frequencies. In particular, the stiffness was shown to have the greatest effect within the frequency range analysed, i.e. 30 - 500 H_z.

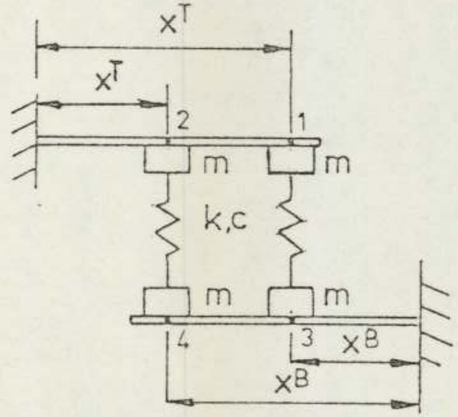

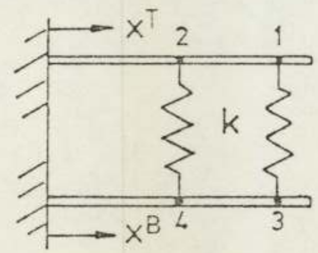

		CANTILEVERS				CONNECTORS			
System Ident.	Cant. Ident.	x_1^T mm.	x_2^T mm.	x_3^B mm.	x_4^B mm.	m_1, m_2 grams	m_3, m_4 grams	k kN/m	c Ns/m
1	a	920	558	-	-	0	0	4×10^3	0
	b	-	-	558	920				
2	a	920	558	-	-	6·2	23·4	43·5	15
	b	-	-	558	920				
3	c	918	461	-	-	0	0	4×10^3	0
	d	-	-	465	920				
4	a	920	558	-	-	0	0	4×10^3	0
	a	-	-	920	558				
5	a	920	558	-	-	0	0	4×10^5	0
	a	-	-	920	558				

TABLE 2·2 DESCRIPTION OF CANTILEVER SYSTEMS

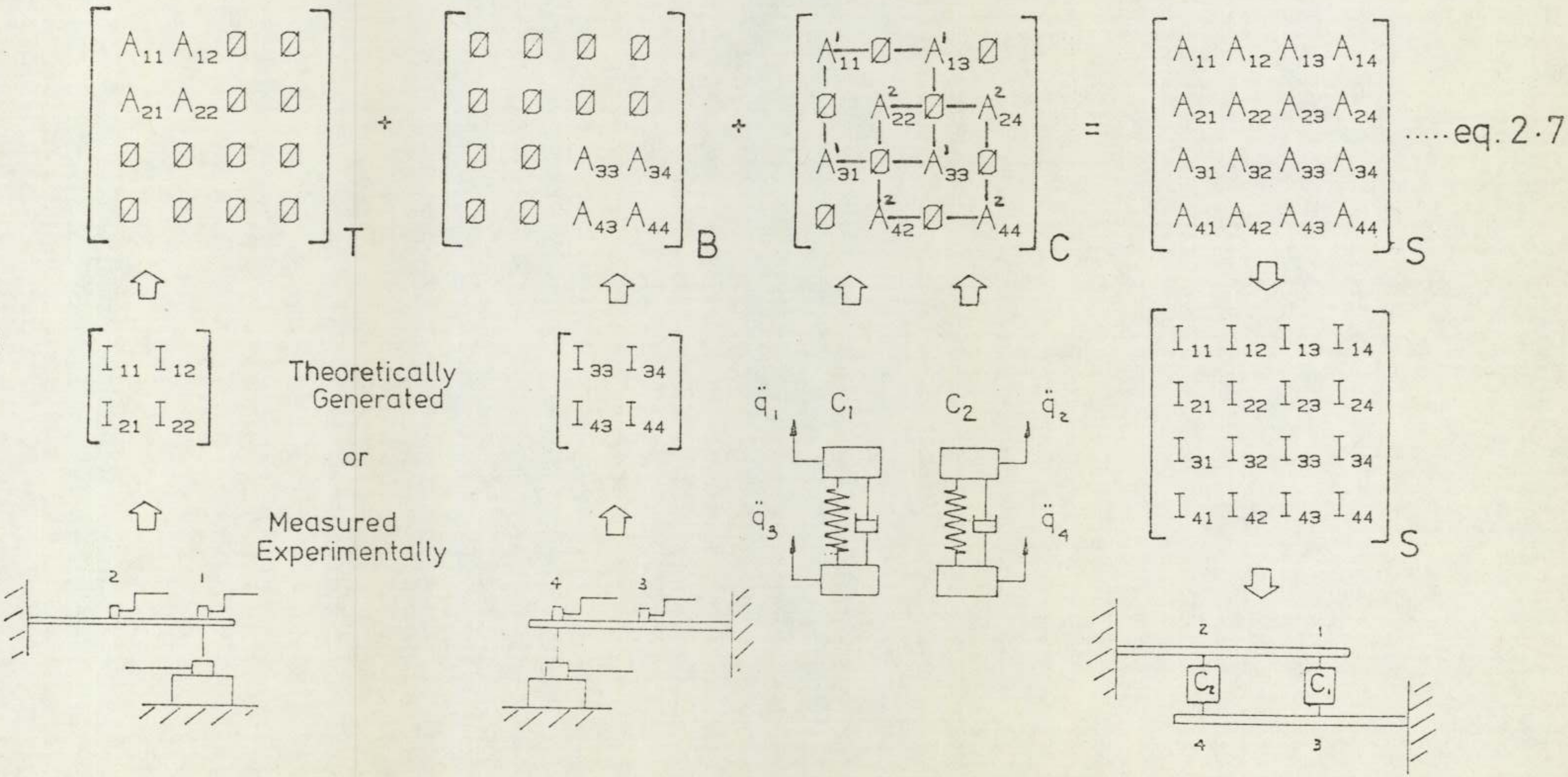

Fig. 2.5 'IMPEDANCE COUPLING TECHNIQUE'

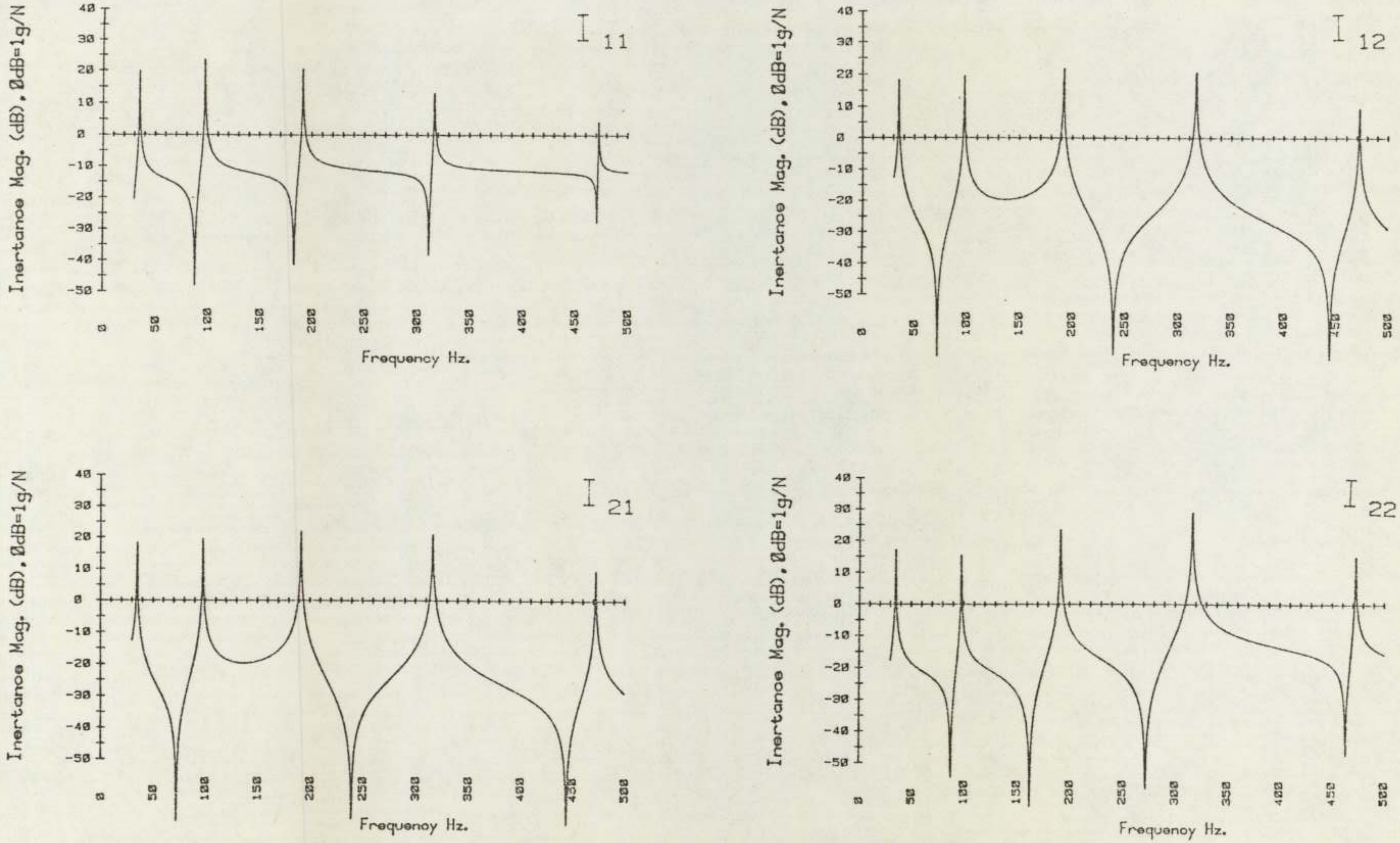

Fig. 2.6 THEORETICAL INERTANCES OF CANTILEVER (a)

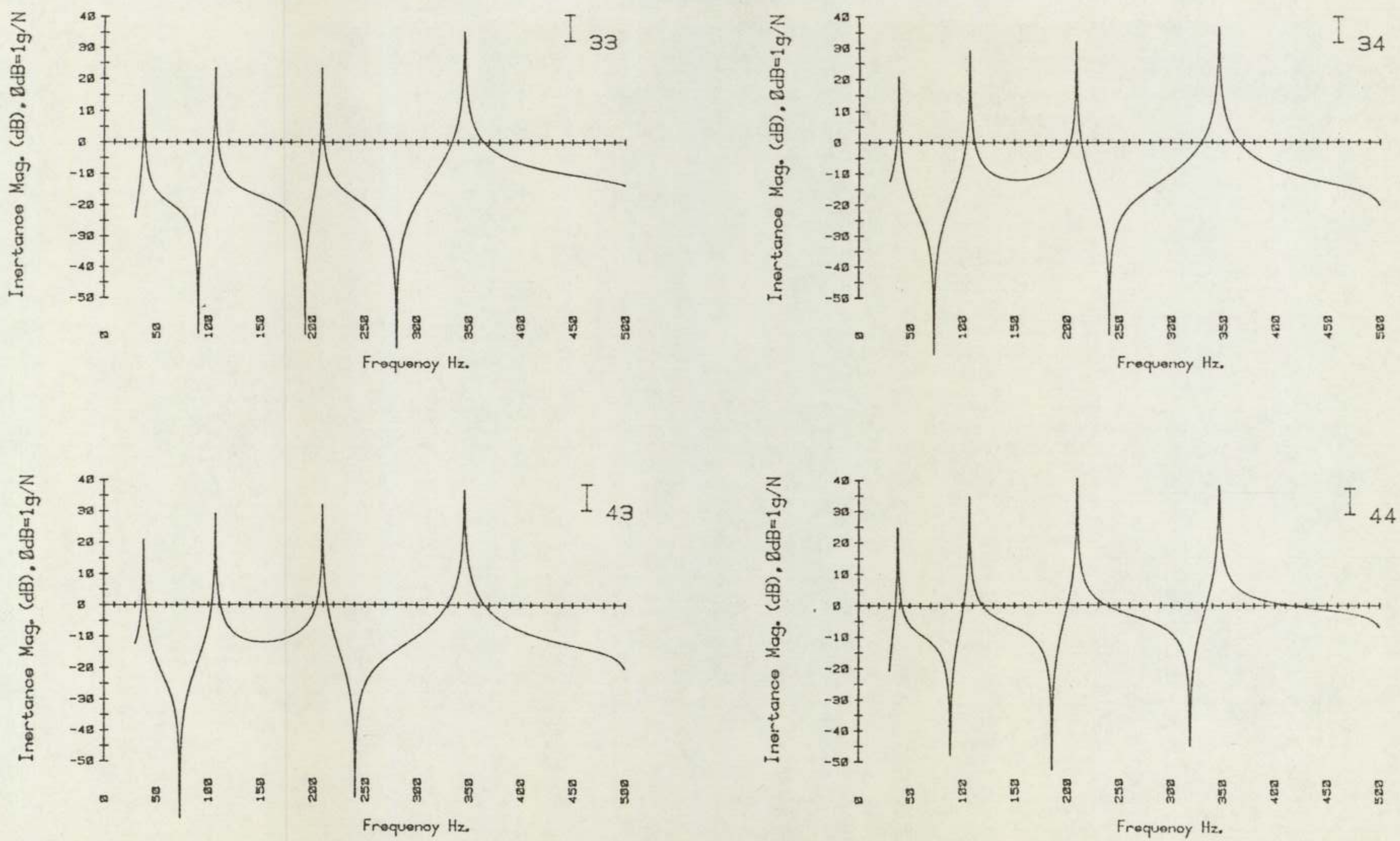

Fig. 2.7 THEORETICAL INERTANCES OF CANTILEVER (b)

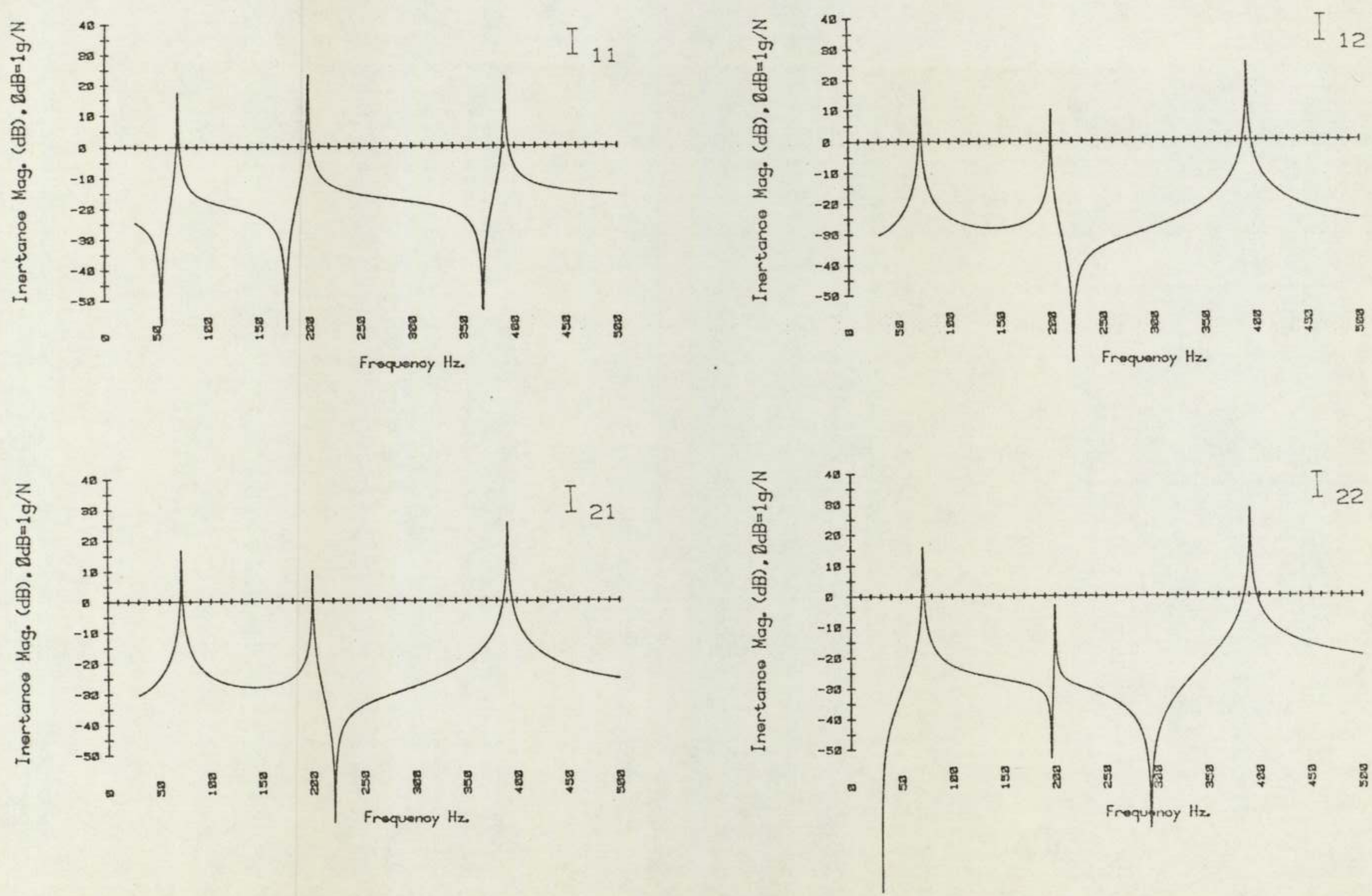

Fig. 2.8 THEORETICAL INERTANCES OF CANTILEVER (c)

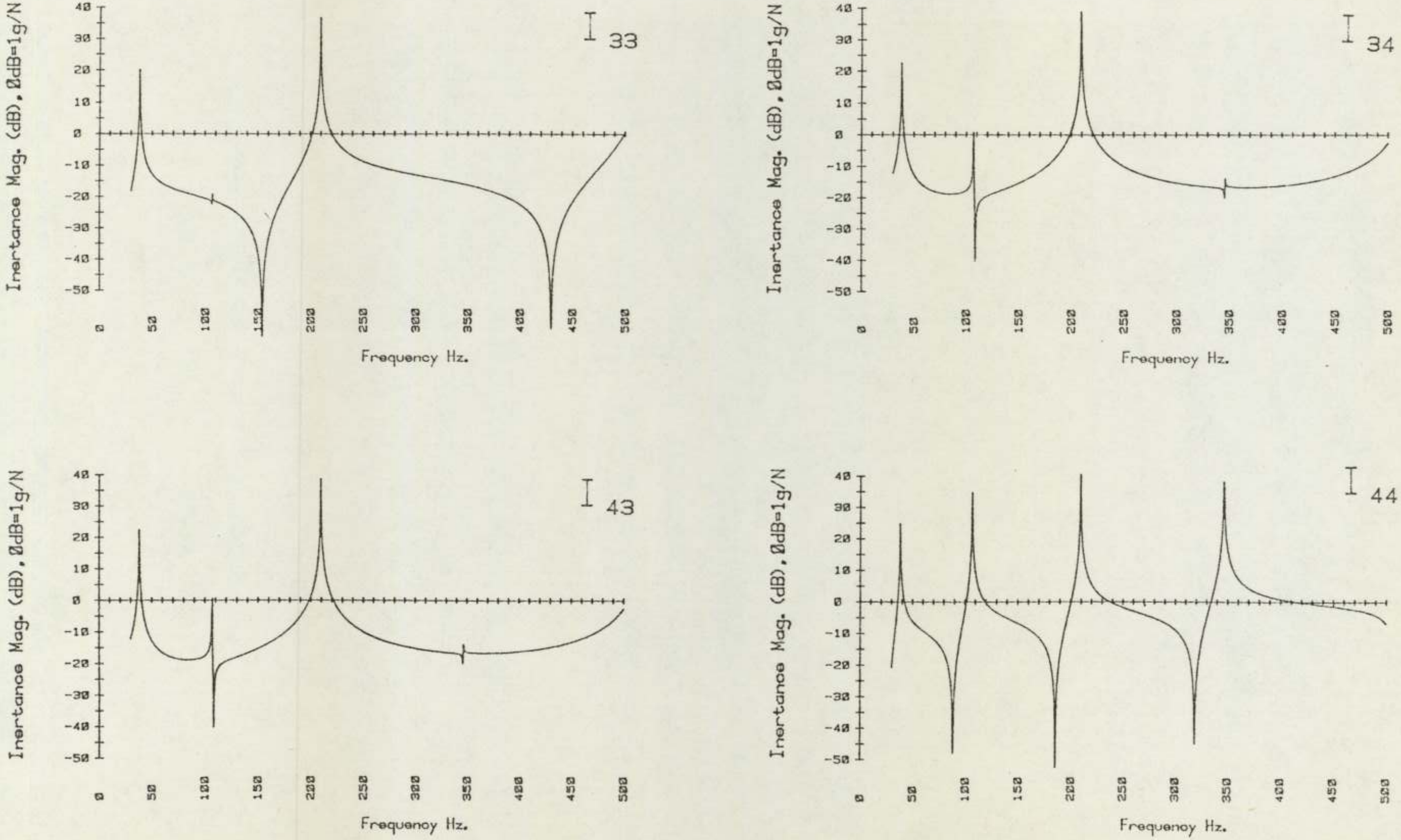

Fig. 2.9 THEORETICAL INERTANCES OF CANTILEVER (d)

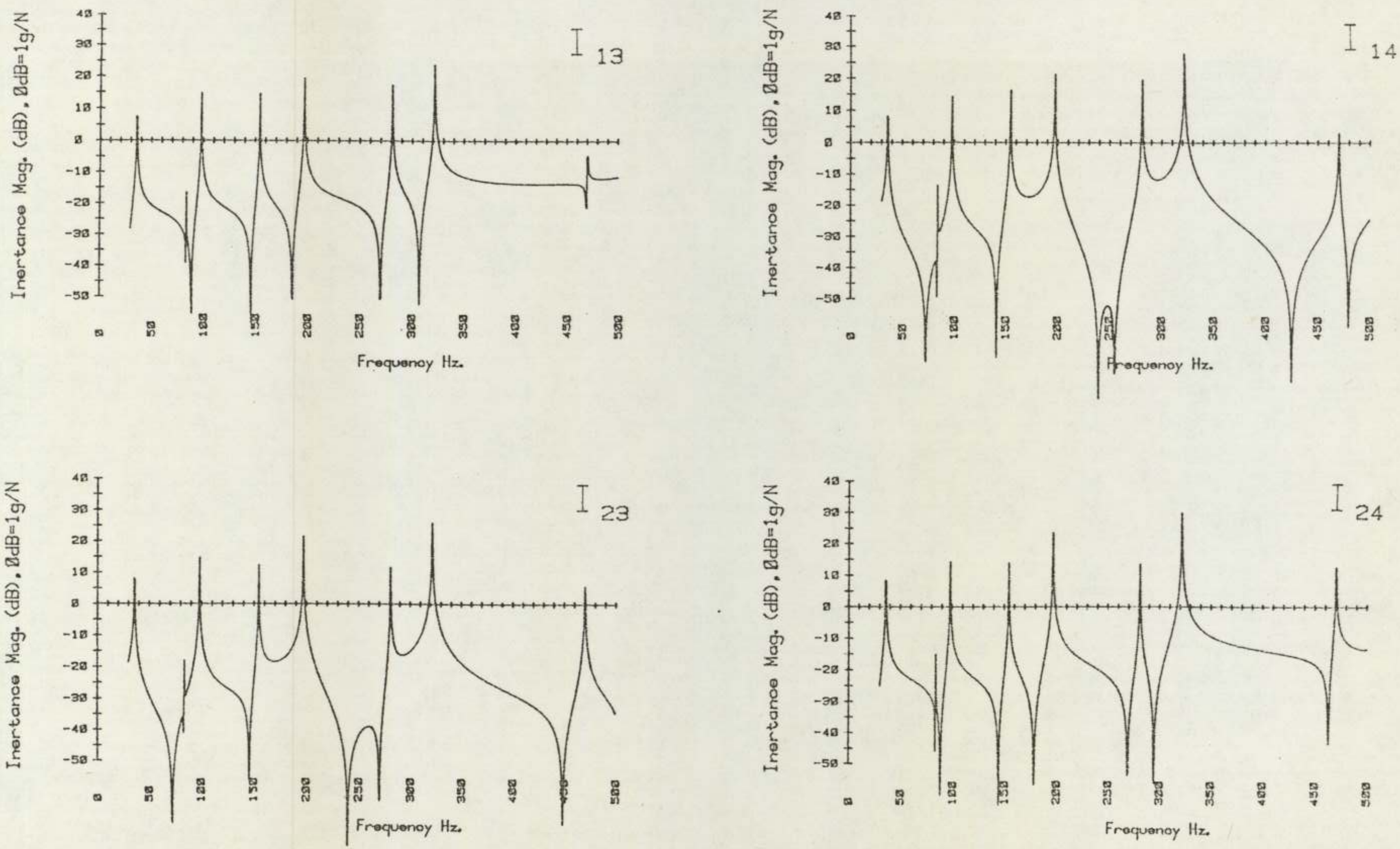

Fig. 2.1Ø THEORETICAL INERTANCES OF SYSTEM 1 - k=4MN/m

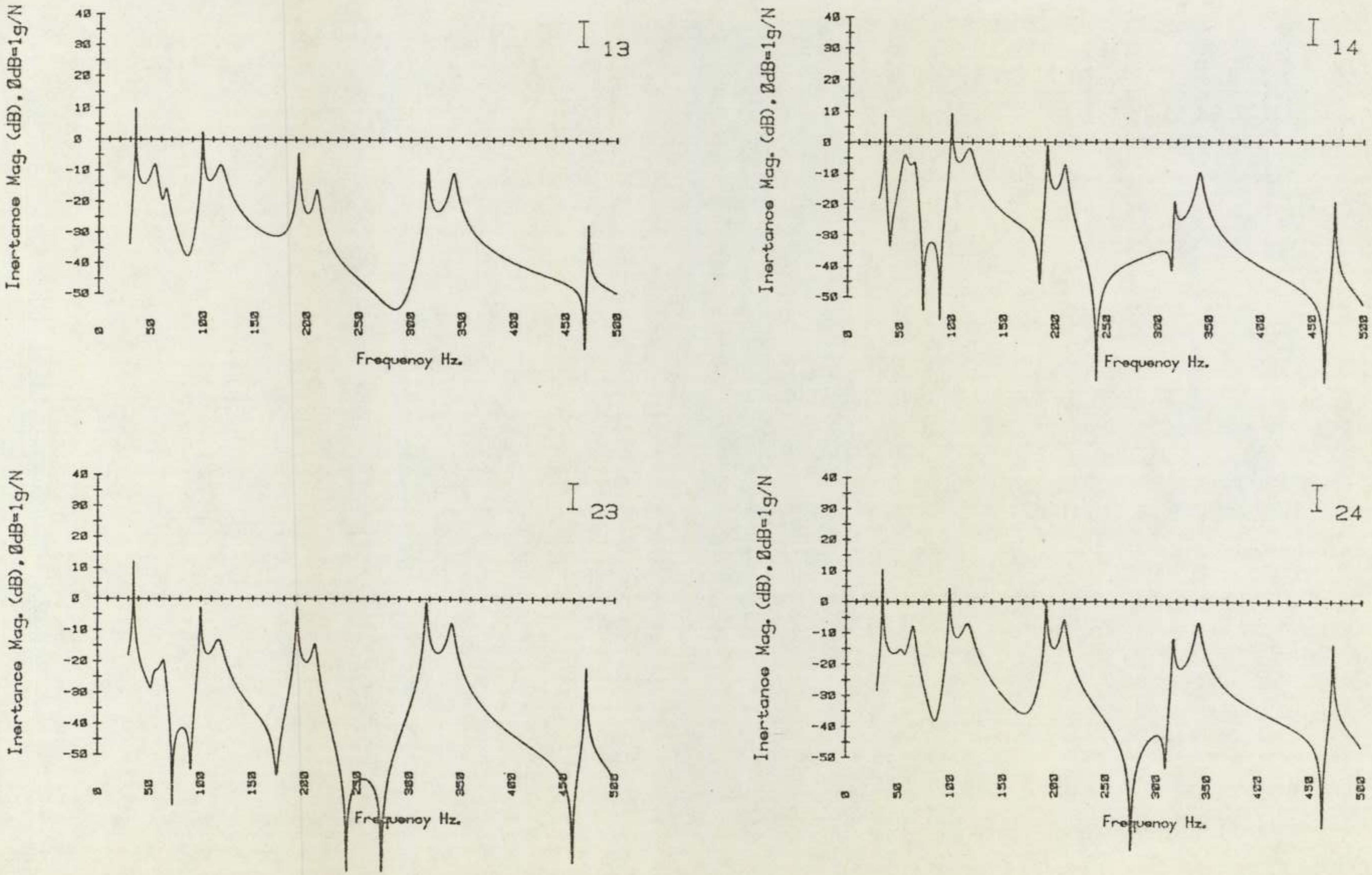

Fig. 2.11 THEORETICAL INERTANCES OF SYSTEM 2

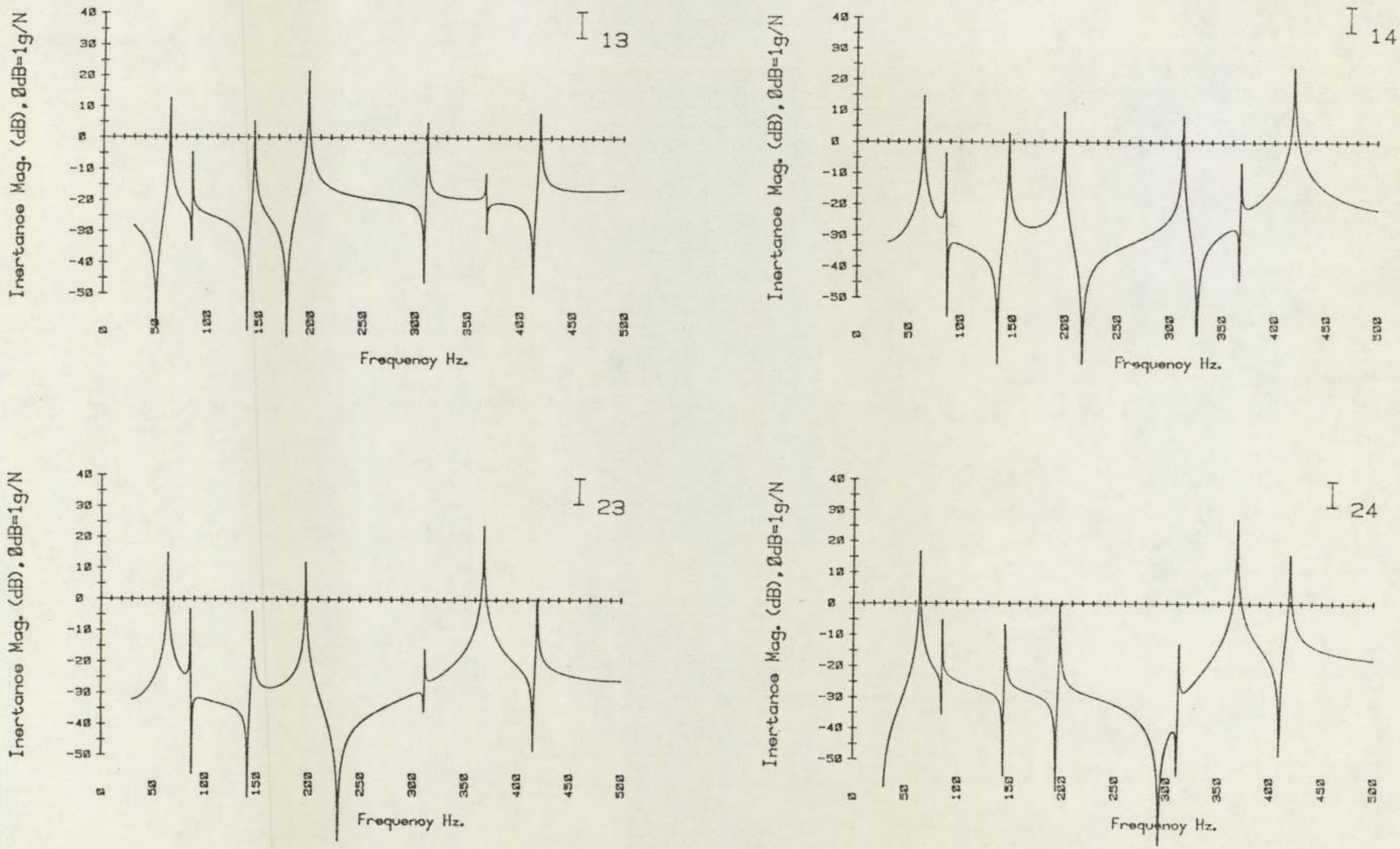

Fig. 2.12 THEORETICAL INERTANCES OF SYSTEM 3 - k=4MN/m

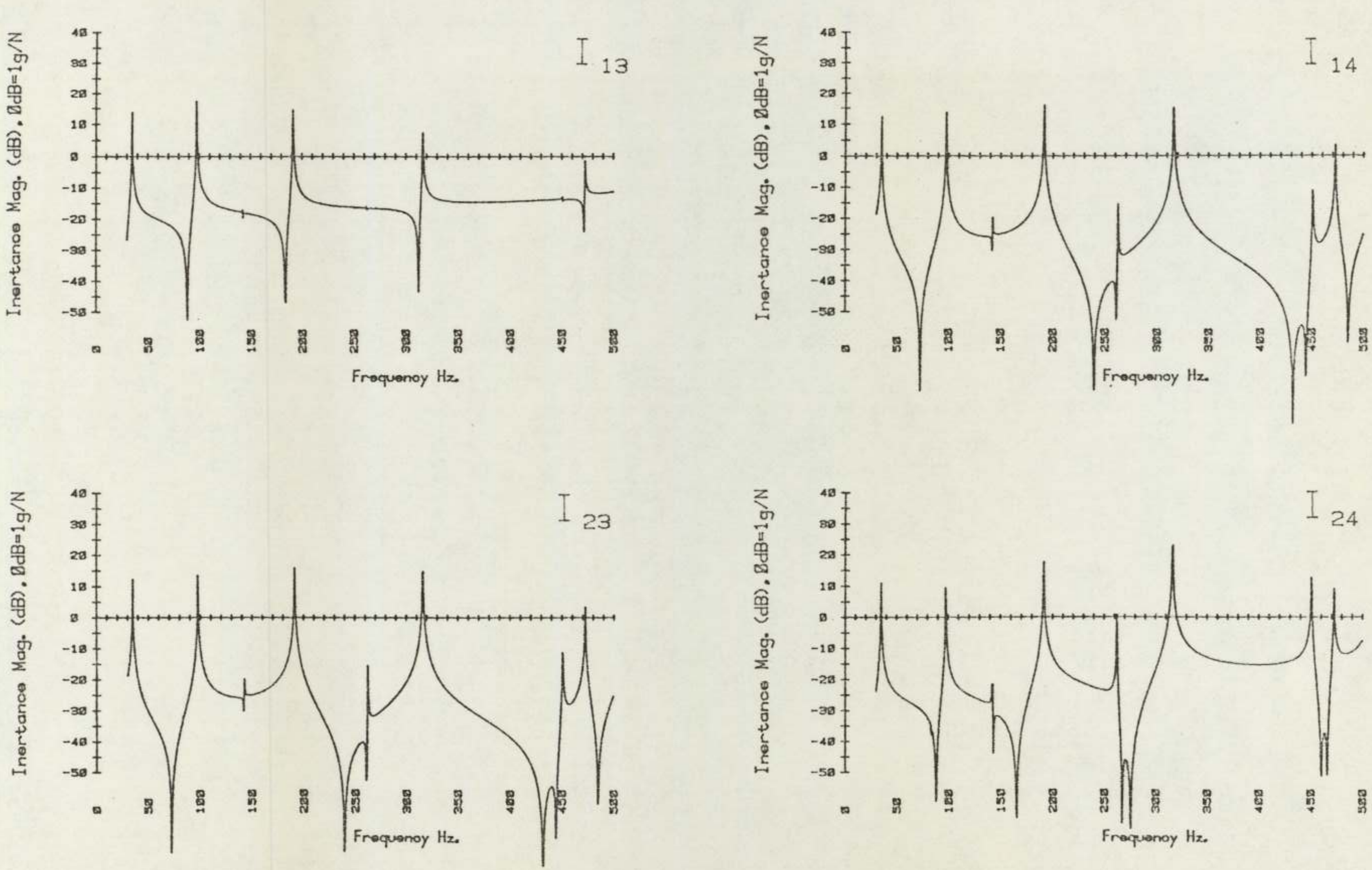

Fig. 2.13 THEORETICAL INERTANCES OF SYSTEM 4 - k=4MN/m

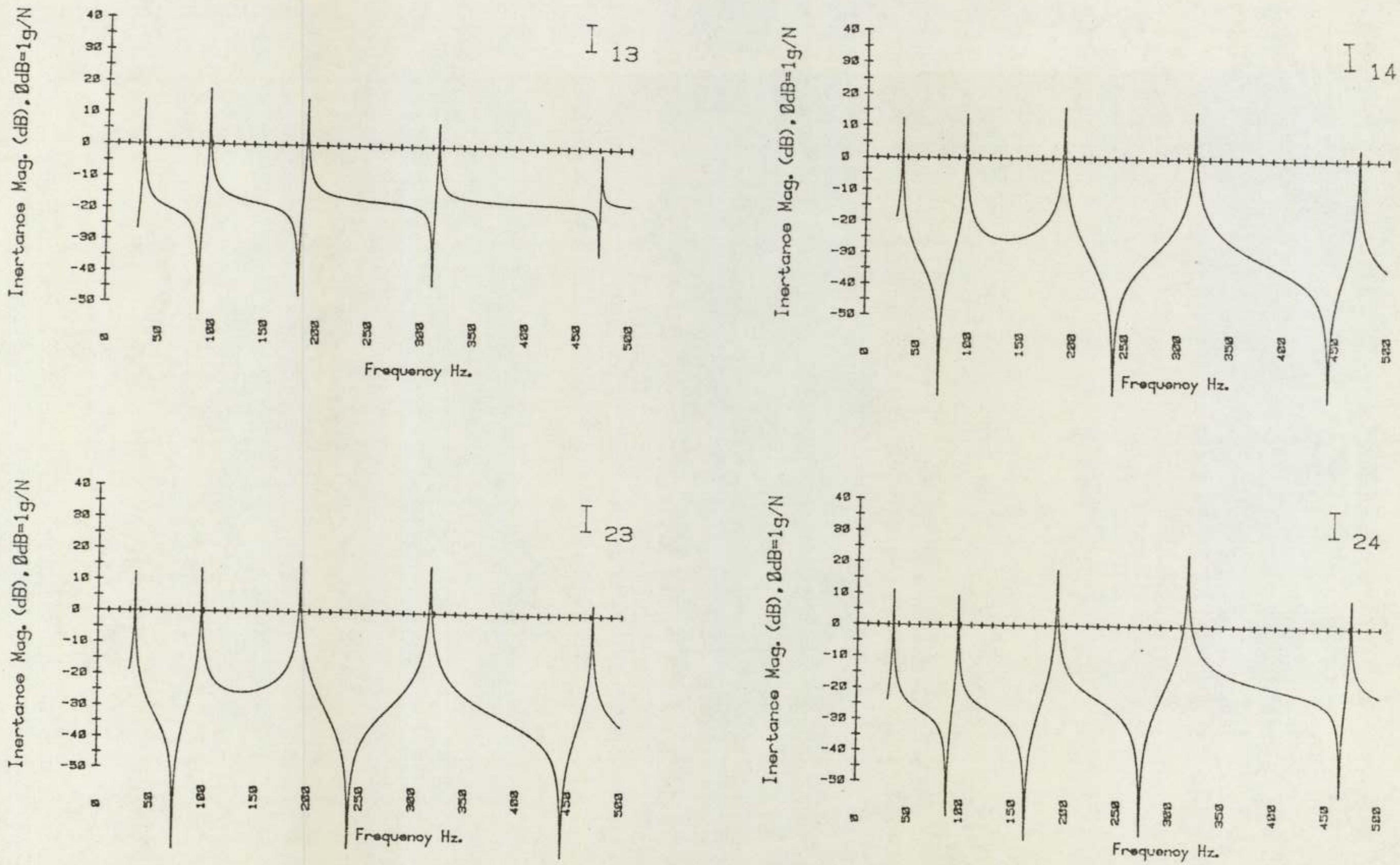

Fig. 2.14 THEORETICAL INERTANCES OF SYSTEM 5 - k=400MN/m

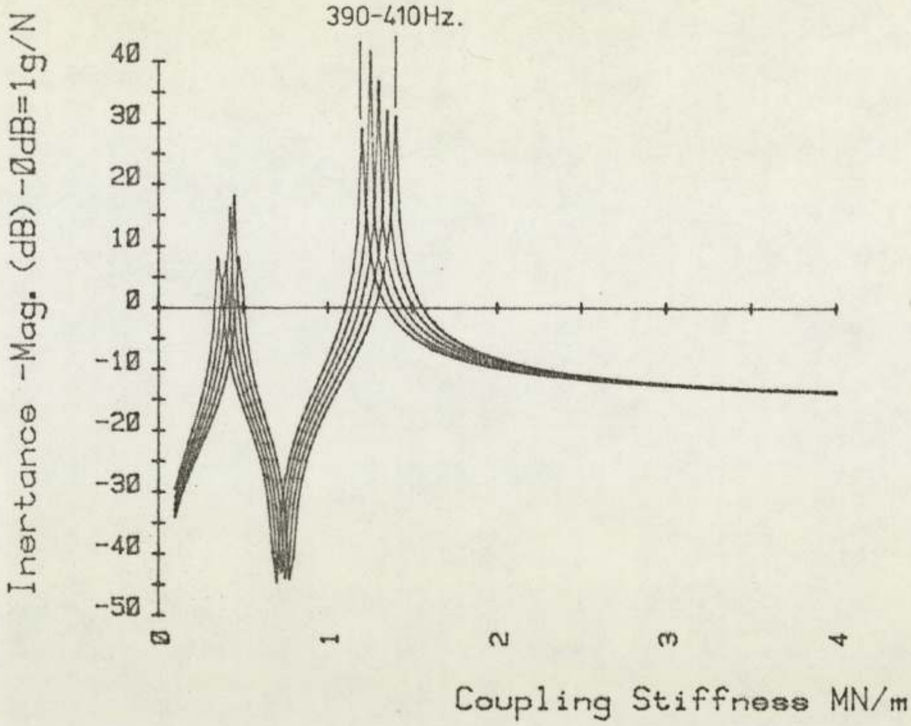

Fig. 2. 15 EFFECT OF COUPLING STIFFNESS ON SYSTEM 1 INERTANCE I_{13}, FREQUENCY RANGE 39Ø-41ØHz.

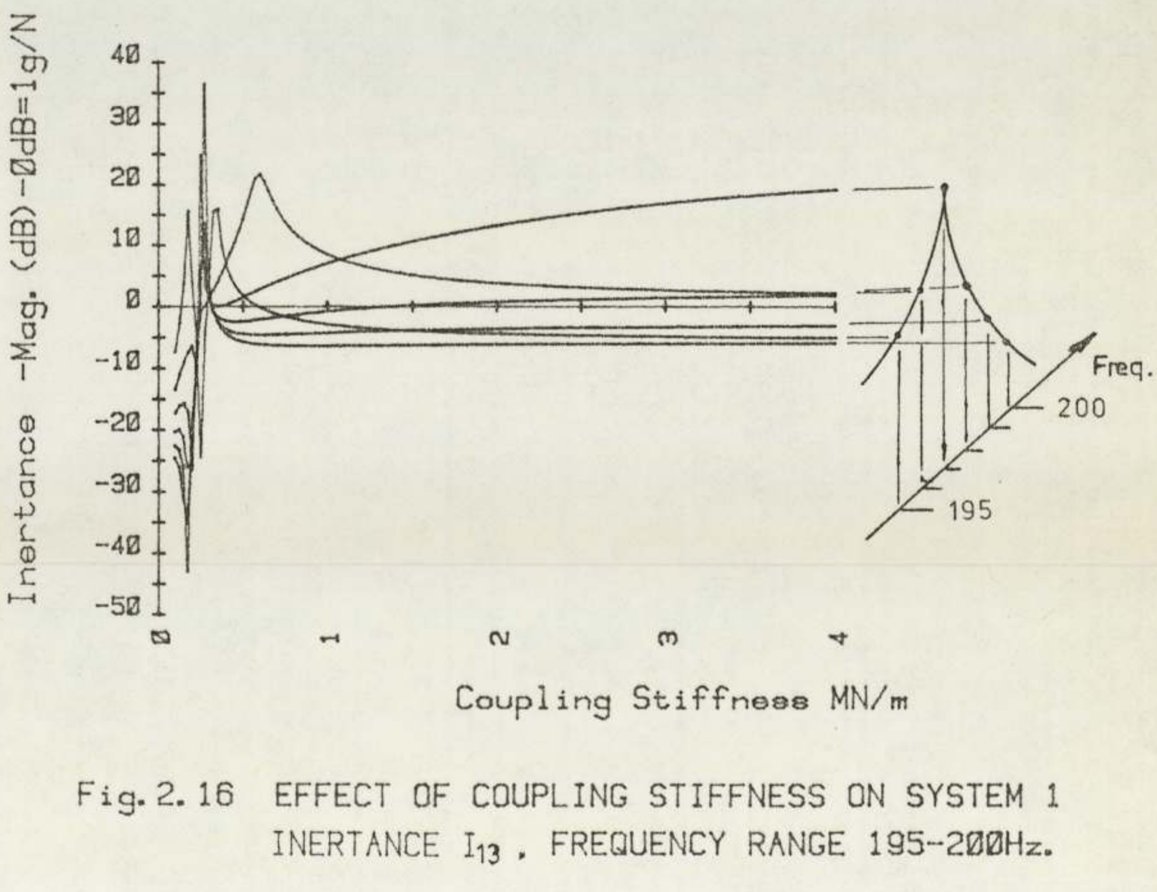

Fig. 2. 16 EFFECT OF COUPLING STIFFNESS ON SYSTEM 1 INERTANCE I_{13}, FREQUENCY RANGE 195-2ØØHz.

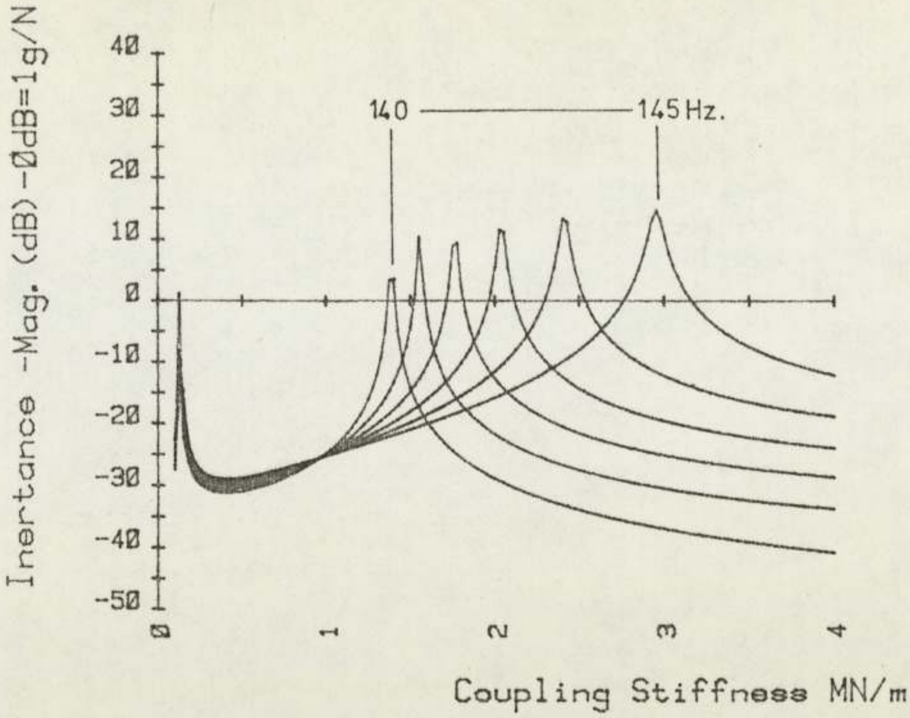

Fig. 2.17 EFFECT OF COUPLING STIFFNESS ON SYSTEM 3 INERTANCE I_{13}. FREQUENCY RANGE 140-145Hz.

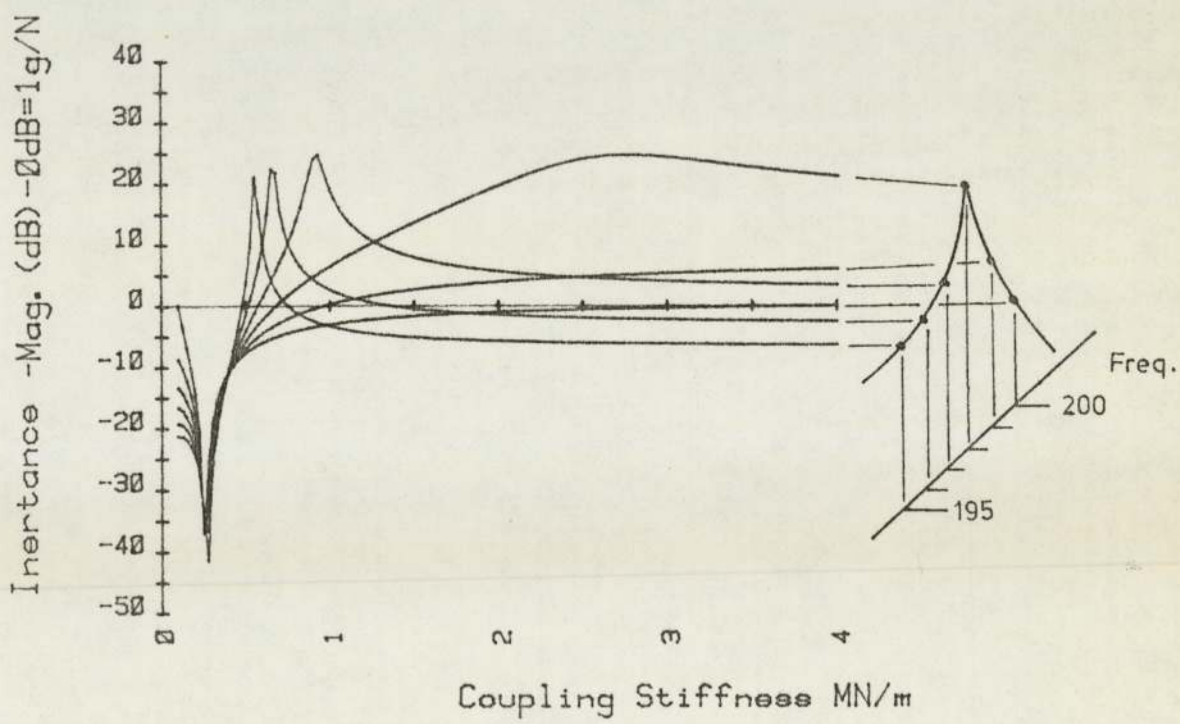

Fig. 2.18 EFFECT OF COUPLING STIFFNESS ON SYSTEM 3 INERTANCE I_{13}. FREQUENCY RANGE 195-200Hz.

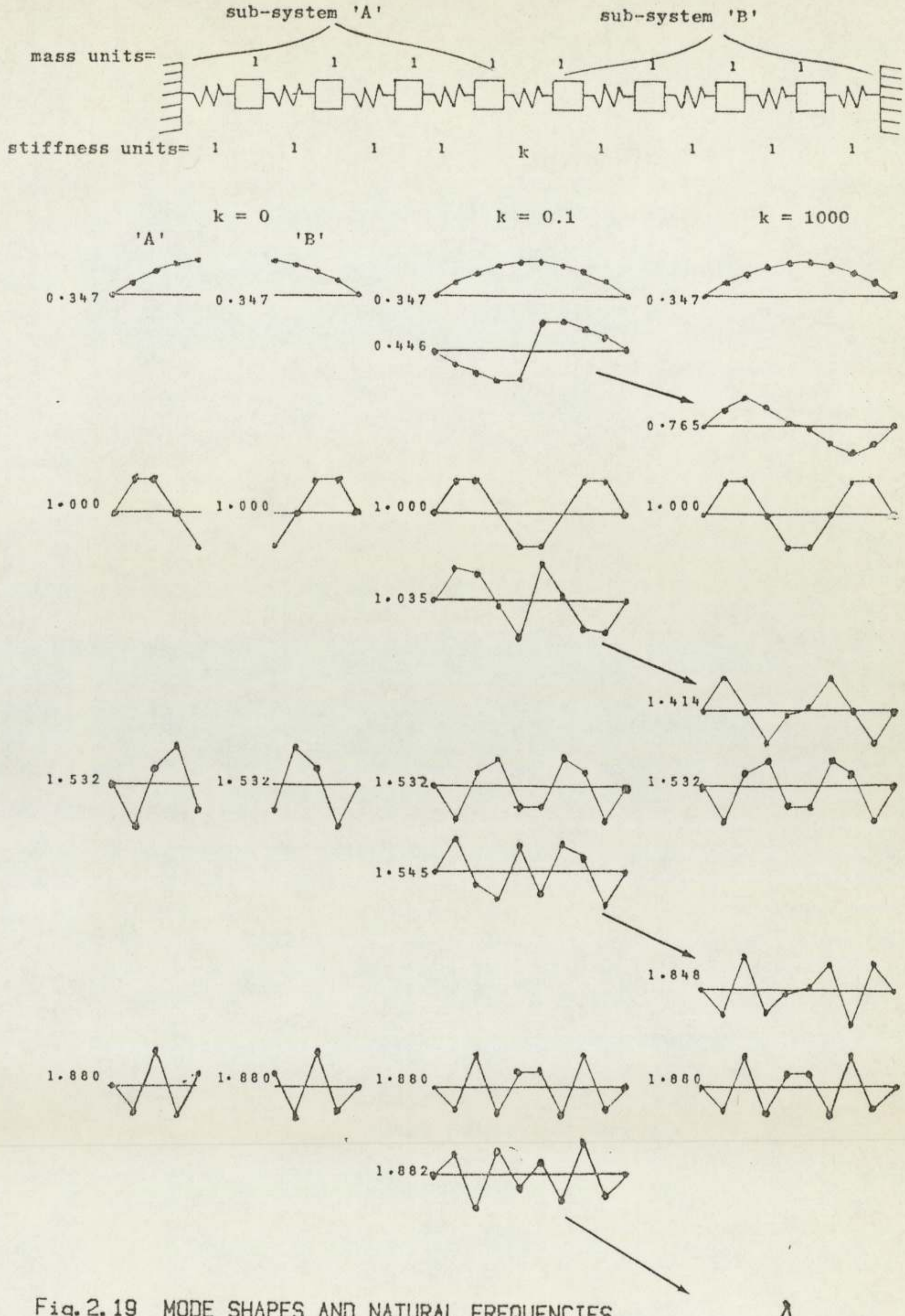

Fig. 2.19 MODE SHAPES AND NATURAL FREQUENCIES OF DISCRETE COUPLED SYSTEMS EXAMPLE 1

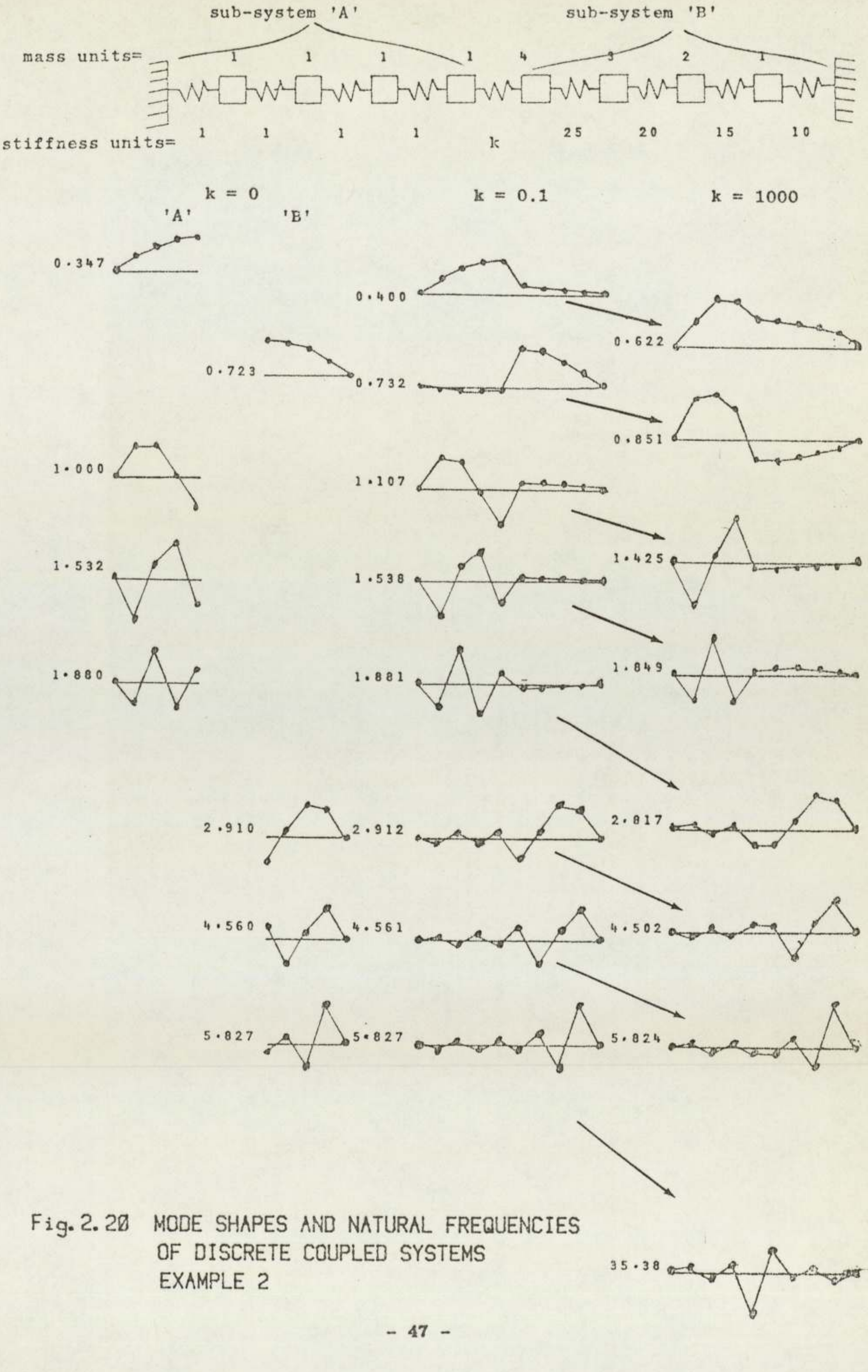

Fig. 2.20 MODE SHAPES AND NATURAL FREQUENCIES OF DISCRETE COUPLED SYSTEMS EXAMPLE 2

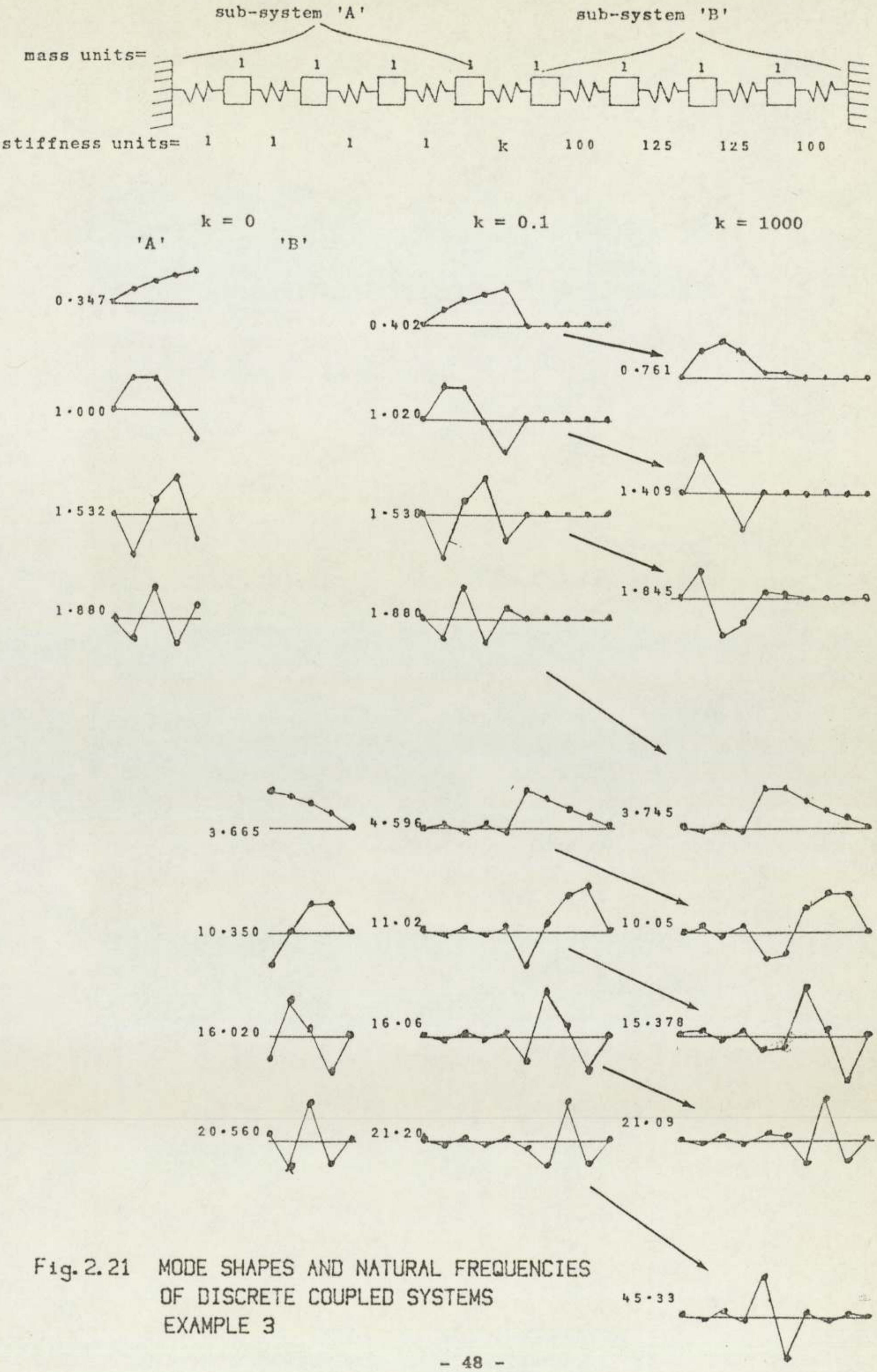

Fig. 2.21 MODE SHAPES AND NATURAL FREQUENCIES OF DISCRETE COUPLED SYSTEMS EXAMPLE 3

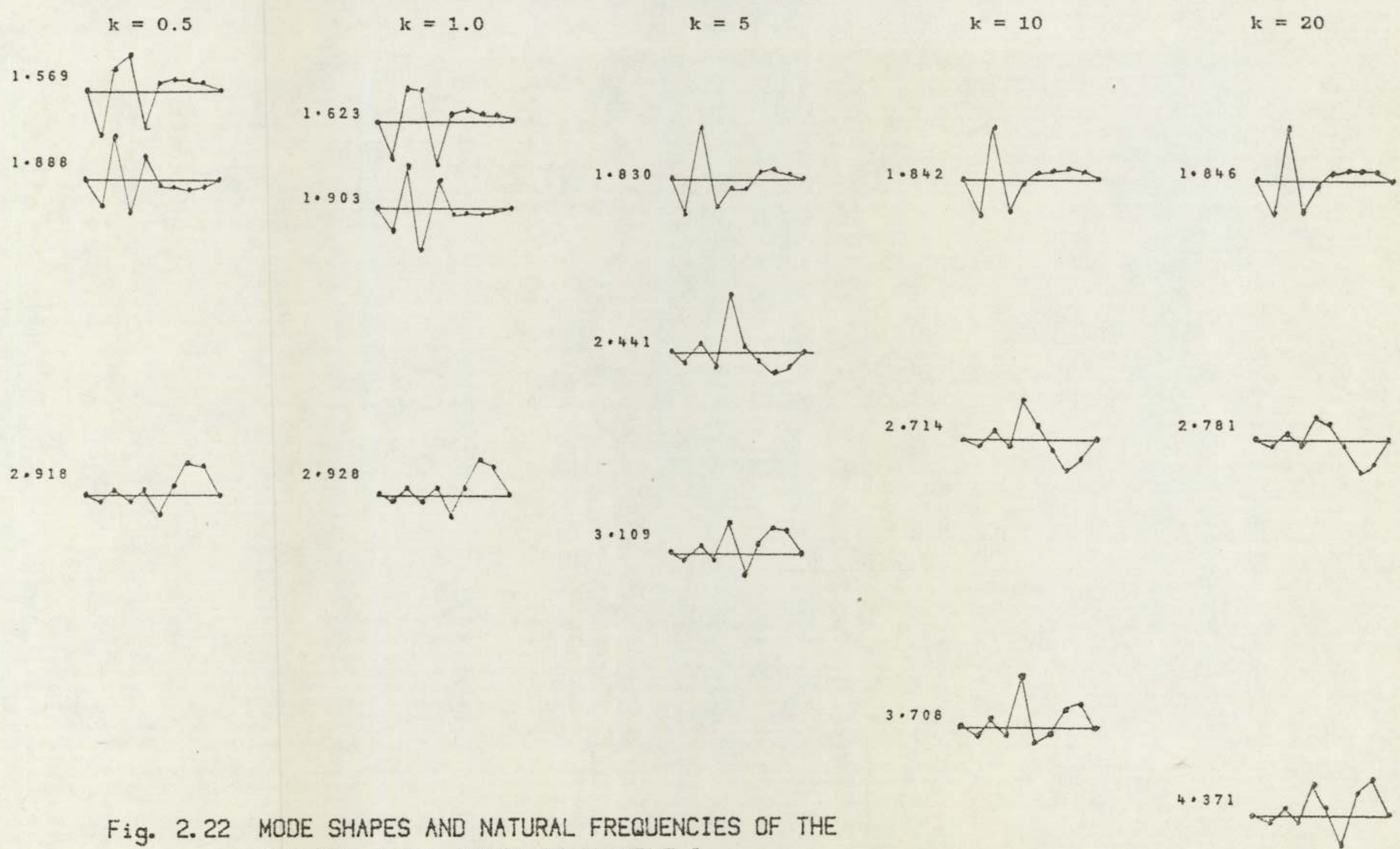

Fig. 2.22 MODE SHAPES AND NATURAL FREQUENCIES OF THE 4th, 5th & 6th MODES OF EXAMPLE 2

CHAPTER THREE

INSTRUMENTATION AND COMPUTING SOFTWARE

CHAPTER THREE

INSTRUMENTATION AND COMPUTING SOFTWARE

3.1 INTRODUCTION

During the investigation it was necessary to continually revise and update instrumentation techniques in order to attain the required level of accuracy. In particular the measuring instrumentation changed from an analogue to a digital system allowing greater frequency discrimination with a dynamic range in excess of 80 dB's. The digital system finally adopted utilised a digital Frequency Response Analyser controlled by a desk-top computer. The computer was also used to process both experimental and theoretical data in the 'Impedance Coupling Equation.' Extensive software had to be developed to perform these tasks.

3.2 TRANSDUCERS AND SIGNAL CONDITIONERS

Transducers

D J Birchall miniature piezo-electric seismic accelerometers were used. These transducers were approximately 3 grams total mass with a nominal charge sensitivity of 3 pC/g. Bees wax was usually used to attach these accelerometers to the test structure.

A Brüel and Kjaer piezo-electric force transducer type 8200 was used to measure the force input to the test structure. The force range of this transducer is 1 kN tensile to 5 kN compressive. Its total mass is 21 grams and it has a nominal charge sensitivity of 4 pC/N.

Signal Conditioners

Charge amplifiers, type CA1, manufactured by Environmental Equipment Ltd, were used to condition the output from the transducers. The gain of the amplifier can be adjusted by a multiturn potentiometer. These charge amplifiers give a 4.6 volt dc bias to the conditioned signal. Therefore, it was necessary to construct a dc balancing circuit which was inserted between the amplifier and the analyser in order to utilise the full dynamic range of the instrument.

Calibration

The transducers together with a B & K Standard accelerometer were mounted on a vibrator table and subjected to a known level of excitation at various frequencies. The gains of the charge amplifiers were adjusted such that their output sensitivities were set to 100 mV/g for the accelerometers and 100 mV/N for the force transducer. Details of the calibration procedure and the frequency response characteristics of the transducer/charge amplifiers are recorded in Appendix 2 of this report.

3.3 ANALOGUE DYNAMIC ANALYSER SYSTEM

At the beginning of the investigation sweep tests were performed using an analogue spectrum analyser system as shown in Fig 3.1. The system centred around two dynamic analysers: these were essentially bandpass filters tuned such that their centre frequencies were varied over the frequency range of interest. This is effected by a B & K sweep frequency oscillator which also drives the electro-dynamic vibrator via a power amplifier. The filtered force signal is fed back to a compressor circuit in the oscillator and forms a feed-back loop which controls the force input to the structure under test. Since the force input remains constant then the filtered acceleration signal is proportional to the frequency response. The dynamic analysers have a constant 100 k Hz phase coherent filtered output which may be compared to give the phase difference between the force input and accelerometer signals. Both analyser and phase meter have dc outputs which are proportional to acceleration and phase respectively and this output is used to drive the X-Y plotter.

It was apparent, after taking preliminary sweep tests, that this method of instrumentation had serious limitations. The compressor circuit which controlled the force input was only capable of giving a constant force within ± 3 dB limits using a realistic sweep rate; the worse conditions were encountered at the high rates of change of force input in the region of resonances due to the lightly damped structures under test. Another disadvantage was that the outputs from the analyser and phase meter are of analogue form which require digitising in order to manipulate the data in an 'Impedance Coupling Technique.' This was not possible with the equipment available at that time. Fortunately, a Solartron Frequency Response Analyser and a Hewlett Packard 9825A desk-top computer became available which provided all the advantages of a digital analyser system. Work was then discontinued on the analogue system.

3.4 FREQUENCY RESPONSE ANALYSER

The FRA analyses two input analogue signals by a correlation technique using its own signal generator output. It, therefore, operates in a closed loop measuring system where the signal generator output is used to excite the structure under test. The instrument is programmable such that a sweep test may be set up by inputting frequency limits and incremental frequency steps. A further facility of the FRA is a digital interface; this allows a computer to be used as a remote controller and data acquisition system. At each frequency the magnitude and phase measurement from both input channels is passed to the computer.

If force input and response is measured then the frequency response may be computed without the need to compress the force input as in the analogue analyser system. This insures a more accurate measurement providing the system under test is linear elastic since the force may vary considerably during the sweep. Fig 3.2 shows how the force, response and computed inertance vary with frequence during a test on a cantilever. The curves show the importance of computing the frequency response since the response characteristics on their own give an inaccurate representation of natural frequencies[24]. In fact the response does not alter at the first natural frequency. It is only by observing the force input that this natural frequency is detected.

The dynamic measuring range of this instrument is potentially very large, in excess of 80 dB's (attained during experimental work), due to its ability to automatically select its measurement range from 10 mV to 100 V in 20 dB steps.

3.5 CONTROLLER AND DATA ACQUISITION SYSTEM

A Hewlett Packard 9825A desk-top computer was used to control the FRA and to accept the digital results. The results were then passed to a mass store, which was a floppy disc capable of storing up to 0.4 mega-bytes. Hard copy output was attained by the use of an X-Y Plotter. These peripheral devices were connected to the computer via an interface bus system. Several bus systems are available for this computer but only two systems were necessary for this work. A 16 bit input/output bus was used for the mass storage since this bus has very high data transfer rates. For the FRA and

X-Y plotter a General Purpose Interface Bus (GPIB), IEEE 488 Standard was used. Fig 3.3 shows the instrumentation set-up for the frequency response experiments.

HP 9825A Desk-Top Computer

The 9825A has a work space of 22 k bytes of random access read/write memory. The program language HPL is interpreter type which is stored in Read Only Memory (ROM) and is similar to BASIC. The language allows matrix manipulations and was found to be adequate for all the necessary processing of theoretical and experimental data.

IEEE 488 Standard Interface Bus

This bus allows data to be transferred bi-directionally between computer and peripheral device via 8 data lines in an 8 bit parallel, byte serial mode. A further 8 lines are used for bus management and data validation purposes.

3.6 COMPUTING SOFTWARE

During this work various computer programs were written and developed to enable the computer to perform its task as controller to the FRA and to manipulate or generate 'Impedance' data via the procedures outlined in Chapter 2 of this thesis. Some of these programs are summarised below and a more detailed description may be found in Appendix 3.

SWFRA: To set up the FRA for a sinusoidal sweep test and read the measured data from the FRA internal store during its incremental sweep. The data is then passed to the floppy disk store.

PMOB: A general plotting program for experimental or theoretical frequency responses which plots magnitude and phase against frequency.

IMPC: Computes the theoretical coupling apparent mass matrix, based on a simple two mass, spring and damper system, for a specified frequency range. This data is then passed to the floppy disk.

CMOBB: 'Impedance Coupling' program for 2 beams and 2 connectors. Computes system inertance as in equation 2.7 (4th order matrix equation). Inputs experimental or theoretical frequency response data for the beam sub-system and combines them with the coupling data previously computed by 'IMPC'.

TCMOB: Computes theoretical inertances of cantilever beams, as equation 2.29, over a selected frequency range. Required inputs are: dimensions of beam; modal damping ratios and number of modes to be summed.

DET: Computes a particular system inertance with differing coupling stiffnesses at selected discrete frequencies. Plots results in graphical form.

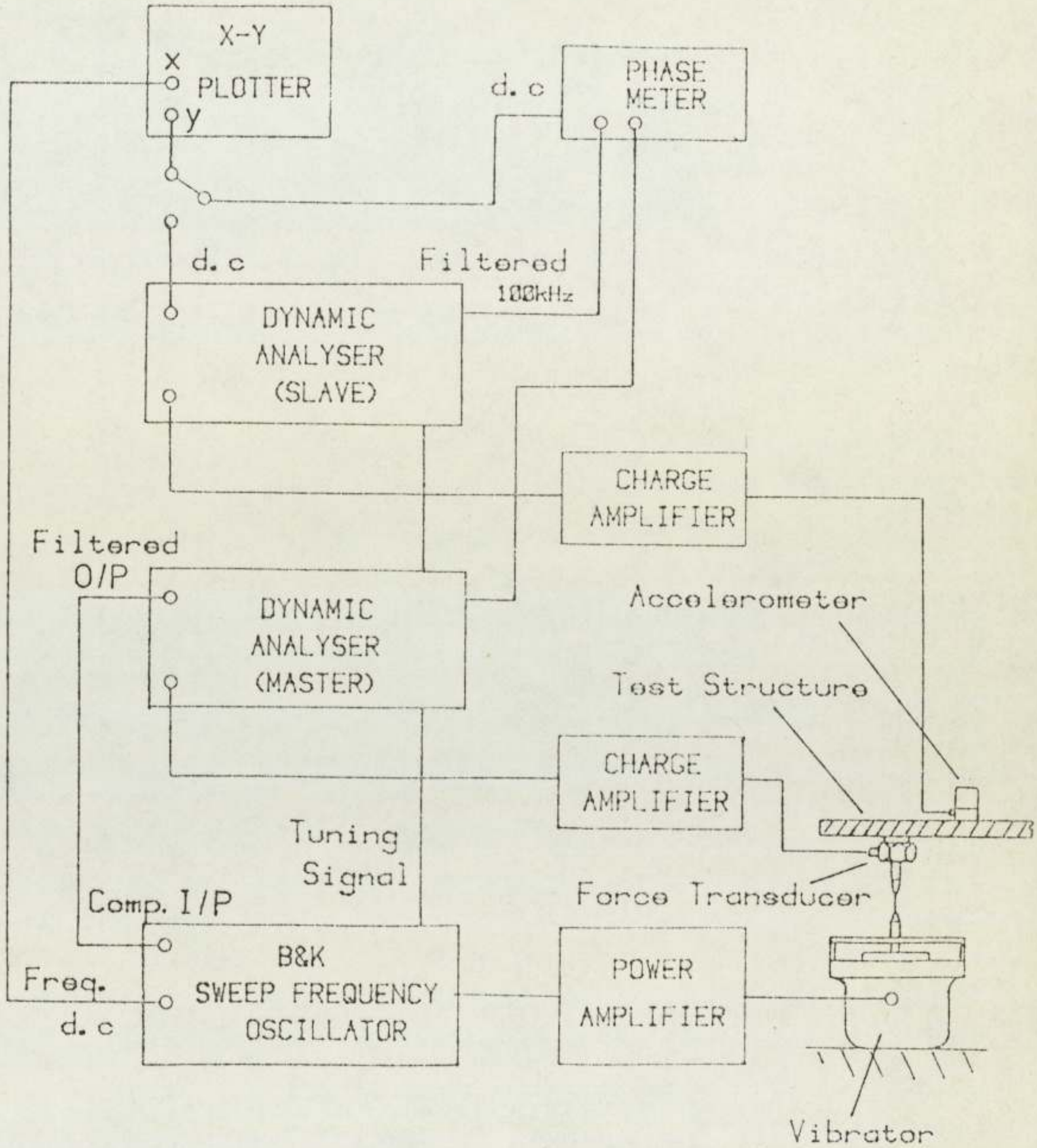

Fig. 3.1 ANALOGUE SPECTRUM ANALYSER SYSTEM

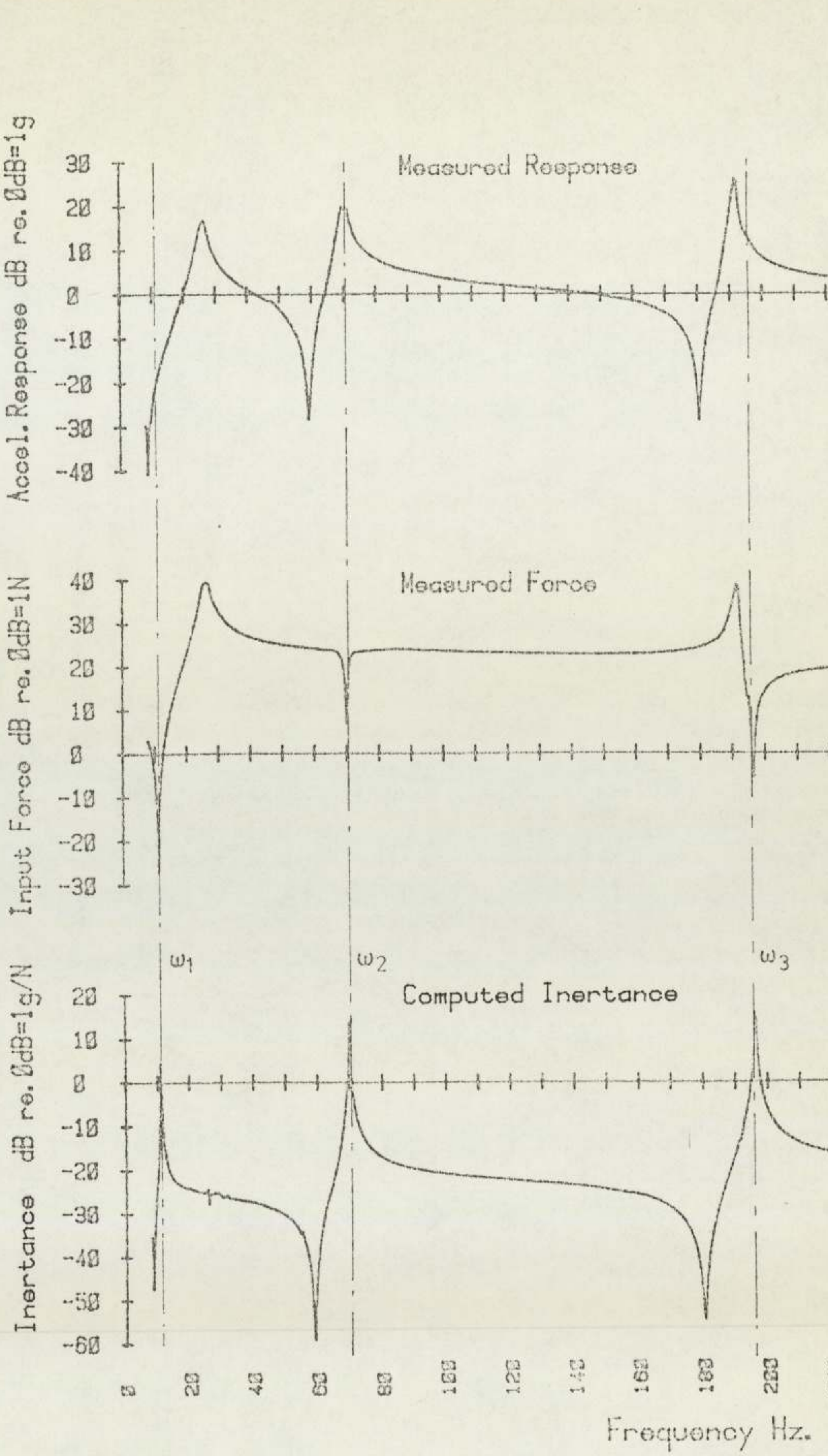

Fig. 3.2 SWEEP TESTS ON A CANTILEVER USING A FREQUENCY RESPONSE ANALYSER

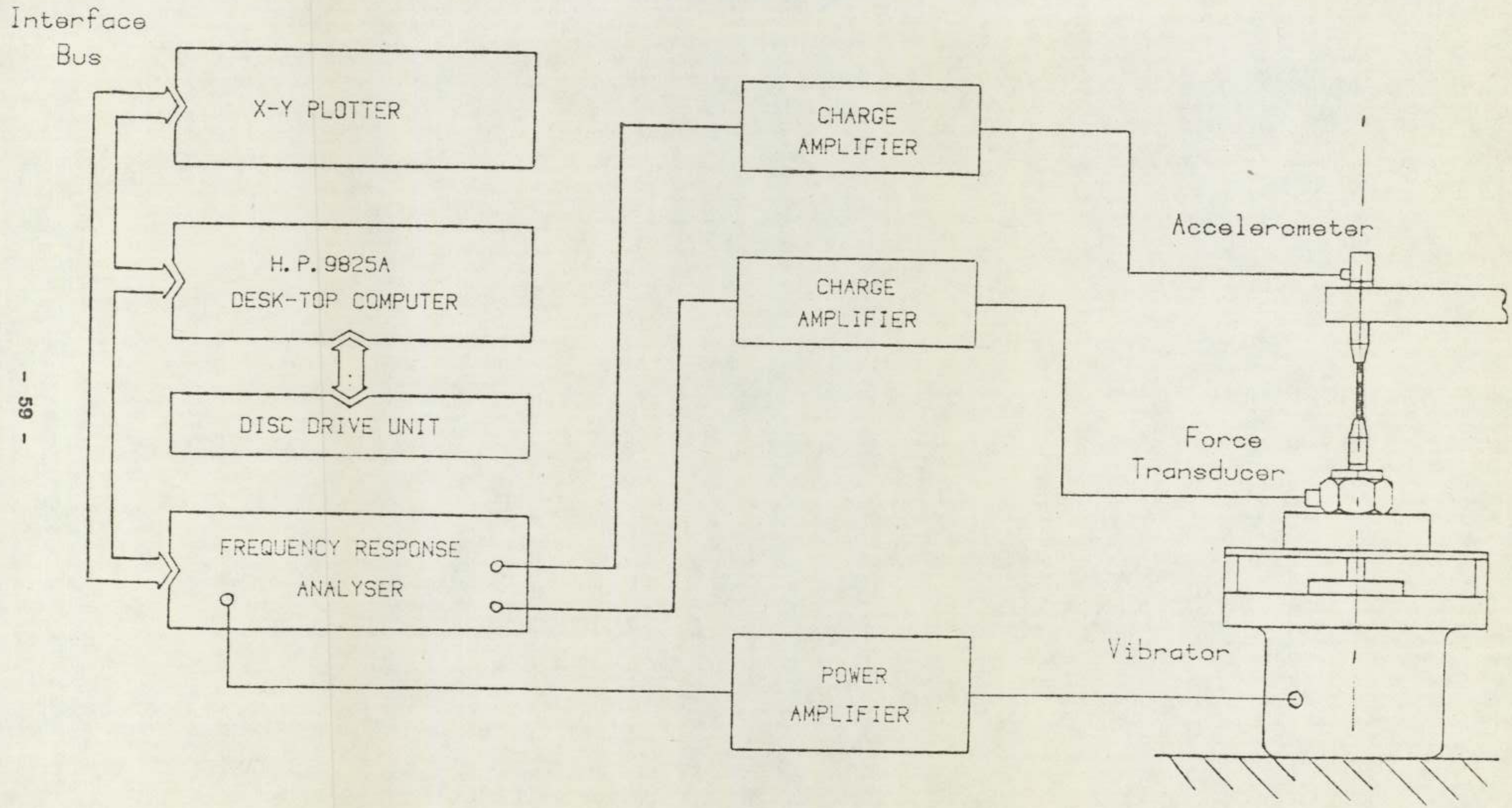

Fig. 3.3 INSTRUMENTATION FOR FREQUENCY RESPONSE TESTS

CHAPTER FOUR

DEVELOPMENT OF EXPERIMENTAL TECHNIQUE

CHAPTER FOUR

DEVELOPMENT OF EXPERIMENTAL TECHNIQUE

4.1 INTRODUCTION

The object of the experimental work was to verify the predictions made by the theoretical study in which a coupled system could be detuned at chosen frequencies by careful selection of connector dynamic characteristics.

This work involved the measurement of the sub-systems inertance matrices which were then processed together with connector information in the 'Impedance Coupling Equation' 2.7 as shown in Fig 2.5. Since the manipulation of the experimental results involved three matrix inversions it was essential that the measurements should be very accurate. This chapter outlines the development of the techniques required to measure these inertances covering the initial experiments on a 'free-free' plate and then progressing to work on the two cantilever system where the measurements proved to be of sufficient accuracy to be used in the 'Impedance Coupling Technique'. The computer controlled Frequency Response Analyser System, as described in section 3.5 and Fig 3.3, was used throughout this experimental work.

The predicted system response was then checked by connecting the two cantilevers together. Two different types of connectors were used, a 'rigid' piano wire connector and a 'flexible' rubber connector. Both connectors were subjected to 'blocked Impedance' tests in order to obtain their frequency response characteristics.

4.2 EXPERIMENTAL MEASUREMENTS

The 'Impedance Coupling Technique' requires the measurement of the apparent mass matrix of each sub-structure to be coupled. Direct 'Impedance' type measurements of a complex structure is often a difficult or even impossible task. In order to measure each element in the matrix the translational and rotational responses at all except one of the co-ordinates of the structure needs to be restrained to zero. Measurements are then taken of the response at the free co-ordinate and of the restraining forces and moments at all other co-ordinates. Each co-ordinate in turn is left free until all the elements in the matrix have been obtained. This procedure is termed as a 'blocked Impedance'* test.

The alternative to this test is to measure the inertance matrix which is then inverted to give the apparent mass matrix. The method of measuring the inertance matrix is the reverse of the 'blocked Impedance' test. A force is applied to each co-ordinate in turn while the responses at the other co-ordinates are measured. An example of this procedure can be demonstrated on the cantilever shown in Fig 2.4. If a force is applied to position 2 by means of a vibration generator - the inertance equation 2.22 becomes:-

$$\begin{bmatrix} I_{11} & I_{12} \\ I_{21} & I_{22} \end{bmatrix} \begin{bmatrix} 0 \\ F_2 \end{bmatrix} = \begin{bmatrix} \ddot{y}_1 \\ \ddot{y}_2 \end{bmatrix}$$

or

$$I_{12} = \frac{\ddot{y}_1}{F_2}$$

and $$I_{22} = \frac{\ddot{y}_2}{F_2}$$

* A 'blocked Impedance' test measures the dynamic stiffness or the mechanical impedance or the apparant mass depending on the type of motion measured.

The force is then applied to position 1 to obtain the remaining inertance elements. Hence it is evident that this procedure is analogous to that adopted in the theoretical study in section 2.4.

Care must be taken to ensure that a pure force is transmitted to the structure, ie no restraining or associated moments. This is usually successfully accomplished by inserting a de-coupler assembly between the structure and the vibrator[14]. The de-coupler assembly is designed such that the transmission of an axial force is very efficient but the assembly offers negligible angular restraint. Since this design requirement is the same as that of the piano wire connector used to couple the cantilevers, these connectors were also utilised as de-coupler assemblies.

4.3 INERTANCE MEASUREMENTS OF A FREE-FREE PLATE

The free-free plate consisted of a steel plate 620 mm by 437 mm and 1.22 mm thick suspended at the four corners by thin elastic. The plate was designed to have four connecting points; at each of these points there was an 18 gram concentrated mass which provided the means of connection. Four accelerometers were fixed to the top of the masses whilst the excitation input was attained by connecting a vibrator to the underside of the plate directly beneath the masses. The force transducer was located at the junction point in contact with the plate and was uncoupled from the vibrator by a de-coupler assembly which was manufactured from 1 mm diameter piano wire.

Sinusoidal sweep tests were performed on the plate in order to measure its inertance matrix for the four connecting points (vertical translational inertances only). This, by necessity, required 16 tests since the Frequency Response Analyser could measure only one inertance at a time. In these tests it was only possible to sweep a maximum of 100 discrete frequencies due to software limitation at that time.

Figure 4.1 shows a typical frequency response curve. The frequency range is 750 - 850 Hz, swept in 1 Hz steps, which is in the vicinity of the 50th plate mode. The two curves are reciprocal transfer inertances I_{14} and I_{41}, I_{14} being the acceleration response at position 1 divided by the input force at position 4 and I_{41} being the response at position 4 divided by the input force at position 1. From theoretical considerations these transfer inertances should be identical for a linear elastic system, see equation 2.29, section 2.4. The curves exhibit serious discrepancies from this theory, in particular the resonant frequencies appear to have shifted by as much as 3 Hz when moving the input position. At this stage it was not known whether these discrepancies were due to experimental error or inherent in the structure due to non-linearity. It was therefore decided to proceed with the experimental investigation on a simpler structure with fewer connection points; a cantilever beam with 2 connection points was chosen.

4.4 INERTANCE MEASUREMENTS OF A CANTILEVER BEAM

Measurement tests were carried out on a cantilever beam which consisted of a rectangular section steel bar clamped at one end to a massive machine bed plate as shown in Fig 4.2. The cantilever was designed to have two connecting points - one near the free end and the other near its mid-point. In the initial tests the configuration of the de-coupler assembly and the force transducer was the same as in the plate tests.

The force transducer measures the force transmitted to its diaphragm which is connected to the test structure. This adds mass to the structure which may be cancelled electronically or mathematically[24]. However, for the purpose of this demonstration, it was easier to redefine the cantilever sub-system to include this extra mass and also the accelerometer masses. Since the measurement of the inertance matrix requires the movement of the force input from one position to the other, then the diaphragm mass (3 grams) must be 'balanced' out by adding an equivalent mass to the system at the non-excited position.

Inertances were measured at two frequency ranges centred at the 3rd and 7th mode of the cantilever. Again, as with the plate tests, serious discrepancies were evident between the reciprocal transfer inertances. In particular the 7th mode resonant frequency differed by 20 Hz when changing the force input from position 1 to 2 and also the antiresonant frequencies were not compatible.

A series of tests were devised to establish the effects of varying the test procedure and changing the test configuration on the inertance measurements.

The first three tests, comprising repeatability of test, changing the sweep direction and altering the sweep rate were performed to assess the reliability of the measured results. These tests are summarised below:

Repeatability

Repeating the same test after a week and dismantling the vibrator connections had no significant effect on the inertance measurement.

Sweep Direction

An increasing frequency sweep was always programmed for these tests. Changing the sweep direction to decreasing frequency had little effect on the measurements.

Sweep Rate

The sweep rate of the Frequency Response Analyser can be altered by judiciously selecting the following parameters:-

(i) frequency step value,

(ii) integration time,

(iii) measurement delay.

A low sweep rate with a step value of 0.1 Hz, a delay of 0.1 second and selecting x 100 integration time greatly improved the smoothness of the curves but there was no fundamental difference to the previous sweep test results which utilised 0.5 Hz steps, 0.1 second delay and minimum integration time.

Having established the reliability of the measurements the next three tests were performed to indicate how sensitive the results are to changes in test configuration. In particular the transfer inertances and resonant frequencies were compared for each of these tests in order to find out any possible causes for the previous discrepancies. These tests are summarised as follows:-

Adding a Concentrated Mass to the System

A mass of 18 grams was added to one of the connecting points on the cantilever. This mass was comparable to the force transducer and six times that of the accelerometer. It had the effect of increasing the 7th mode resonant frequency by 10 Hz but the transfer inertances showed similar discrepancies to the initial cantilever tests.

Altering Mass and Stiffness of Vibrator Moving Parts

The stiffness of the vibrator moving parts was decreased by removing the protective diaphragm. Altering the vibrator stiffness and adding mass to the moving parts did not effect the inertance measurements.

Two Vibrators Simultaneously Coupled to the Cantilever

Two vibrators were used, one connected to each of the connecting points. The object was to excite each point in turn without disturbing the system mechanically. Sweep tests showed that resonant frequencies exhibited the same discrepancies depending on which vibrator was energised.

These experiments were invaluable in helping to obtain a 'feel' for the measurement process and its sensitivity to changes of the cantilever structure. It was concluded that this shift in resonant frequency was not due to non-linearities in the structure but to an error in the measuring process. Usual instrumentation checks were carried out including a complete change of transducers and a re-calibration. The methods of attaching the transducers to the structure were then inspected and it was at this stage that the cause of the error became known. It was noticed that the piano wire, used in the de-coupler assembly, was cemented into its adapters with Araldite, thus giving a 'soft' joint. The method of connecting the vibrator to the cantilever was redesigned such that the force transducer was fixed directly to the vibrator, the de-coupler assembly being situated betwen the transducer and the cantilever. The piano wire of the de-coupler assembly was soldered into its adaptors thus giving a more 'rigid' joint.

Repeating the inertance measurements indicated that the previously found discrepancies between the transfer inertances had been significantly reduced such that the resonant and antiresonant frequencies coincided to within approx. 0.5 H_z throughout the frequency range of 30-500 H_z. Therefore, it was concluded that the experimental technique was sufficient to provide frequency response measurements to an acceptable accuracy such that they could be used in the 'Impedance Coupling Equation'.

4.5 INERTANCE MEASUREMENTS OF THE CANTILEVER SYSTEM FOR USE IN THE 'IMPEDANCE COUPLING TECHNIQUE'

The experimental set-up which proved to give the most accurate frequency response is shown in Figure 4.3. The cantilever sub-system consisted of the cantilever together with the two accelerometers, de-coupler assembly and a 'balance' mass. The 'balance' mass was equivalent to the mass of the de-coupler assembly plus the force transducer diaphragm mass.

The de-coupler assembly was therefore considered to act as a rigid body over the frequency range of the tests. This assumption was based on the frequency response results of the piano-wire connector shown in Fig 4.12 and discussed in section 4.7, since the de-coupler assembly was the same as the piano-wire connector used to couple the cantilever systems. The apparent mass measurements of the piano-wire connector shown in Fig 4.12 indicate a very high stiffness of 5.4 MN/M, with a first, natural frequency at 2200 H_Z.

The accuracy of the frequency response measurements was first checked by comparing the reciprocal transfer inertances. In Fig 4.4 the two transfers inertances for cantilever b, I_{34} and I_{43} were compared to verify that all the resonances and anti-resonances were coincident. Experience has shown that the mass balance was required to be within 1 gram of the optimum for the frequency range of interest. This mass is relative to a cantilever mass of 2.5 kg and a de-coupler mass of 15 grams.

The 2nd order inertance matrix was measured for two cantilevers a and b in tables 2.1 and 2.2. These matrices were then manipulated, together with various mathematical models of connectors, by the use of the 'Impedance Coupling Equation', equation 2.7, in order to obtain the predicted system inertances.

The cantilevers were then coupled with the two different types of connector in order to measure the system inertances and compare them with the predicted results. The experimental set-up for these tests is shown in Figures 4.5 and 4.6. These connectors were designed using piano-wire or rubber to give either a 'rigid' or 'flexible' coupling.

4.6 LINEARITY CHECKS ON CANTILEVER SYSTEMS

The most important assumption in applying the 'Impedance Coupling Technique' is that the structures to be coupled must behave as linear elastic systems within their environmental operating range, ie the maximum forces encountered in service must lie within the system's elastic range and this range must be linear.

Since the cantilever systems were used as laboratory models, then the maximum exciting force that these systems were likely to be subjected to was restricted by the maximum possible output of the vibration generator used throughout the tests. Furthermore, when the initial tests were performed, an optimum input to the power amplifier was set to avoid overdriving the systems under test. Therefore, the maximum exciting force possible under these conditions was obtained when the power amplifier gain was set to its highest value.

The linearity of the structures under test was checked by repeating inertance measurements with different gain settings on the power amplifier.

Figure 4.7 is a typical result from cantilever b. These tests indicated that the assumption of linearity was valid within the operating range of the equipment used.

4.7 CONNECTOR DESIGN AND TESTING

Two types of connector were manufactured to enable the two cantilever sub-systems to be coupled. One type, considered to be 'rigid' was made of piano-wire; the other connector, made of rubber, represented the flexible end of the stiffness range of interest. The connector assembly included a force transducer which was initially added to allow the measurement of forces in the connector. Although unnecessary in the investigation the transducers remained in situ to save modifying the rig. The connectors were designed to give a minimum of angular restraint at the coupling points, thus giving the connectors long and slender proportions which allowed high transverse flexibility.

'Blocked Impedance' Tests on Connectors

The connectors were subjected to dynamic tests in order to obtain apparent mass data for use in the 'Impedance Coupling Equation.'

Due to their high transverse flexibility the 'blocked Impedance' test, as described in section 4.2, was more suitable than the inertance test used in the plate and cantilever tests. This 'blocked Impedance' test was greatly simplified due to the assumption that the connectors transmitted only axial forces since the effective apparent mass matrix is reduced to a 2nd order matrix as shown in Figure 4.8.

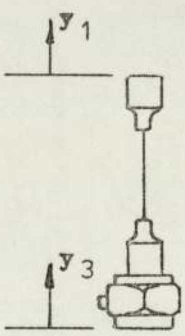

$$\begin{bmatrix} A_{11} & A_{13} \\ A_{31} & A_{33} \end{bmatrix} \begin{bmatrix} \ddot{y}_1 \\ \ddot{y}_3 \end{bmatrix} = \begin{bmatrix} F_1 \\ F_3 \end{bmatrix}$$

FIG 4.8 EFFECTIVE APPARENT MASS MATRIX EQUATION FOR CONNECTORS

A sequence of tests, as shown in Figure 4.9, was necessary to obtain the complete apparent mass matrix. Each coordinate was 'blocked' in turn by fixing one end of the connector to a large mass via force transducer, whilst the other end was connected to the vibrator. A force transducer and an accelerometer were inserted to measure the force input and response at the 'free'end.

Figures 4.10 and 4.11 show some initial apparent mass measurements on the piano-wire and rubber connectors respectively. It can be seen that the curves are not very smooth or well defined, especially at the low frequencies, which may be attributed to the fundamental difficulties associated with 'Impedance' testing of this type of structure.

Attempts were made to use this low quality experimental data directly in the 'Impedance Coupling Equation' but the results proved to be unsatisfactory. The errors compounded to such an extent that the shape of the predicted system inertance was completed masked by numerical 'noise'.

To overcome this problem it was necessary to re-generate these curves from a suitable mathematical model. In order to obtain sufficient data to construct and test such a model the apparent mass measurements were repeated and extended to a higher frequency. The results obtained from each connector are discussed separately as follows:

(i) <u>Piano Wire Connector</u>

The apparent mass measurements on the piano wire connector are shown on a logarithmic frequency base in fig 4.12. The results clearly show a connector resonant frequency at 2200 H_z and an anti-resonant frequency at 12000 H_z. This anti-resonant frequency was thought to be associated with the rig characteristics and to investigate this more closely a separate test was conducted on the rig with the connector removed. Apparent mass measurements of the rig, at the force transducer, indicated that the rig stiffness was about 150 MN/ m. A stiffness line representing the rig stiffness is shown on the same graph as the apparent mass measurements of the connector and it can be seen that the connector measurements taken at frequencies in excess of about 5000 H_Z are completely dominated by the dynamic characteristics of the rig and as such will be invalid. When this is taken into account the results show the typical characteristics of a grounded one degree of freedom system which is mathematically described by the apparent mass element A_{33} in equation 2.32 of section 2.5. The mass, stiffness and damping for the mathematical model was obtained by estimating the stiffness from the low frequency results. Then accurately measuring the resonant frequency and calculating the mass from the relationship.

$$m = \frac{k}{\omega_1^2}$$

The calculated mass was compared with the mass found by direct measurement and was accurate to within one gram which was equal to five percent of the total mass. The damping, which was assumed to be viscous was estimated from the apparent mass measured at the resonant frequency. In order to obtain an accurate measurement a separate sweep test was performed with small frequency increments in the vicinity of the resonant frequency. It was assumed, since the damping ratio was very small that the resonant frequency was coincident with the natural frequency. Therefore the damping ratio may be calculated for a one degree of freedom system by the following relationship.

$$\zeta = \frac{A}{2m} \Bigg|_{\text{when } \Omega = \omega_1}$$

Where A is the apparent mass measured at the natural frequency ω_1.

The frequency response of the mathematical model of equation 2.32 using these measured dynamic properties is also shown in Fig 4.12. The frequency response of the model is in close agreement with the experimental results up to approximately 4000 H_z. Above this frequency the experimental results deviate from the model but is due to the limitations of the rig as previously discussed. In conclusion the two degrees of freedom model of equation 2.32 using the mass stiffness and damping coefficients computed from the experimental results was shown to be of sufficient accuracy such that it may be used in the 'Impedance Coupling Technique'. The measured parameters used in this model are shown in Fig 4.16.

(ii) Rubber Connector

The apparent mass measurements on the rubber connector are shown in Fig 4.13. Measurements at frequencies above 5000 H_z are not shown because, as in the piano wire connector experiments, the rig dynamic properties have a dominant effect on the results above this frequency.

The results indicate a fundamental resonant frequency at approximately 240 H_z and a second resonant frequency in the region of 1600 H_z. This second resonant frequency is only just detectable. There is evidence of very high damping and the low and high frequency response is characteristic of a spring and mass respectively.

In contrast to the piano wire connector, obtaining a model for the rubber connector presented a more difficult problem principally due to the following reasons.

(a) The stiffness of the rubber increased as the frequency increased and as such could not be accurately modelled by a linear stiffness coefficient.

(b) The damping properties of the rubber could not be accurately modelled by a viscous damping coefficient since the damping was not proportional to velocity.

(c) The specification of the rubber was unknown and as such it was not possible to obtain accurate values of Young's modulus of elasticity and the loss factor.

Initially the apparent mass measurements were compared with the frequency response obtained by equation 2.39 using realistic values of Young's modulus of elasticity (E) and loss factor (δ) together with the measured values of cross-sectional area, density, length and end mass. The theoretical frequency response showed characteristics which closely corresponded to the measured results. However, the apparent mass levels were in error up to approximately 500 H_Z and the first resonant frequencies were not coincident. These discrepancies indicated an error in the stiffness properties of the theoretical model which implied an error in the value used for Young's modulus since the stiffness of the rubber is proportioned to E. An improved value of E was estimated from the low frequency apparent mass measurements since the stiffness is the pre-dominate dynamic property at these frequencies. To illustrate this point the apparent mass equation of the connector, eq 2.37, shown below, must be considered:

$$\frac{F_3}{\ddot{y}_3} = \frac{-m_R \cos \beta \ell}{\beta \ell \sin \beta \ell} + m_3$$

where

$$\beta = \sqrt{\frac{\Omega^2 \rho}{E}}$$

If Ω is very low ($\Omega \ll 1$ rad/s) then by using the expansions of the sine and cosine functions and discarding the cubic and higher frequency terms, such that

$$\frac{F_3}{\ddot{y}_3} = \frac{-m_R \left(1 - \dfrac{\beta^2 \ell^2}{2}\right)}{\beta \ell \, (\beta \ell)} + m_3$$

and observing that $m_R = \rho A \ell$ then

$$\frac{F_3}{\ddot{y}_3} = \frac{-EA}{\Omega^2 \ell} + \frac{\rho A \ell}{2} + m_3$$

Since the static stiffness of the rubber rod, k is

$$k = \frac{EA}{\ell}$$

and the second term is the effective mass of the rod at low frequency, the low frequency response is characteristic of the one degree of freedom system used in the piano wire model. Furthermore, since at low frequency the stiffness term is very large compared to the mass terms the latter terms may be neglected. In practice, as the measurements of the rubber and piano wire connector show, the stiffness may be accurately determined from the frequency response at frequencies up to approximately one octave below the first natural frequency.

A more accurate value of E was therefore computed from the low frequency response together with a value of the loss factor, δ which was calculated from the ratio of the real and imaginary parts of the apparent mass using equation 2.38. These new values gave a much improved frequency response function, however, the theoretical natural frequencies were lower than that measured. Closer inspection of the real and imaginary parts of the measured apparent mass indicated that the stiffness, hence E, and the loss factor were not constant over the frequency range 0-5000H_z but both increased with frequency.

This second attempt to obtain a mathematical model of the connector was not considered to be accurate enough to be used in the 'Impedance Coupling Equation'. Therefore the investigation proceeded by obtaining experimentally derived values of E* (i.e. E and δ) against frequency such that they could be used in the mathematical model. The experiment to obtain accurate values of E* involved repeating the 'blocked Impedance' test on the rubber connector but with the end mass (i.e. the dummy force transducer) removed. This was necessary in order to increase the stiffness dominated frequency range thereby giving accurate results to a higher frequency. The measured apparent mass at selected frequencies was used in the iteration formula of eq 2.42 to obtain values of E and δ and these values are plotted in figs 4.14 and 4.15 respectively. The results indicate a significant increase in both values as the frequency is increased. The scatter of the results at the high frequency is because the high frequency response is mass dominated and as such it is difficult to obtain accurate stiffness properties at these frequencies. Curves were fitted to the results to assist in the generation of the mathematical model using polynomials of 1 and 2 degrees for δ and E respectively. The theoretical apparent mass using the frequency dependent values of E and δ is shown on the same graph as the experimental results in fig 4.13. It can be seen that the correlation is very good up to about 3000 H_Z. The experimental results start to diverge from the theoretical results above this frequency and this is due to the effects of the rig as discussed in the piano wire connector experiment in the previous section.

An accurate mathematical model of the rubber connector was found. However, the method used was both complex and time-consuming.

An alternative to this modelling technique is to use a simple mathematical model similar to the one used for the piano wire connector. The dynamic properties may be optimised depending upon the frequency range in which the connector is to be modelled. Since the connector in this investigation is used up to 500 H_z then the stiffness property is dominant over most of this range. The damping is dominant in the vicinity of the natural frequency and the mass is dominant at the higher frequencies. A model may be found by optimising on the mass such that the natural frequency is accurately modelled and by using an equivalent viscous damping coefficient. The apparent mass of such a model is shown on the same graph as the experimental results and the theoretical model discussed in the preceding paragraphs, fig 4.13. It can be seen that the mass used in this model is lower than measured but this parameter was purposely reduced so that the natural frequency of the model coincided with the measured natural frequency. This was necessary because of the increase in the stiffness properties of the rubber at this frequency. The equivalent viscous damping was obtained by accurately measuring the imaginary component of the apparent mass at the natural frequency and by using the relationship

$$\mathrm{Imag}\,(A_{35}) = \frac{-c}{\omega_1}$$

where c is the viscous damping coefficient. The phase characteristics of the apparent mass show that the damping is inaccurate at the lower frequencies but is adequate at the natural frequency. However, this optimised model proved to be of sufficient accuracy when used in the 'Impedance Coupling Technique' and as such was used throughout the investigation.

The optimised dynamic properties used in the 2 degrees of freedom model of the rubber connector are shown in fig 4.16.

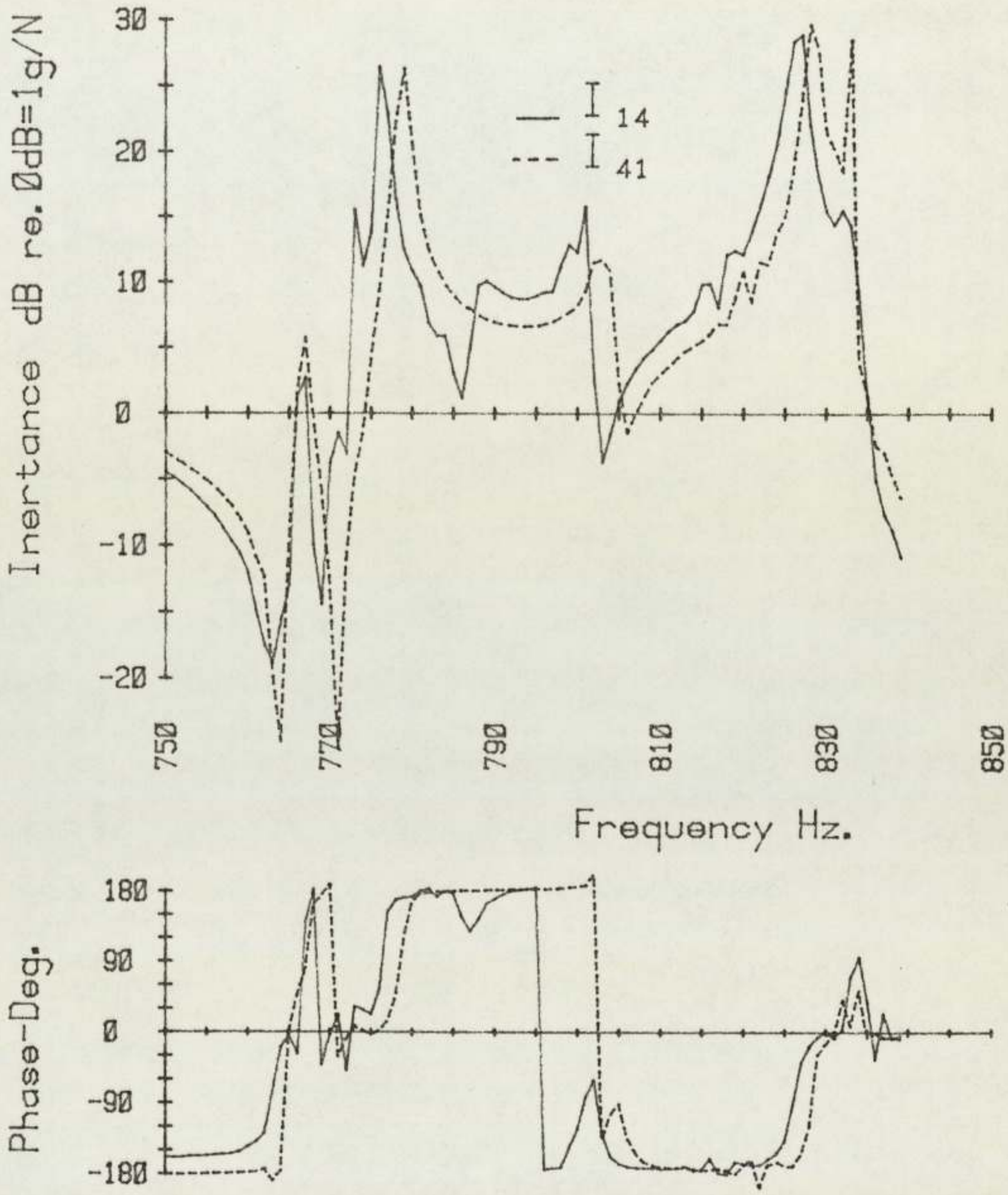

Fig. 4.1 RECIPROCAL TRANSFER INERTANCES OF 'FREE-FREE' PLATE

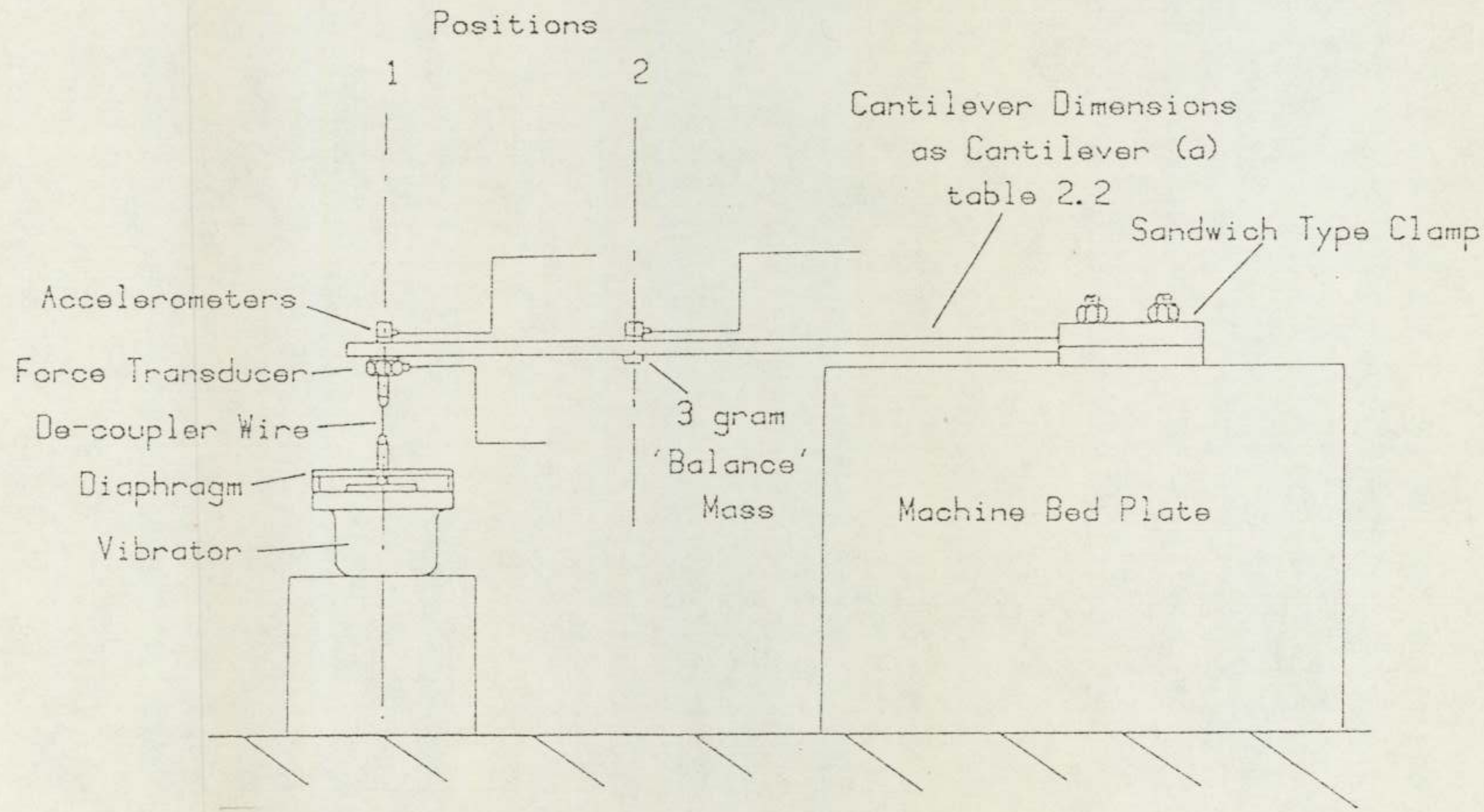

Fig. 4.2 SET-UP FOR INITIAL CANTILEVER FREQUENCY RESPONSE TESTS

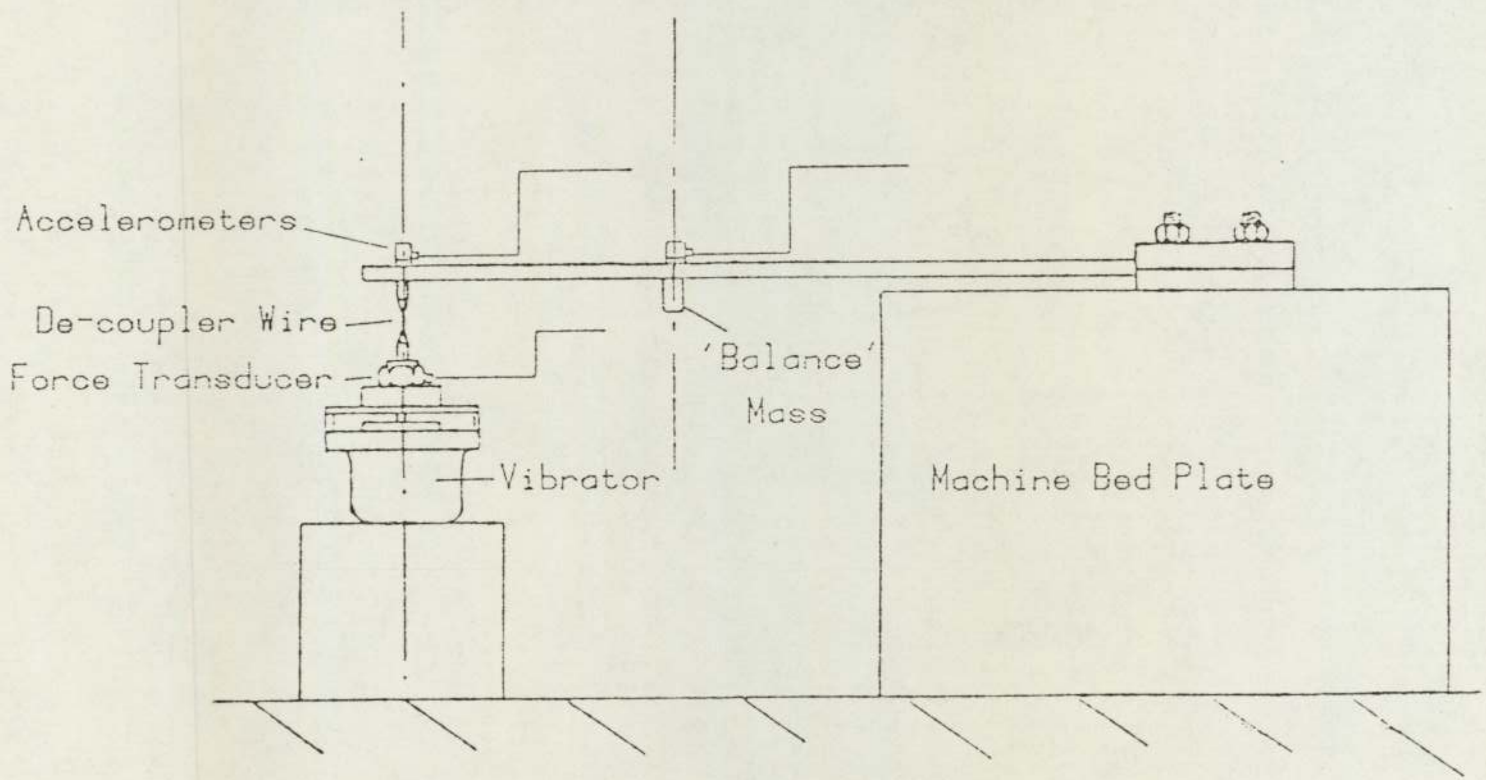

Fig. 4.3 SET-UP FOR BOTTOM CANTILEVER FREQUENCY RESPONSE TESTS

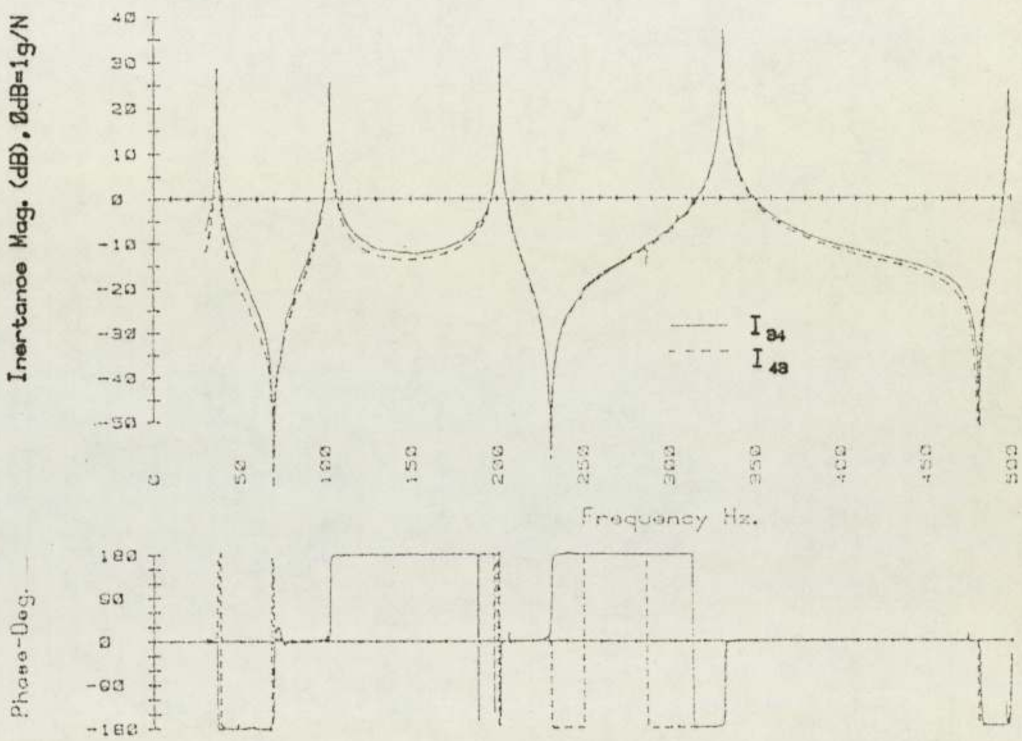

Fig. 4.4 TRANSFER INERTANCES FOR BOTTOM CANTILEVER

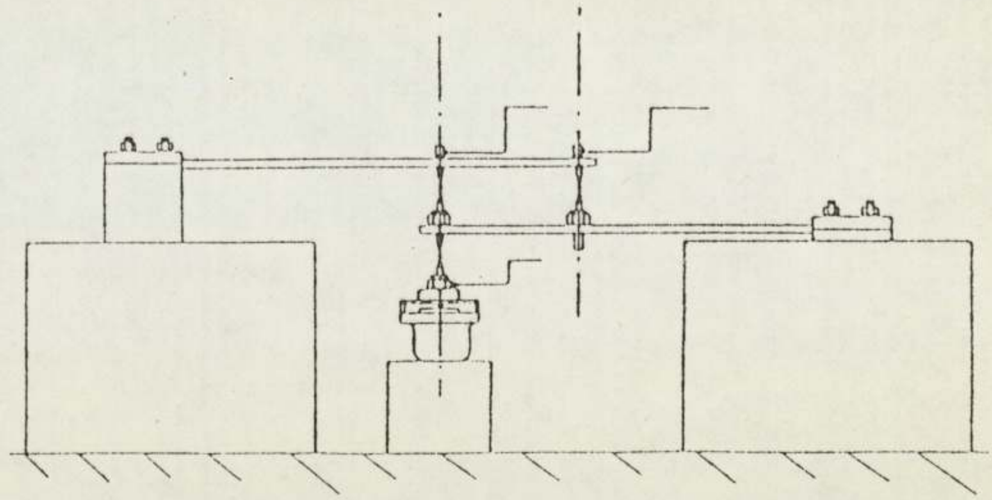

Fig. 4.5 SET-UP FOR SYSTEM FREQUENCY RESPONSE TESTS WITH PIANO WIRE CONNECTORS

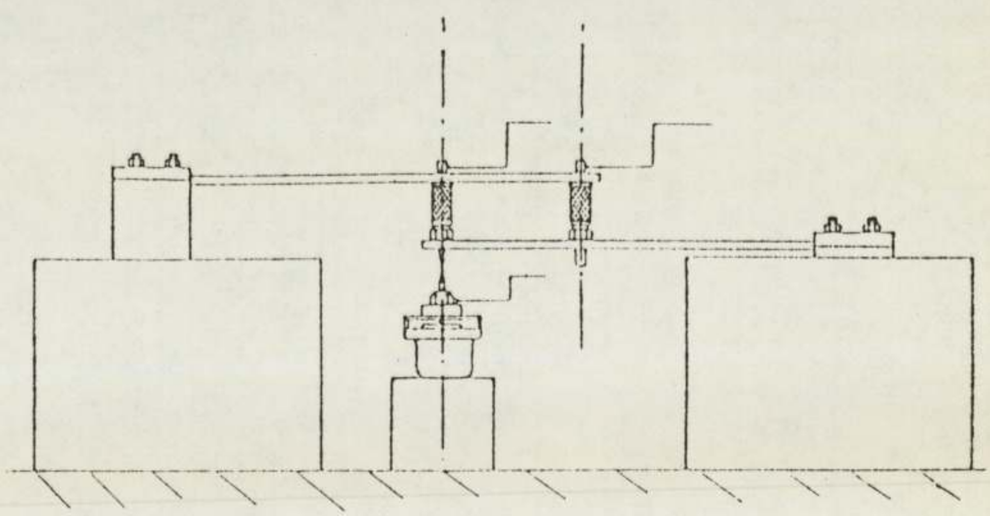

Fig. 4.6 SET-UP FOR SYSTEM FREQUENCY RESPONSE TESTS WITH RUBBER CONNECTORS

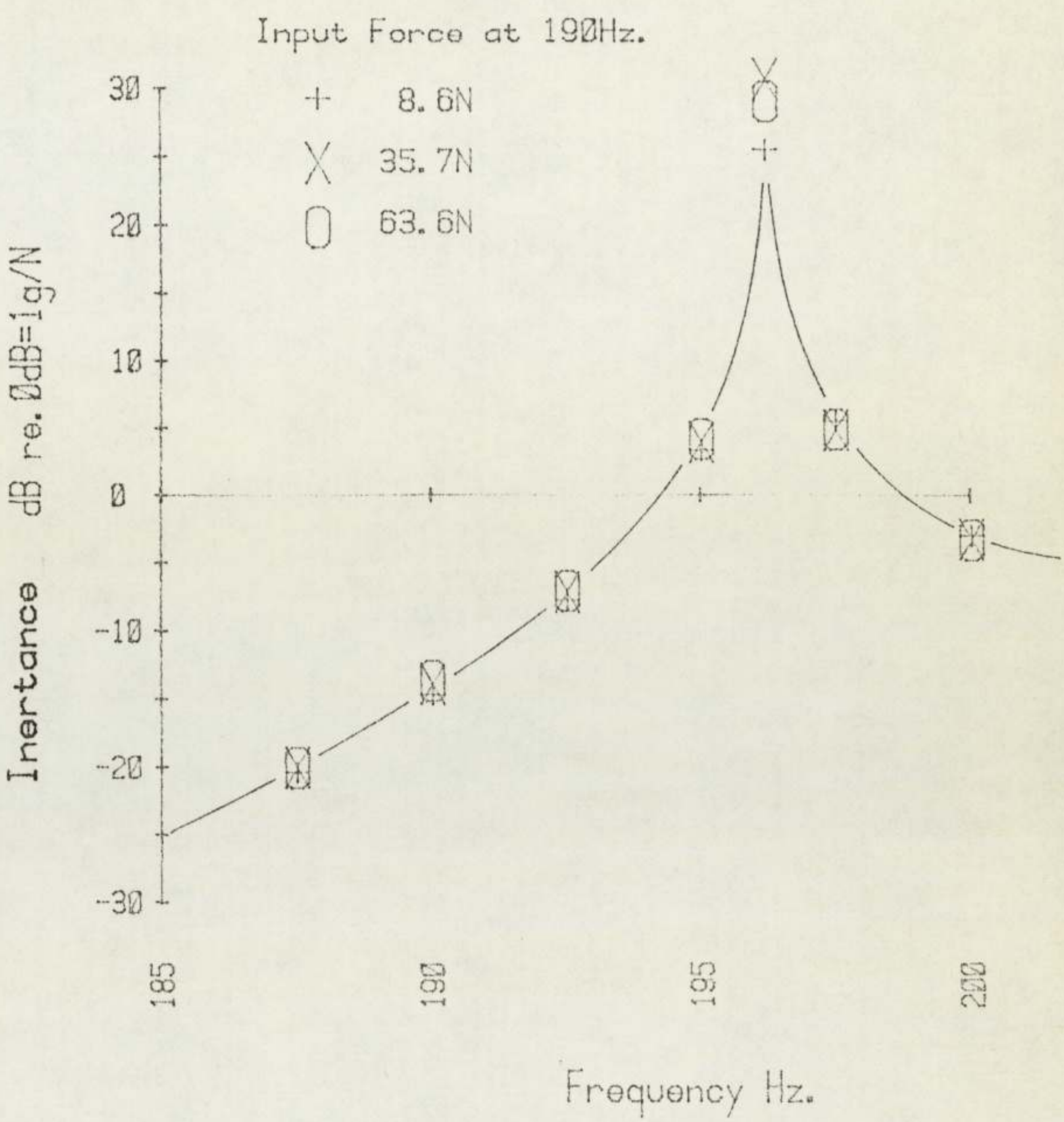

Fig. 4.7 LINEARITY TEST ON CANTILEVER b

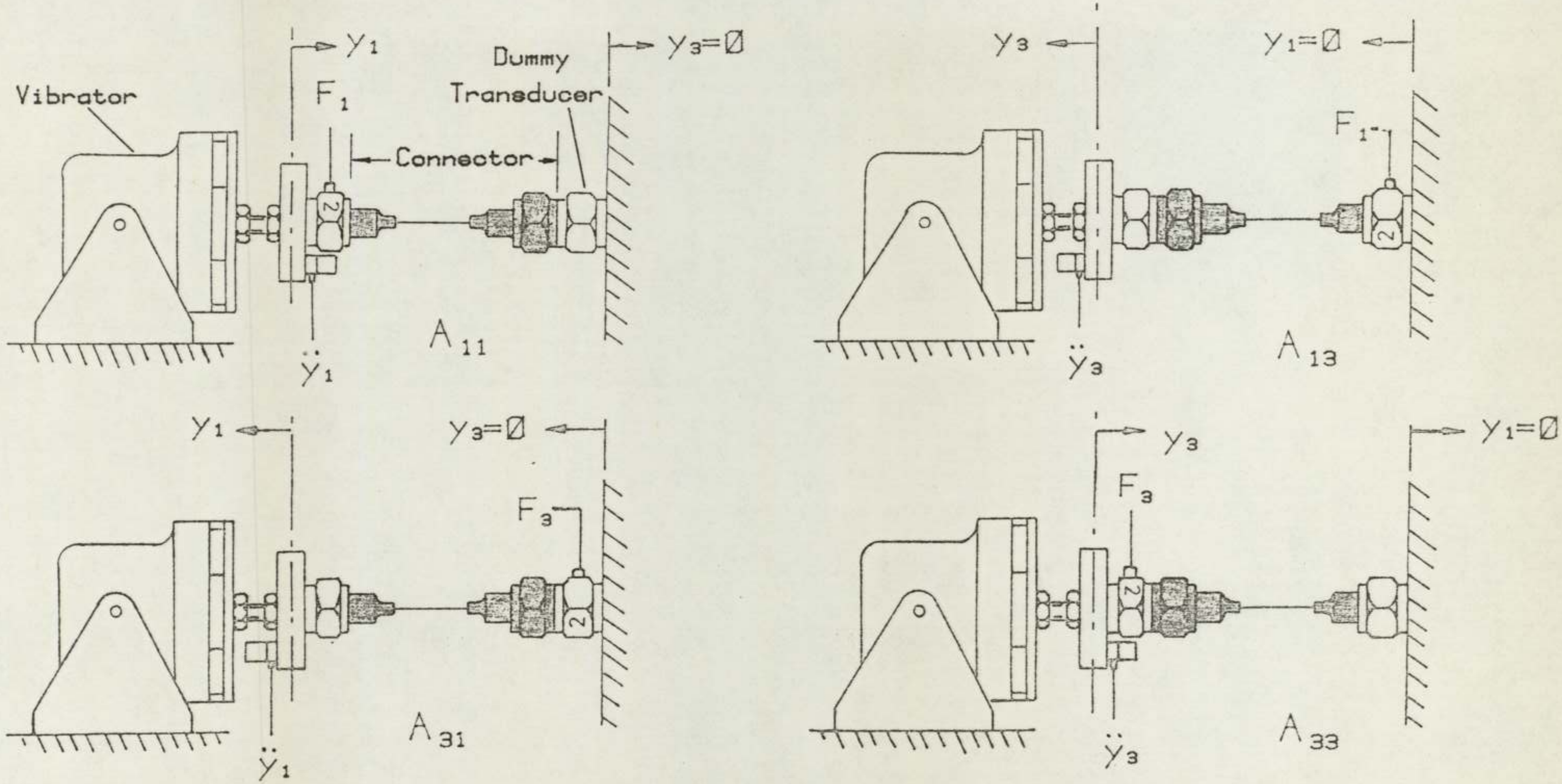

Fig. 4.9 'BLOCKED IMPEDANCE' TESTS ON CONNECTORS

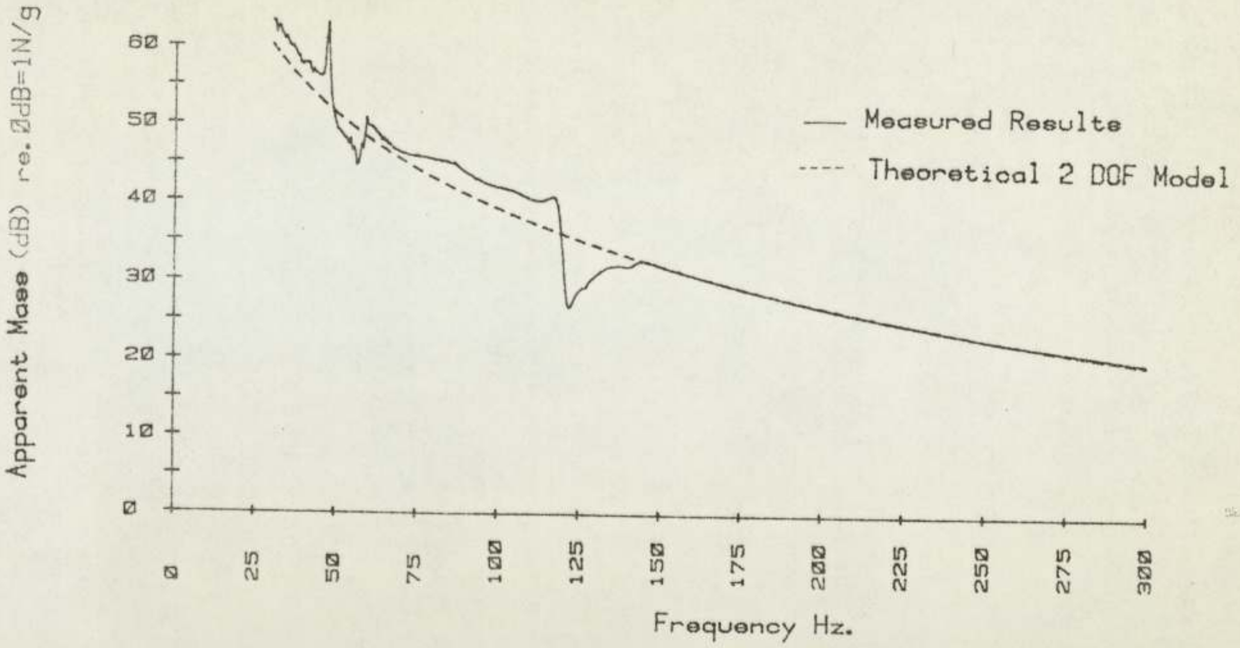

Fig. 4.10 APPARENT MASS OF PIANO WIRE CONNECTOR A_{33}

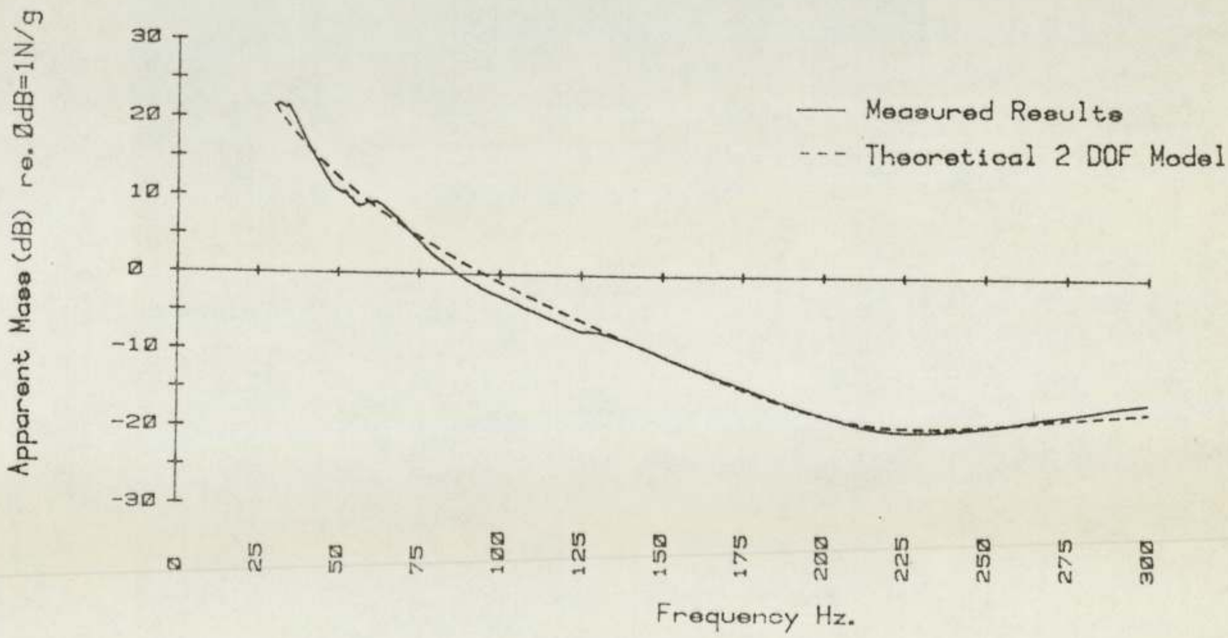

Fig. 4.11 APPARENT MASS OF RUBBER CONNECTOR A_{33}

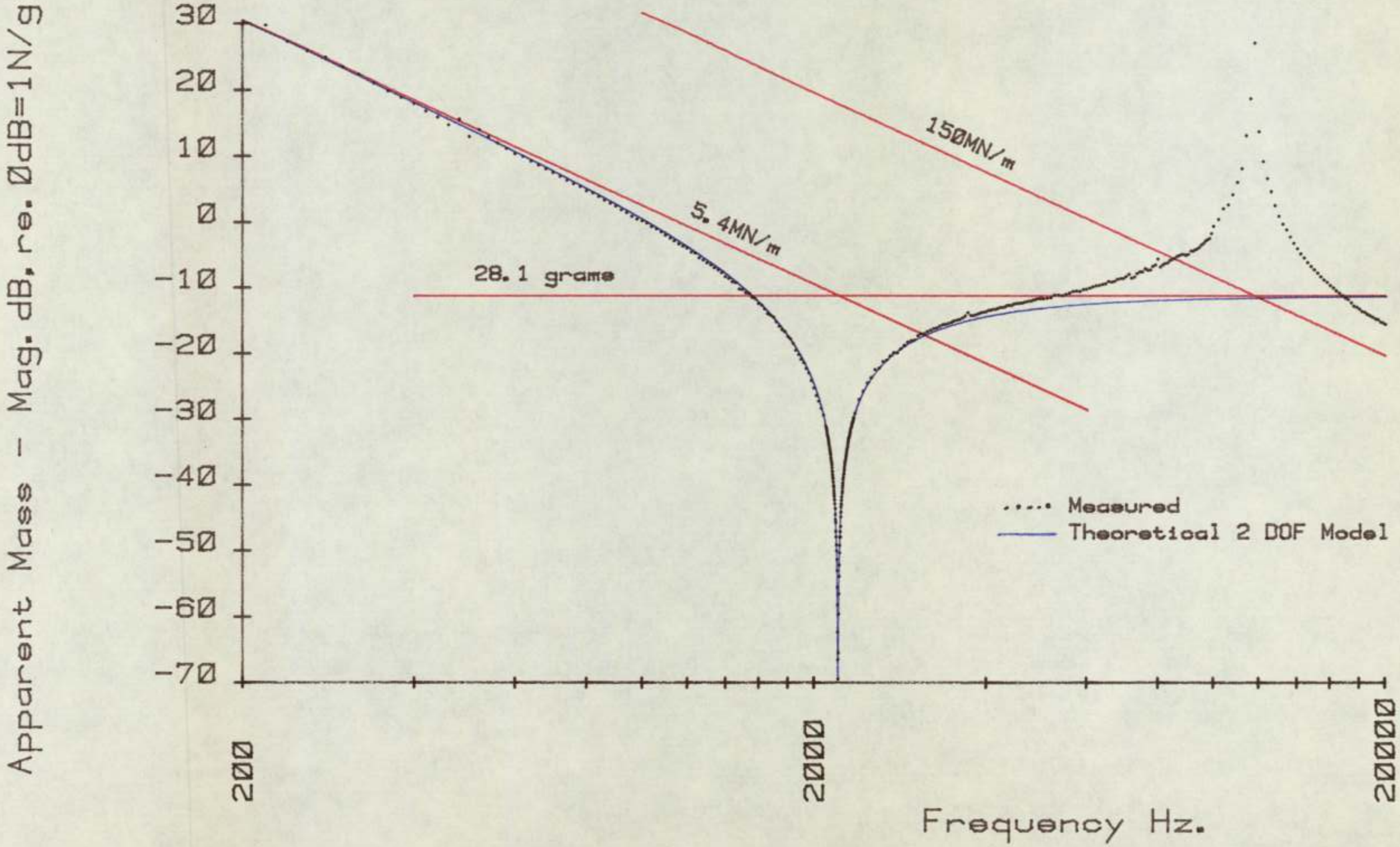

Fig. 4.12 APPARENT MASS MEASURMENTS & THEORETICAL MODEL FOR PIANO-WIRE CONNECTOR - A_{33}

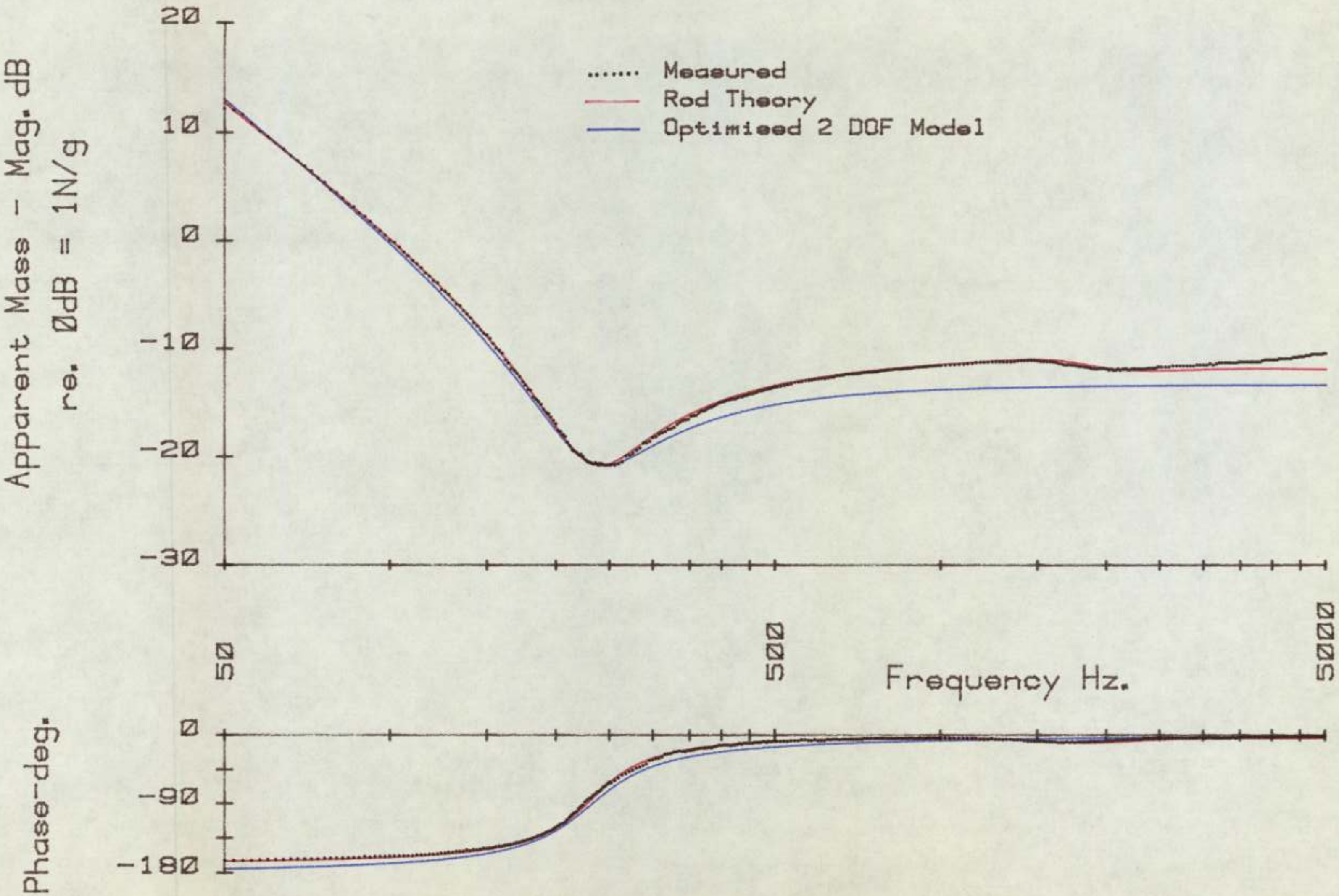

Fig. 4.13 APPARENT MASS MEASURMENTS & THEORETICAL MODELS FOR RUBBER CONNECTOR - A_{33}

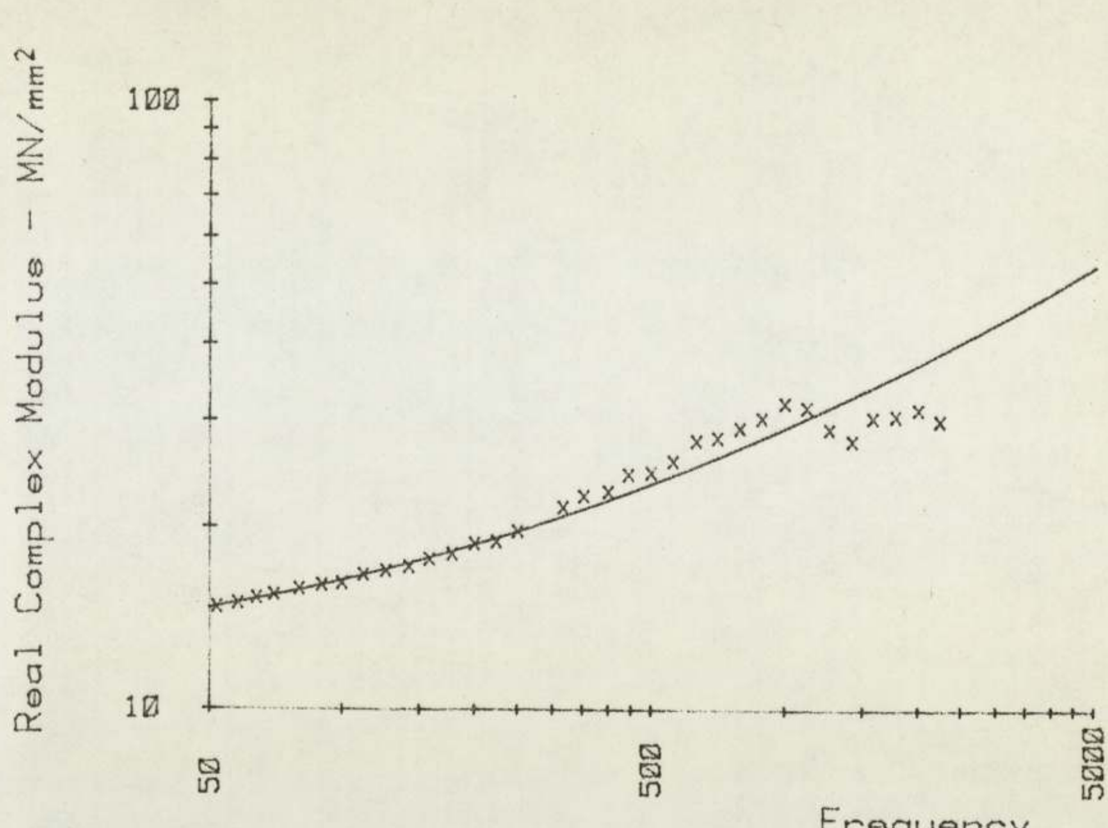

Fig. 4.14 REAL PART OF COMPLEX MODULUS v FREQUENCY

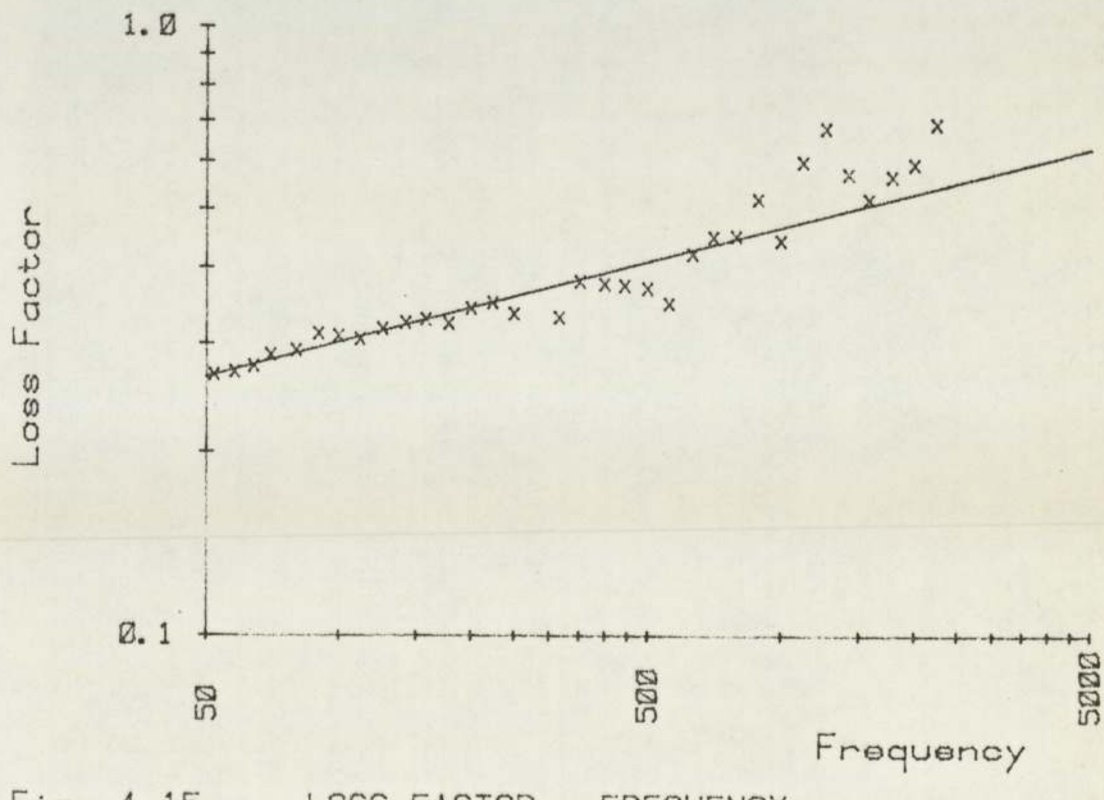

Fig. 4.15 LOSS FACTOR v FREQUENCY

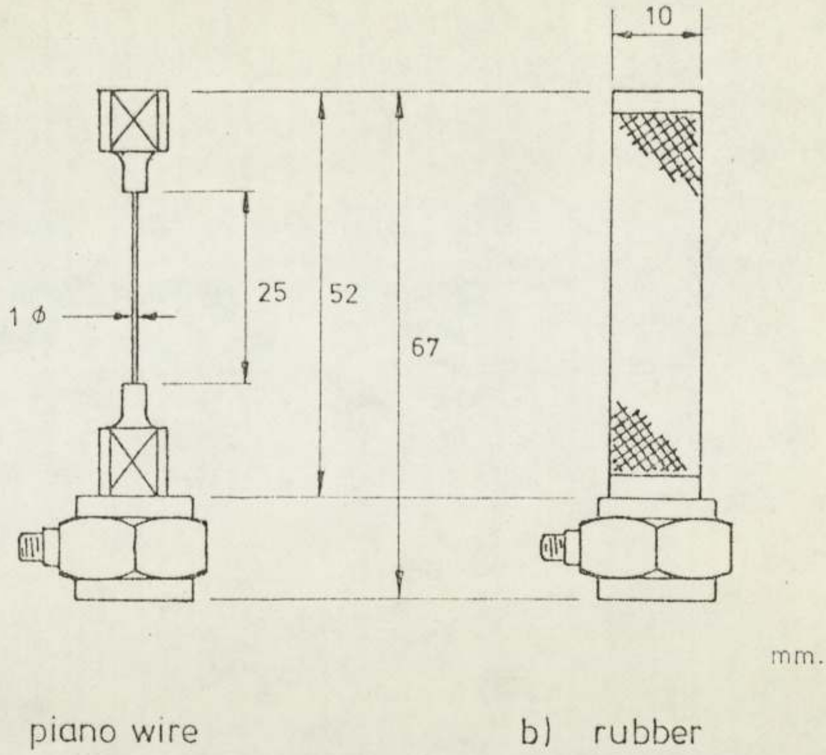

Dynamic Properties for 2 d.o.f. model	Piano Wire	Rubber
$m_{1,2}$ grams	3·0	5·0 +
$m_{3,4}$ grams	28·1	22·0 +
c Ns/m	0·468	14·0 +
k kN/m	5400	47

+ optimised

Fig. 4.16 DIMENSIONS AND ESTIMATED DYNAMIC PROPERTIES OF CONNECTORS

CHAPTER FIVE

EXPERIMENTAL RESULTS OF CANTILEVER SYSTEMS

CHAPTER FIVE

EXPERIMENTAL RESULTS OF CANTILEVER SYSTEMS

5.1 INTRODUCTION

The results included in this chapter are those obtained from the measured inertance data of the two cantilevers a and b of table 2.1. Comparisons between the measured system inertances and those predicted by using the experimental data of the individual cantilevers and the re-generated coupling data in the 'Impedance Coupling Technique' are given for the two types of connector. This comparison may be used to indicate the validity of the experiments, mathematical manipulation and assumptions made in the prediction process. Having gained confidence in the process the cantilever data was further manipulated with hypothetical coupling data. In particular, coupling was effected with pure stiffness elements since this parameter was shown to have the most significant effect on the system inertances in the frequency range of interest.

Finally, a theoretical dynamic absorber was coupled to the system by extending the 'Impedance Coupling Technique' to show the use of this type of device and to demonstrate the flexibility of the Technique.

All the results span the frequency range 30-500 Hz in frequency steps of 0.5 Hz. This frequency range was covered by two sweep tests 30-300 Hz and 250-500 Hz.

Most of the results quoted are of system inertance I_{13}, i.e. the ratio of the acceleration response at position 1 (on the top cantilever - a) to the input force at position 3 (on the bottom cantilever - b). These positions are directly across one connector so that the inertance I_{13} gives a measure of the vibration transmission from the bottom to the top cantilever.

5.2 MEASURED INERTANCES OF CANTILEVERS a AND b

(as shown in Figures 5.1 and 5.2)

The inertance magnitudes are presented in matrix formation. The dimensions and position locations are the same as cantilevers a and b in systems 1 and 2 of the theoretical study (see tables 2.1 and 2.2). These curves may be usefully compared with the theoretical results of Figures 2.6 and 2.7. The first resonant peak in these curves are the cantilevers' second natural frequencies since the fundamental resonant frequencies are below 30 Hz. In general the experimental results show that the cantilevers' natural frequencies are below those predicted by classical theory; this is primarily due to non-idealised boundary conditions at the clamped end and the inclusion of transducer, de-coupler and balance masses within the cantilever sub-system.

5.3 PREDICTED INERTANCES OF SYSTEMS 1 AND 2

(as shown in Figures 5.3 and 5.4)

The experimental results of cantilevers a and b, Figures 5.1 and 5.2, were manipulated together with the re-generated connector data in the 'Impedance Coupling Technique' to obtain these predicted system inertances. System 1 comprises the two cantilevers coupled with the mathematical model of the piano-wire connectors and in system 2 the cantilevers are coupled with the 2 D.O.F. mathematical model of the rubber connectors. These results may be usefully compared with systems 1 and 2 in the theoretical study, ie Figures 2.10 and 2.11.

5.4 MEASURED INERTANCES OF SYSTEMS 1 AND 2

(as shown in Figures 5.5 and 5.6)

The cantilevers a and b were coupled with the two types of connector (ie piano-wire and rubber), cantilever a being the top cantilever in the coupled system. Figure 5.5 shows the experimentally measured inertance magnitudes of system 1 which was coupled by the piano-wire connectors and Figure 5.6 shows the results from system 2 where the rubber connectors were used.

5.5 COMPARISON OF PREDICTED AND MEASURED INERTANCES FOR THE TWO TYPES OF CONNECTOR

(as shown in Figure 5.7)

This figure shows in detail the differences between predicted and measured system inertances. The system inertance I_{13} is taken from the preceding graphs and is shown on the same graph for comparison. The upper two curves correspond to the piano-wire connected system and the lower two to the rubber connected system.

The correlation between the predicted and measured inertances is good considering the simplicity of the mathematically re-generated connector models used. Furthermore, the inertance plots show that when using the flexible connectors the coupled system exhibits resonances that are basically the individual cantilever resonances. When the systems are rigidly coupled extra resonances appear in the frequency range but the top cantilever resonances, in particular, are still evident. This is a characteristic feature when coupling two similar structures with such a simple connector, see section 2.8 for a detailed discussion.

5.6 PREDICTED SYSTEM INERTANCE I_{12} WITH VARIOUS STIFFNESSES

(as shown in Figure 5.8)

The upper two curves in this graph are the measured point inertances of the two uncoupled cantilevers. The lower five curves were obtained by applying the 'Impedance Coupling Technique' to combine the experimental cantilever data with hypothetical flexible connectors (with no mass or damping properties) to predict the overall system characteristics. The stiffnesses of the connectors were chosen to cover the range 250-4000 kN/m, the lower stiffness being approximately 5 times greater than the rubber connector stiffness and the upper stiffness being approximately equal to the piano-wire connector stiffness. It can be observed that at the higher frequencies the system resonances vary dramatically with change in connector stiffness but at low frequencies (< 100 Hz) connector stiffness has much less effect on the inertance predicted. If the frequency of 390 Hz is taken as an example, the system shows a resonant peak when the coupling stiffness is 500 kN/m but as the stiffness is increased to 1000 kN/m the system shows an anti-resonance.

5.7 EFFECT OF COUPLING STIFFNESS ON SYSTEM INERTANCE I_{12} AT SELECTED FREQUENCIES

(as shown in Figure 5.9)

These figures show the effect of coupling stiffness on system inertance more clearly than Figure 5.8 since the inertance is plotted against coupling stiffness, the frequency remaining constant. At the frequency of 390 Hz, Figure 5.9 (a), it can be seen that the inertance reaches a maximum when the coupling stiffness is 500 kN/m and 1500 kN/m and reaches a minimum when the stiffness is 1000 kN/m. Thus, to detune the system at 390 Hz the optimum coupling stiffness would be 1000 kN/m. Other stiffness-inertance curves at neighbouring frequencies are overlaid to give an indication of the frequency band within which this de-tuning would be effective.

Inertance against stiffness plots for frequencies of 260 Hz and 190 Hz are given in Figures 5.9 (b) and (c) respectively. The plot at 260 Hz shows that de-tuning can again be achieved, but at stiffnesses greater than 1500 kN/m the inertance is extremely sensitive to changes in frequency and the plot at 190 Hz shows that de-tuning is not possible with coupling stiffnesses greater than 250 kN/m. The system resonance at 193 Hz coincides with the fourth natural frequency of the top cantilever - a.

5.8 THE APPLICATION OF A DYNAMIC ABSORBER TO THE TWO CANTILEVER SYSTEM

(as shown in Figures 5.10 and 5.11)

Using the computer programs developed it is relatively easy to examine the theoretical effect of any additional mass/spring/damper element on the real cantilever sub-system. For example, Figure 5.10 shows the effect of adding a mass/spring dynamic absorber to the system when the two sub-systems are connected by springs of 500 kN/m. The absorber was tuned to a frequency of 390 Hz with a mass of 14.5 grams compared with the total system mass of 5.4 kg.

Figure 5.11 shows the response of the mass due to an input force to the system at the point of attachment of the absorber. This shows the increase in activity of the mass in the 390 Hz region.

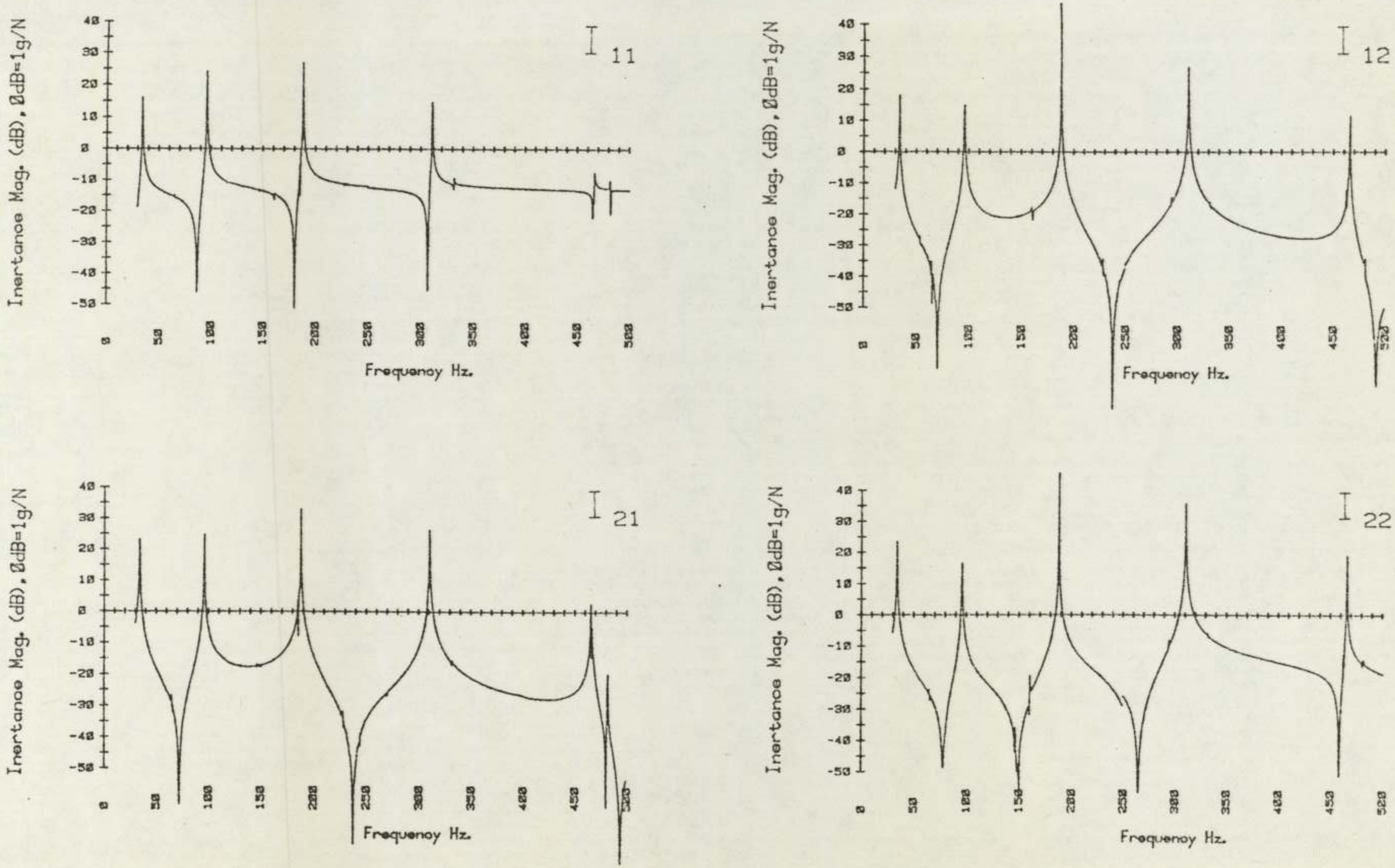

Fig. 5.1 MEASURED INERTANCES OF CANTILEVER (a)

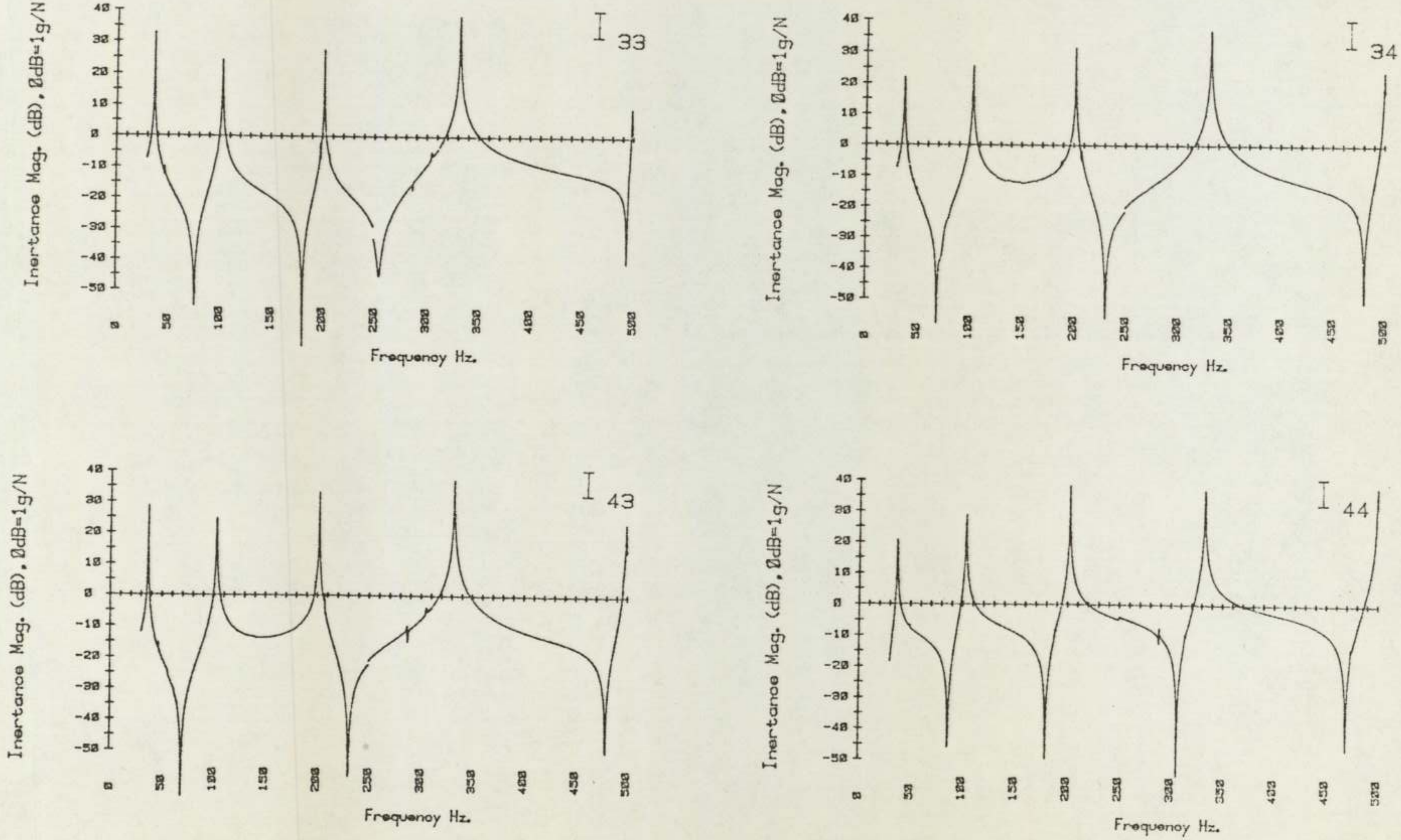

Fig. 5.2 MEASURED INERTANCES OF CANTILEVER (b)

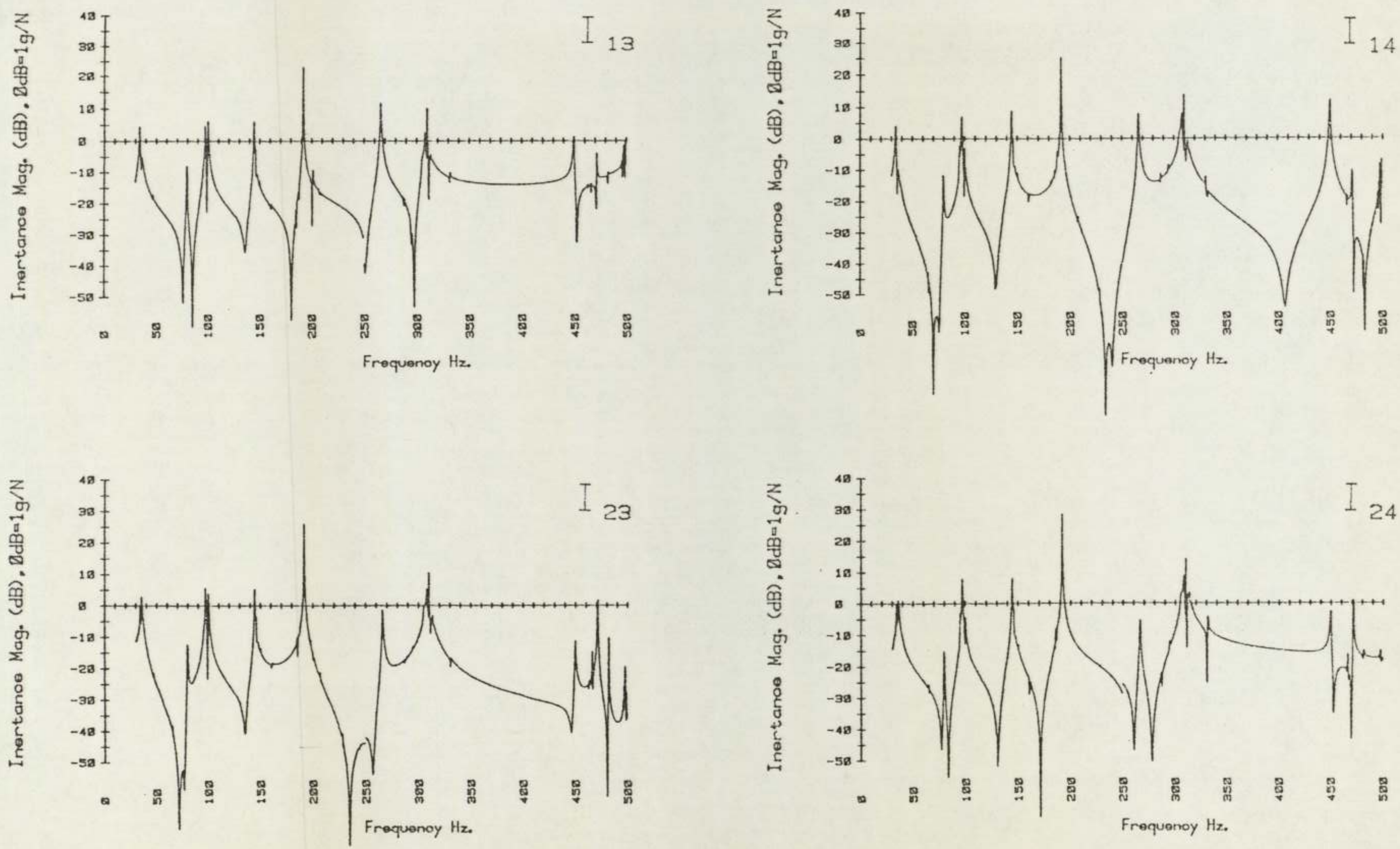

Fig. 5.3 PREDICTED INERTANCES OF SYSTEM 1

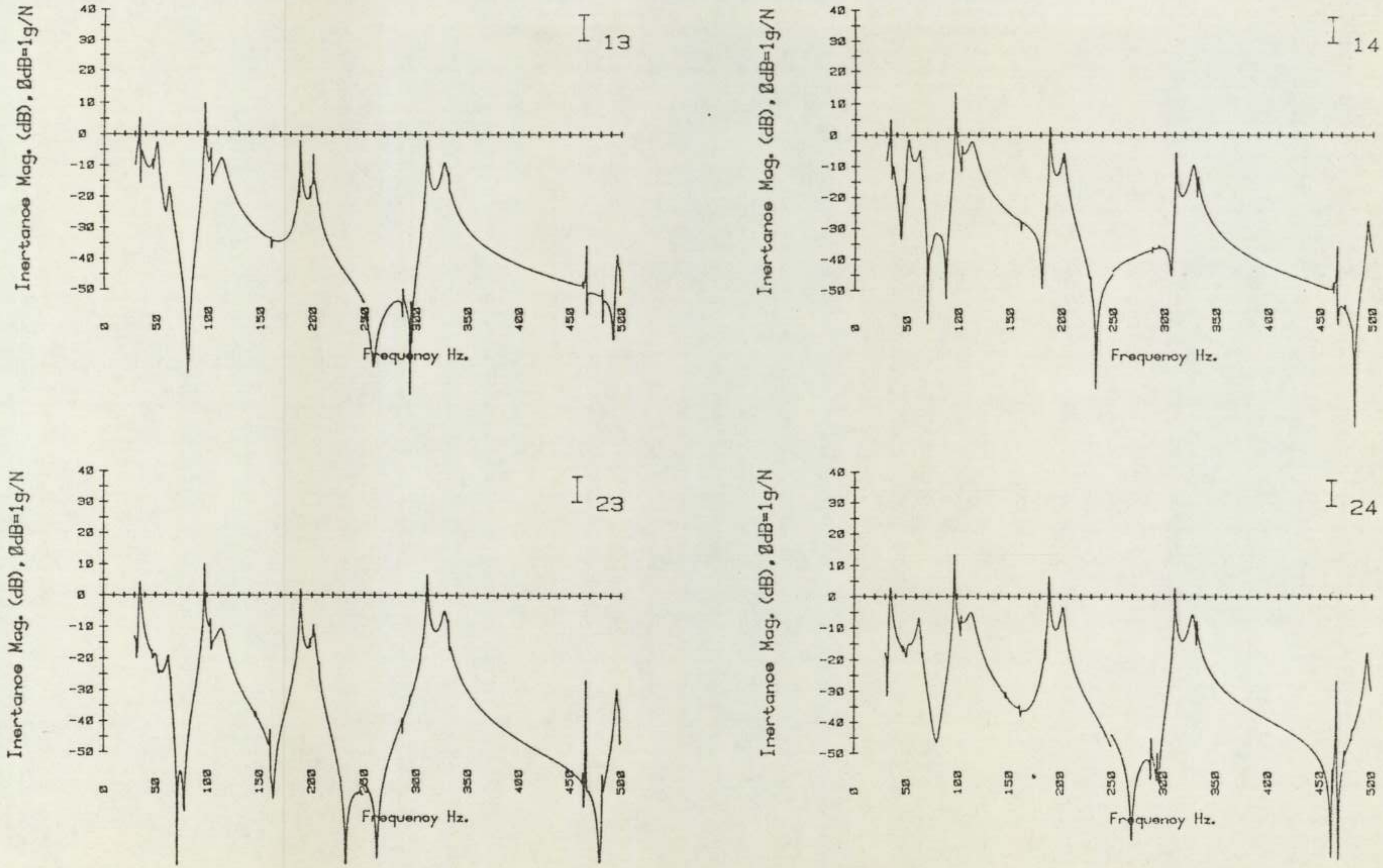

Fig. 5.4 PREDICTED INERTANCES OF SYSTEM 2

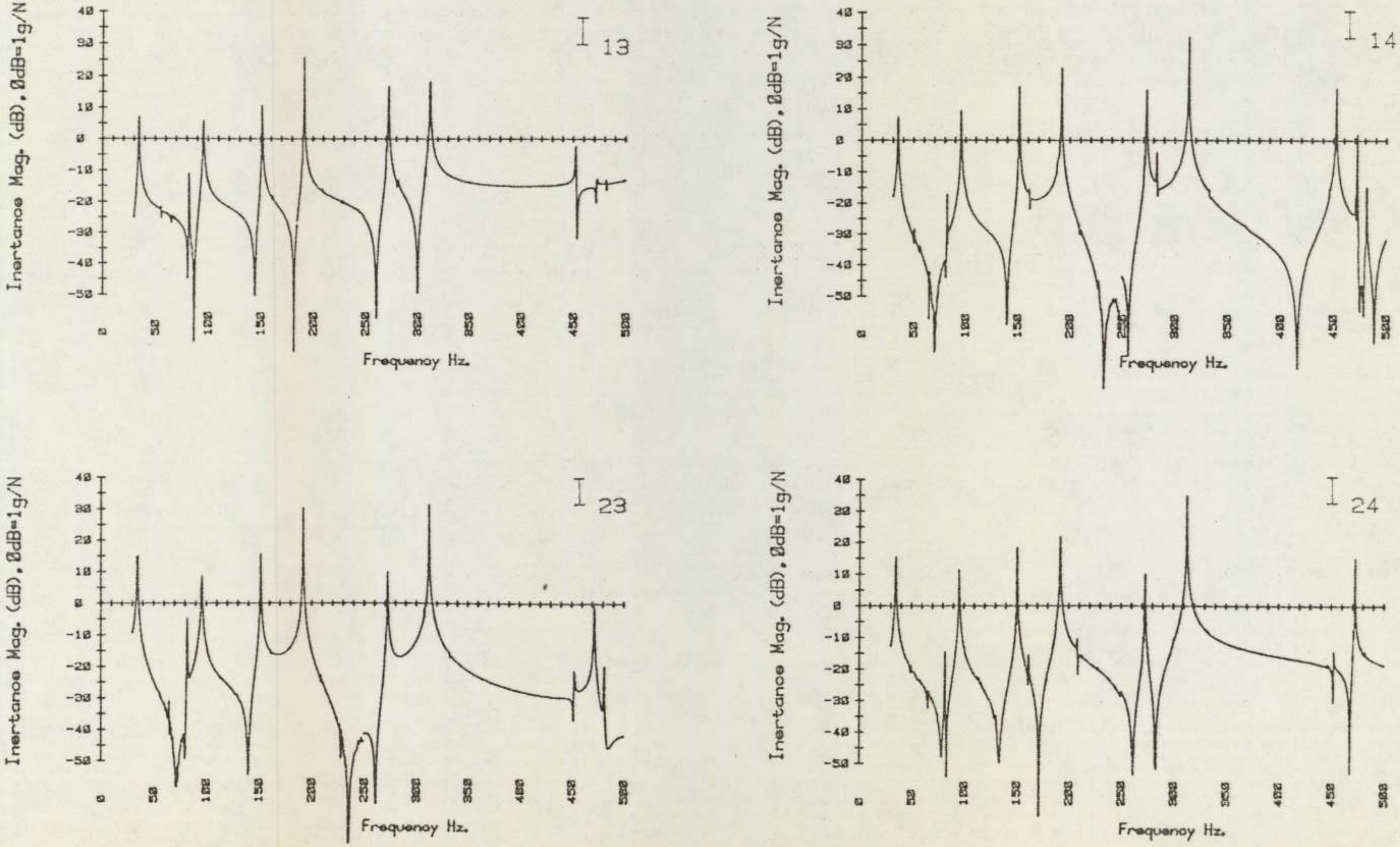

Fig. 5.5 MEASURED INERTANCES OF SYSTEM 1

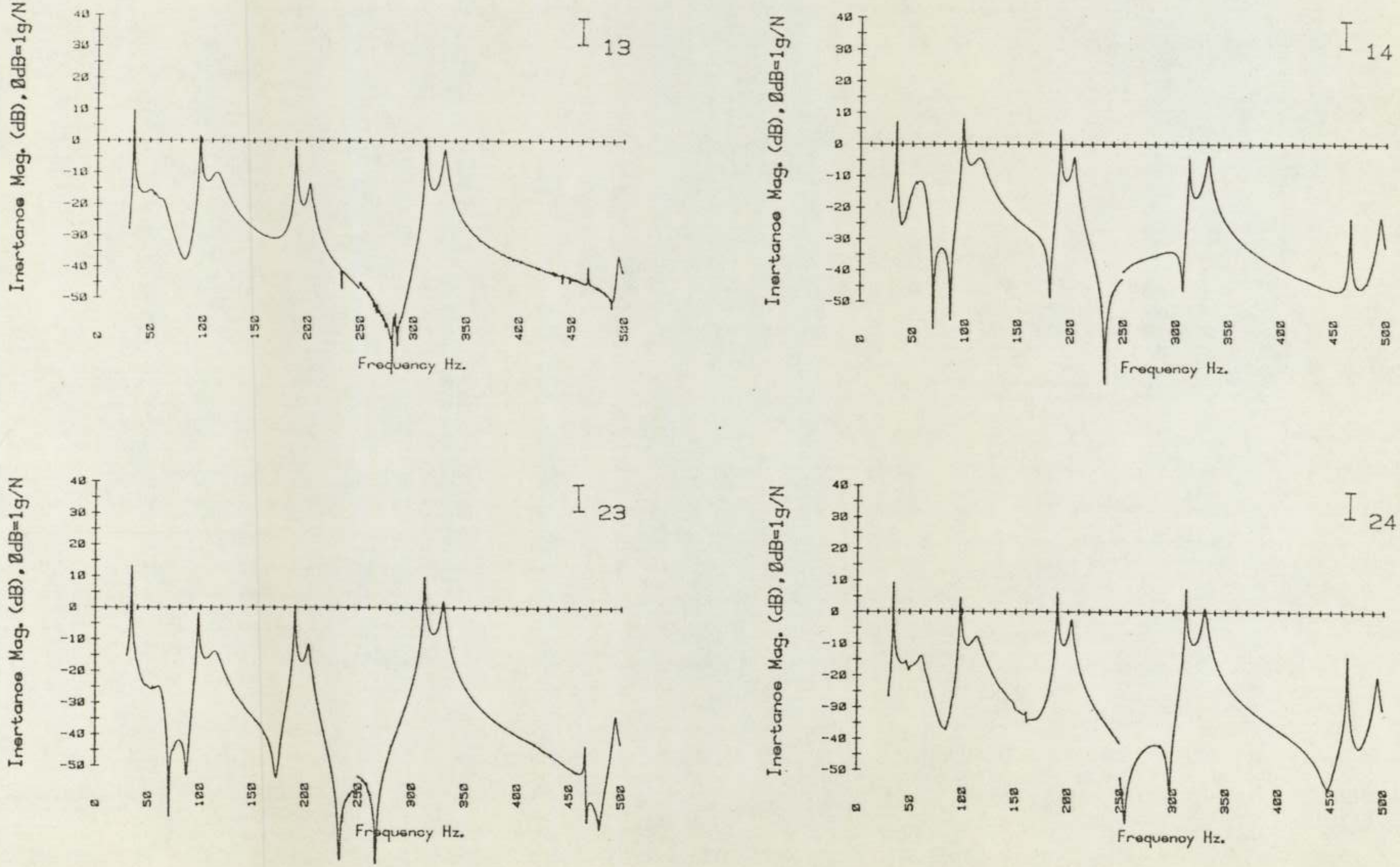

Fig. 5.6 MEASURED INERTANCES OF SYSTEM 2

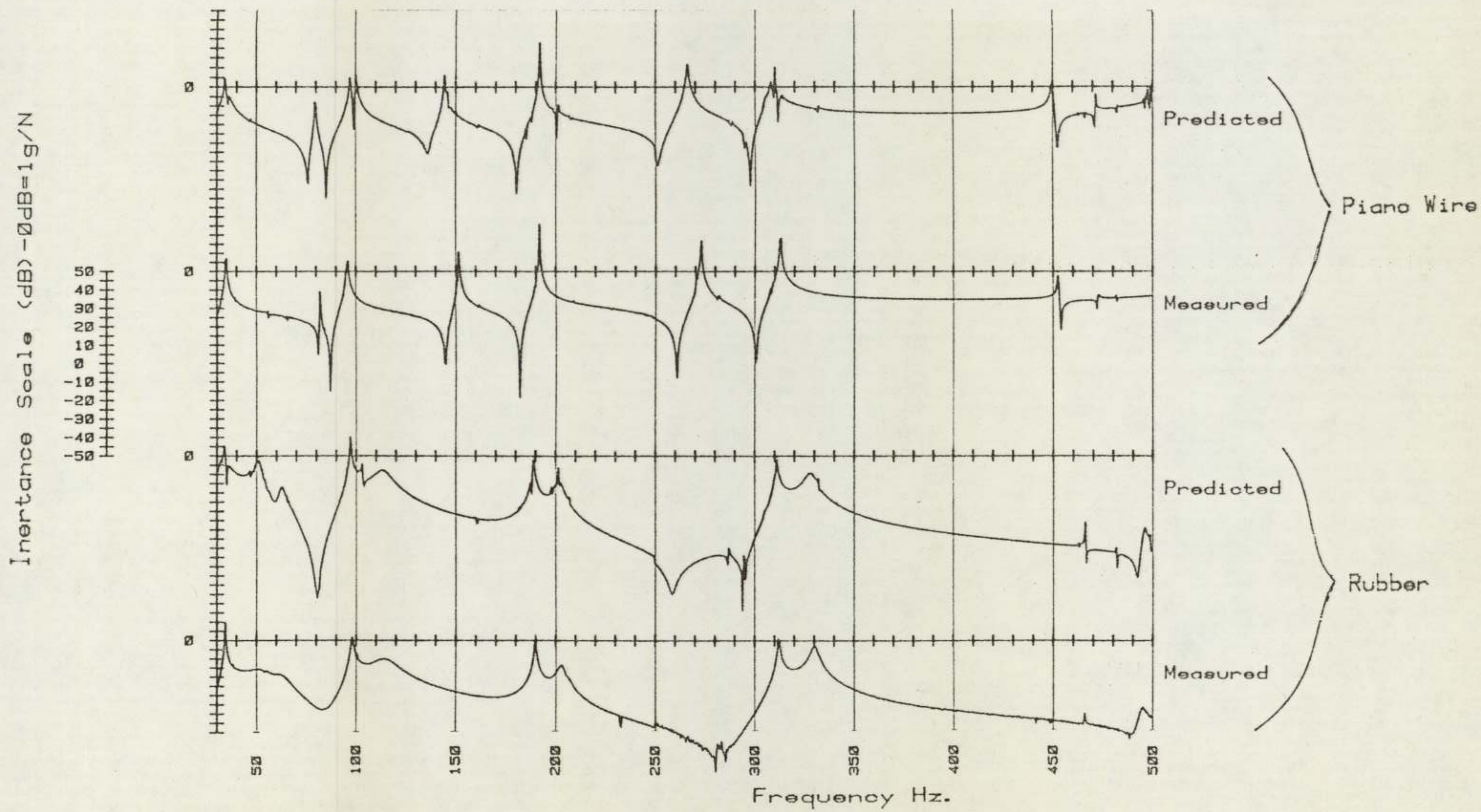

Fig. 5.7 COMPARISON OF PREDICTED AND MEASURED INERTANCE I_{13} FOR 2 TYPES OF CONNECTOR

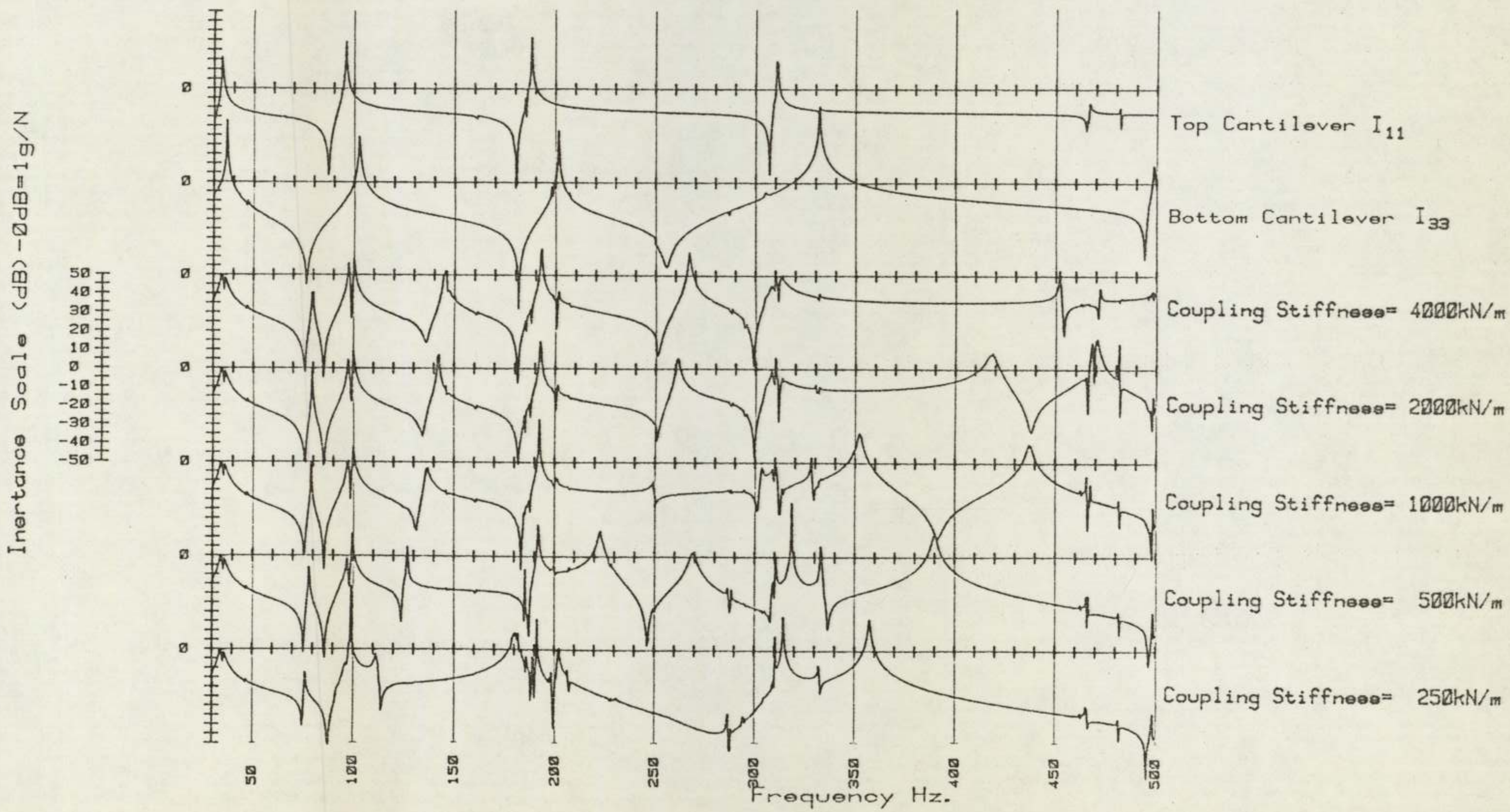

Fig. 5.8 PREDICTED SYSTEM INERTANCE I_{13} WITH VARIOUS STIFFNESSES

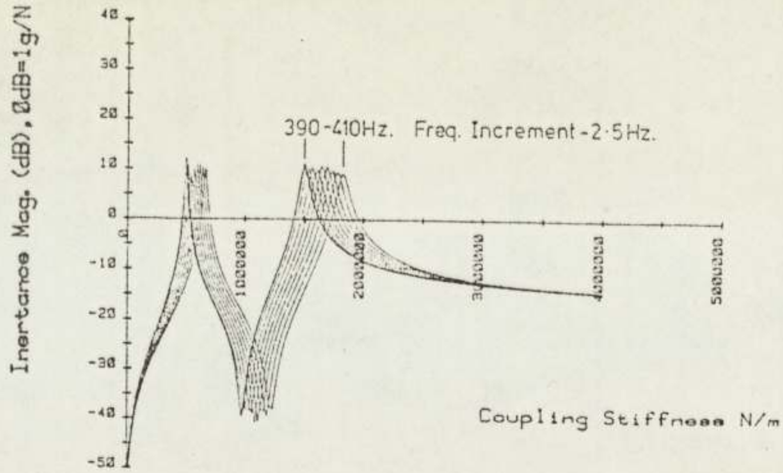

Fig 5·9a EFFECT OF COUPLING STIFFNESS ON SYSTEM INERTANCE I_{13} AT 390-410Hz

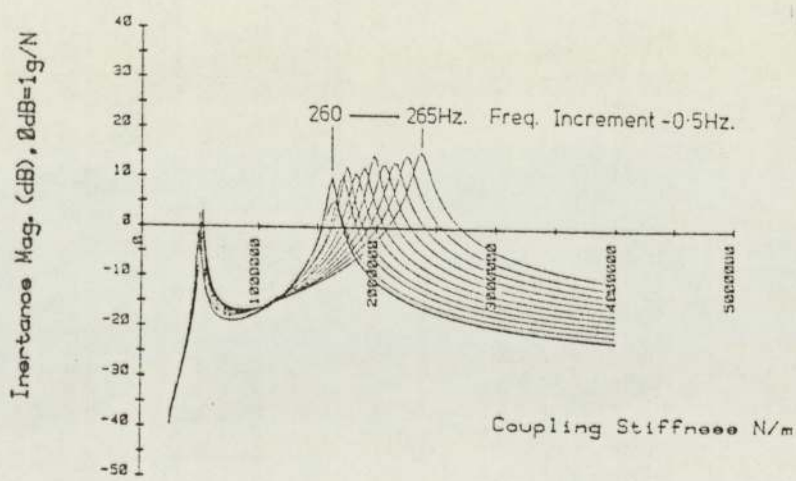

Fig 5·9b EFFECT OF COUPLING STIFFNESS ON SYSTEM INERTANCE I_{13} AT 260-265Hz

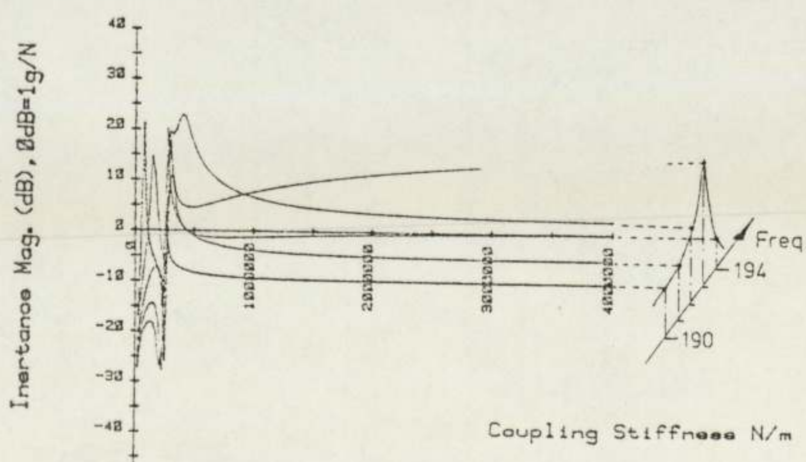

Fig 5·9c EFFECT OF COUPLING STIFFNESS ON SYSTEM INERTANCE I_{13} AT 190-194Hz

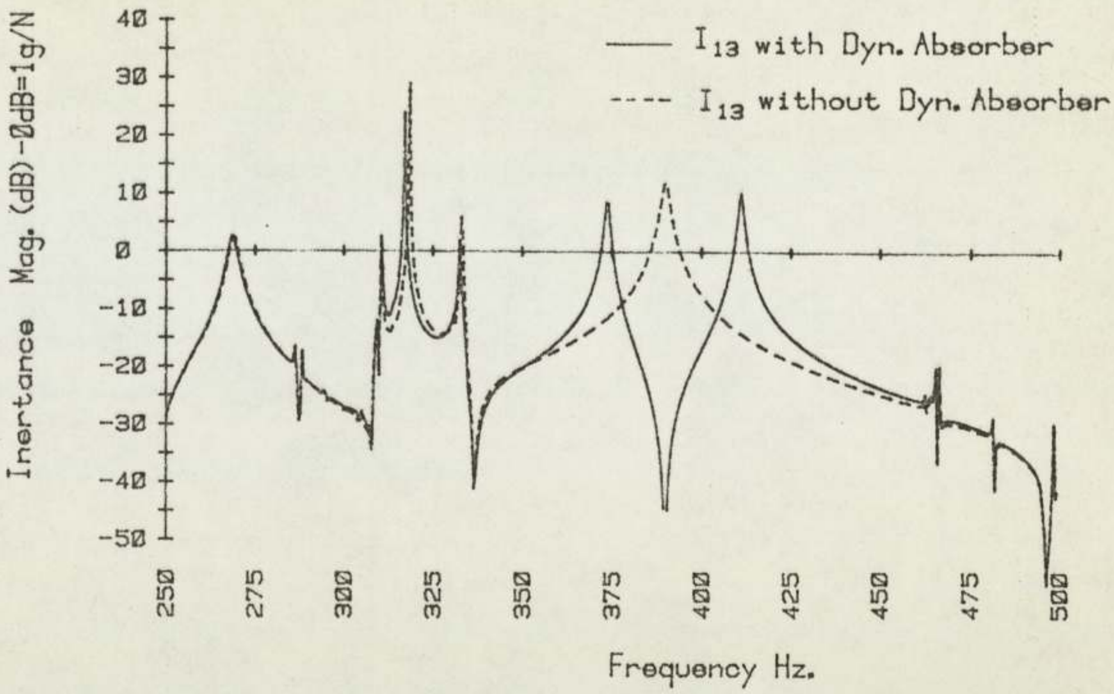

Fig. 5.10 PREDICTED SYSTEM INERTANCE I_{13} WITH DYNAMIC ABSORBER TUNED TO 390Hz. (Mass = 14.5grams)

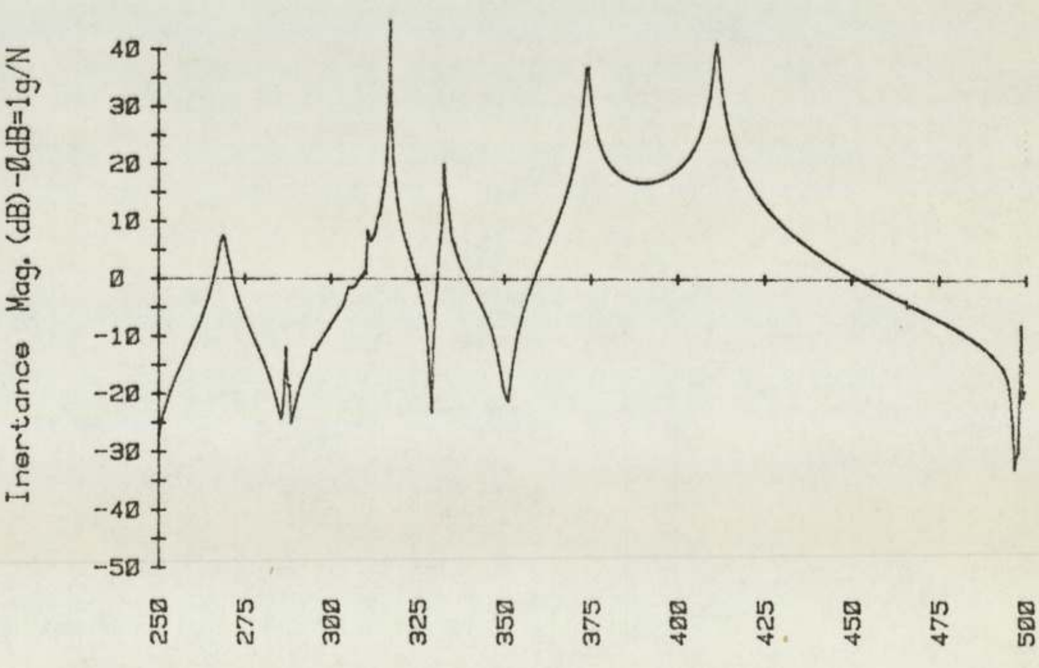

Fig. 5.11 PREDICTED INERTANCE I_{53} OF DYNAMIC ABSORBER MASS

CHAPTER SIX

DISCUSSION

CHAPTER SIX

DISCUSSION

6.1 INTRODUCTION

This chapter conveniently divides into four parts allowing a discussion on the four principal areas of the investigation as follows:

(a) The experimental technique developed in measuring the frequency response to the required accuracy in order that these measurements might be further processed.

(b) The theoretical and experimental results when manipulated by the 'Impedance Coupling Technique.'

(c) The optimisation of the interface dynamic characteristics in order that the system may be de-tuned at selected frequencies.

(d) A general discussion on the 'Impedance Coupling Technique' which forms the basis of the optimisation procedure.

6.2 DISCUSSION OF EXPERIMENTAL TECHNIQUE

The most important part of the investigation was to perfect a measuring technique since the frequency response of a general structure is too complex to predict theoretically. Only then was it possible to manipulate these experimental results together with a theoretical interface in the search for optimum conditions in the overall performance of the coupled system.

The system under investigation comprised two cantilever structures coupled at two points via some interface system. The cantilevers were disconnected and were subjected in turn to frequency response tests in order to accumulate all the necessary impedance data to be able to predict the coupled system response. This post test analysis required experimental data of an extremely high quality which was not only very demanding in terms of instrumentation but also required a high degree of skill in experimental technique.

The cantilever structures used in the investigation offered many advantages for attaining highly accurate frequency response measurements[25] these being due to a relatively flexible structure with well defined frequency response characteristics. The experimental measurements could be checked at every stage with predictions obtained by classical forced response of beam theory. Some of the inaccuracies associated with measuring the frequency response of a structure are due to the incorrect selection of vibration generator or force transducer which may have stiffness characteristics not suited to the type of test structure and the frequency range of interest. In general the force transducer has high stiffness with low mass giving a flat frequency response to a moderately high frequency. However, if the test structure is mass-like, ie it has high stiffness, then the contact stiffness (between the transducer and the structure) and the transducer stiffness elements will become active at somewhat lower frequencies giving incorrect frequency response measurements. Errors of this sort were avoided in the investigation since the cantilevers had lower stiffness properties, although similar errors did occur in the initial tests due to low stiffness joints in the de-coupler assembly which connected the vibrator to the force transducer. This was remedied by soft-soldering the joints giving a high stiffness to the assembly which increased its useful frequency range to approximately 1000 H_z.

The effect of these stiffnesses on the measured inertance is more readily appreciated by constructing a simplified mathematical model of the test configuration[7].

Let the structure to be measured be represented by a simple mass and spring system as shown below:

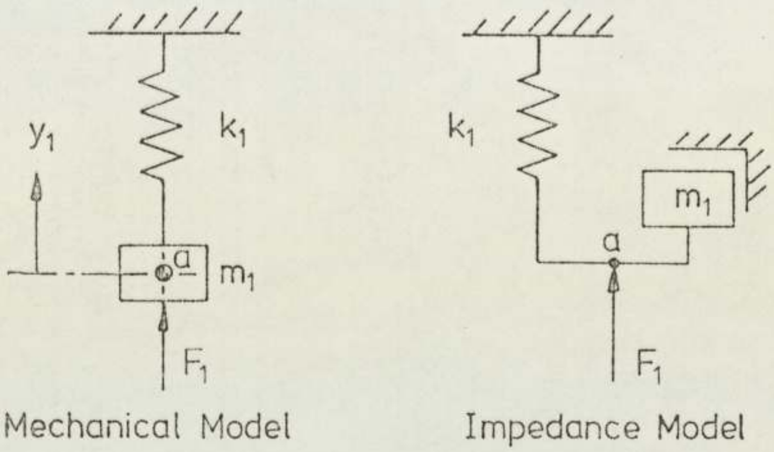

The point inertance at (a) would be:-

$$I_{aa} = \frac{1}{m_1} \cdot \frac{\Omega^2}{\Omega^2 - S_R} \qquad \text{. . . eq 6.1}$$

where $S_R = \dfrac{k_1}{m_1}$

At resonance all elements are active and this resonant frequency would be

$$R_1 = \sqrt{\frac{k_1}{m_1}} \qquad \text{. . . eq 6.2}$$

If extra stiffness and mass elements are introduced between the measured force input and point (a) (as shown **over leaf**)

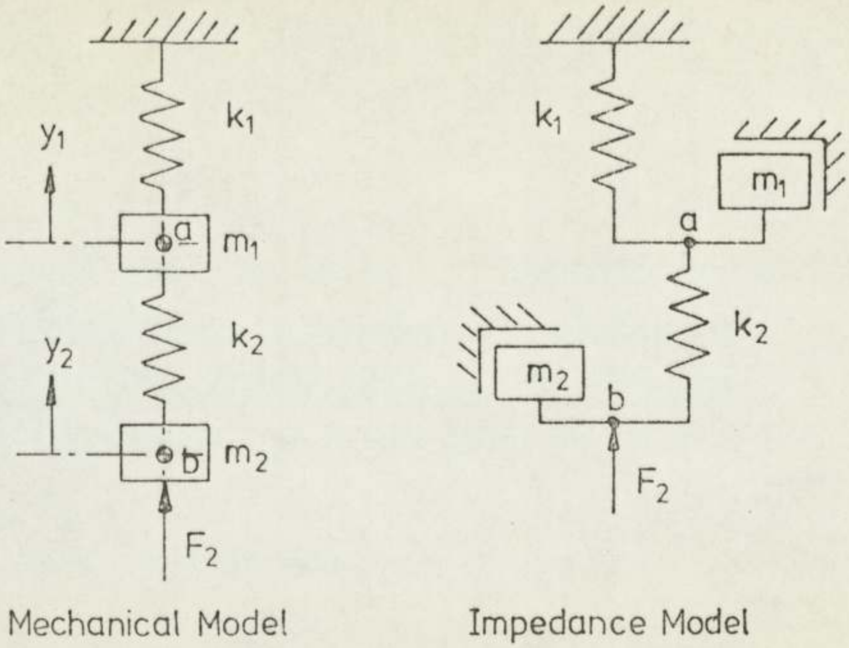

then the input force measured would now be represented by F_2 and the measured acceleration would be at point (a). These extra elements represent the following:

(i) contact stiffness between the transducer and the test structure,

(ii) any concentrated masses added to the structure at the force input point, eg transducer diaphragm mass,

(iii) force transducer stiffness,

(iv) de-coupler assembly mass and stiffness.

The inertance would be

$$I_{ab} = \frac{1}{m_1} \cdot \frac{S_A \Omega^2}{\Omega^2 S_R - \Omega^4 - P_R} \qquad \text{. . . eq 6.3}$$

where $S_A = \frac{k_2}{m_2}$, $S_R = \frac{k_1}{m_1} + \frac{k_2}{m_2} + \frac{k_2}{m_1}$ and $P_R = \frac{k_1 k_2}{m_1 m_2}$

At resonance all elements are active and the resonant frequencies R_1, R_2 may be found by solving the equation

$$\Omega^4 - \Omega^2 S_R + P_R = 0 \qquad \text{. . . eq 6.4}$$

Clearly the inertance of equation 6.3 is not the same as that of equation 6.1. However, as $m_2 \to 0$ and $k_2 \to \infty$ equation 6.3 approaches equation 6.1

This is demonstrated in Fig 6.1 where the theoretical inertances using equation 6.3 is plotted against frequence for various contact stiffness. The mass M_2 is taken as zero and the mass and stiffness values of the model of the test structure are both unity. The true frequency response of the 1 degree of freedom system is mass-like at high frequency i.e. the inertance becomes constant. However, the introduction of a contact stiffness causes the high frequency response to become stiff-like, i.e. the inertance becomes proportional to Ω^2

Further an anti-resonance is introduced into the frequency response function at a higher frequency than the natural frequency. It can be seen from the graphs that a reasonably accurate frequency response may be measured up to one decade higher than the natural frequency when the contact stiffness is 1000 times that of the system stiffness. In the cantilever experiments the contact stiffness included the de-coupler assembly which had a stiffness of approximately 50000 times that of the static stiffness of the cantilever therefore the errors due to contact stiffness were very small. The de-coupler assembly was originally placed in this position for convenience and also to give extra protection to the force transducer since it could be bolted to the vibrator for the duration of the investigation. If higher frequency responses are measured or if the test structure has higher stiffness properties then a higher contact stiffness would be required. To achieve this the force transducer would be connected directly to the test structure giving a much higher contact stiffness.

The advantage gained by using flexible cantilever structures was somewhat offset by the relative ease with which the necessarily attached vibration generating equipment could alter the boundary conditions of the test structure. In the case of a cantilever any restraint at its free end will result in significant errors in the frequency response especially at low frequencies. An example to illustrate this point is to compare the theoretical constants used to evaluate the natural frequencies of a cantilever with free and sliding end conditions - the first natural frequency will be increased by 57% and the third natural frequency by 21% due to the torsional restraint at the sliding end boundary condition. To overcome this problem it was necessary to connect the vibration generating equipment to the cantilever via a de-coupler assembly. This assembly consisted of a short length of piano wire thus ensuring that only axial forces were transmitted giving little rotational restraint because of its high transverse flexibility.

The rotational stiffness of the piano wire was calulated as less than 1% of the cantilever rotational stiffness at the free end, this giving an error in the first natural frequency of less than 1%.

The testing configuration finally adopted in the experimental procedure consisted of a cantilever connected to a vibrator via the de-coupler assembly and force transducer.

It is important to realise, with this testing configuration, that the de-coupler assembly and the accelerometers were within the measuring system boundary and as such the resulting inertance would include the inertances of these extra elements. These elements, which may be considered as concentrated masses, could normally be cancelled by an electronic circuit or simply taken into account in any subsequent matrix manipulation, but since these cantilever structures were used as demonstration sub-systems the accelerometers etc. were considered as an integral part of the measured sub-system. Further, an additional dummy mass was required within this measuring system boundary at the connection point which was not excited in order to maintain consistency when transferring the de-coupler assembly and vibrator from one position to the other. This mass, which was termed as a 'balance' mass, was equal to the de-coupler assembly mass. It was found that a useful way of checking the balance of the system under test was to compare the transfer inertances since the reciprocity relationships should be maintained, i.e. the transfer inertance I_{ij} should be identical to I_{ji} for a linear system. Experience has shown that the 'balance' mass was required to be within 1 gram for the cantilevers tested up to a frequency of 500 Hz and this took into account the small diaphragm mass within the force transducer since it is effectively part of the measuring system. This mass balancing shows how sensitive the system is to relatively small amounts of mass.

However if the system under test is massive then the effect of the transducer masses may be negligible. For example table 1 shows the theoretical change in natural frequences when a concentrated mass (representing the transducer) is placed at the tip of a cantilever.

Mass of transducer as a % of beam mass	Change in ω_1 %	Change in ω_2 %	Change in ω_6 %
0.1	0.2	0.2	0.2
1	1.9	1.9	1.7
10	16	12	6.4

TABLE I

Comparing the reciprocal transfer inertances gave added confidence in the accuracy of the measured frequency response, since a change in the position of excitation can produce a change in the effect of contact stiffness, rotational restraint and the mass of transducers that are moved from one position to another on the measured frequency response.

The cantilevers provided a sufficient number of resonant frequencies within the frequency range of 30-500 Hz to adequately demonstrate the effects of coupling configurations on the overall system response. The low damping inherent in these structures gave an immediate visual check on the positions of resonant frequencies which eliminated the need to subject the sweep test results to further modal identification procedures. However, high dynamic ranges are associated with lightly damped structures and a change of 80 dB's from an anti-resonant to a resonant peak in the inertance levels was found to be typical. Fortunately, the Frequency Response Analyser used in the investigation was able to measure these changes without any loss of data, providing a suitable sweep rate was selected.

The optimum sweep rate was obtained by a trial and error selection of integration time and frequency step value. A long integration time would have had an added advantage of a more accurate measurement but was impractical due to the excessively long sweep time. Careful selection of frequency step value was necessary because too small a value would have increased the amount of discrete frequency data points, and too large a value would have resulted in loss of definition in the response curves. In this respect the selection of the frequency step value is synonymous with effective bandwidth of an analogue filter since a large bandwidth reduces the frequency resolution. A frequency step of 0.5 H_z was selected for all the cantilever tests giving 940 discrete frequency data points within the range 30-500 H_z. The time taken to sweep these frequencies was approximately 45 minutes.

An alternative to this procedure is to concentrate measurements at the resonant frequencies but this requires a knowledge of the position of the coupled system resonances. Further, if these resonances are to be moved by the optimising process then their final positions in the frequency range may not be known before commencing tests of the sub-systems.

6.3 EXPERIMENTAL AND THEORETICAL RESULTS

The experimental frequency response curves for the cantilevers show quite clearly the need to use experimental data when predicting a coupled system response since even with these simple structures classical theory does not predict the response with sufficient accuracy. This is mainly due to the non-idealised boundary conditions at the clamped end and partly due to the extra masses within the measuring system boundary. The discrepancy between the theoretical and experimental results could be improved by taking into account realistic boundary conditions and by including these extra concentrated masses. But it is doubtful whether these modifications would improve the situation to the extent that the results would be practically viable,since the objective is to optimise the coupled system response in a very narrow frequency band. Taking, as an example to illustrate this point, the first few modes of vibration of a general structure, a successful prediction of resonant frequency would be considered to be within 10% and predictions would become more inaccurate for higher modes. Therefore, an optimisation of frequency response within a bandwidth of less than 10% of the centre frequency is not possible. However, the totally theoretical study was extremely useful for the purposes of this investigation which was primarily concerned with the general behaviour of a simple coupled system with respect to alterations in the dynamic properties of the interface mechanism.

The experiment was idealised primarily to avoid unnecessary complications such as measuring rotational inertances and can, as such, be considered as successful since the connectors in particular were shown to be predominantly axial transmitters of energy. This can be seen by the high correlation between the predicted and measured system mobilities for the two types of interface connector, shown in Figure 5.7, since the predicted result was obtained by manipulating the experimental data from the cantilevers with theoretical connectors having purely axial properties. Mass, stiffness and damping values necessary for the theoretical re-generation of the connectors were estimated from 'blocked Impedance' tests. Initially, attempts were made to use the raw connector data from these tests but it was found that the results were of low quality. This is due to the inherent difficulties in carrying out such a test where the structure is required to have perfect restraint at all except one of the prescribed co-ordinates whilst accurately measuring the restraining forces.

6.4 OPTIMISATION OF COUPLED SYSTEM RESPONSE

The results show quite clearly that in certain cases a considerable reduction in energy transmission between two coupled structures can be effected within a narrow frequency band by optimising on the dynamic characteristics of the interface mechanism. This de-tuning process is achieved by varying the interface properties in a mathematical model of the coupled system so that the predicted system resonances are moved away from the selected frequency at which the de-tuning is to be effected. The bandwidth in which de-tuning is effective is therefore dependent on the modal density of the system. The interface in this mathematical model is, by necessity, theoretically generated in contrast to the experimentally obtained data of the sub-systems. The type of interface is therefore restricted to one in which an accurate mathematical prediction is possible, ie interfaces of low modal density. Once the optimum values of mass, stiffness and damping of the interface are found then a prototype may be constructed. During the investigation a simple mass-spring-damper interface was used to demonstrate how each of these elements could be utilised in the de-tuning of a two cantilever system coupled at two positions.

Of these three dynamic properties adjusting the stiffness of the interface was found to produce the most interesting effects on the response of the system. Adjustments to the mass and damping produced effects of a less complex nature. In general the shift in resonant frequencies increases as mass is added to or subtracted from the system and increases in damping and, although having little effect on position of resonant frequencies, does decrease the dynamic range of the system by attenuating the resonant frequencies and increasing the dynamic levels at anti-resonances. It is due to this last point that low damping would be necessary if optimisation of mass and stiffness produce anti-resonant conditions at the de-tuned frequency.

In the two cantilever systems tested two groups of system resonant frequencies were evident. One group was easily moved by adjustments in the coupling stiffness whereas the other group, which comprised the individual cantilever resonances, was not affected by any such adjustments. This phenomenon was principally due to the similar dimensions of the cantilevers but may also hold true in many practical situations in which the connected system exhibits uncoupled modes where the restraints imposed by the interface mechanism are not sufficient to prevent the sub-system acting as an independent system. This effect is more pronounced in the two cantilever system tested since the interface only provided **vertical restraint** at two positions along their length.

In the case of the de-tunable modes relatively large shifts in system resonant frequencies were effected by small changes in coupling stiffness up to a stiffness of about 2 MN/m. Further increases in stiffness had little effect indicating that this figure is, for practical considerations, the 'rigid' limit for the system, ie when the interface acts as a rigid body within the system. Within this limit adjustments to coupling stiffness may be used to a great effect without appreciably altering the overall dynamic response of the system and this may be an important factor if low frequency stability must be maintained.

6.5 IMPEDANCE COUPLING TECHNIQUE

The 'Impedance Coupling Technique' was used to good effect in simulating and optimising the dynamic characteristics of a coupled system. This Technique is particularly useful when combining experimental data with theoretical data in a mathematical model of a proposed system in order to predict the effect of changes within the system on the system response.

One of the major limitations of this Technique is that the system responses are described by a discrete set of co-ordinates and, as such, predicted system behaviour is confined in terms of these co-ordinates. Therefore, any additional information of system behaviour at other locations in the system is not possible without re-collecting the basic data to include any extra co-ordinates. Likewise, adding mass or stiffness to the system is only possible at the chosen co-ordinates. This also applies when the effect of rotations are necessary to the investigation since in this case rotational co-ordinates must be included in the system. Measuring a frequency response which include a rotation is difficult since the sub-systems must be excited by a pure moment and the rotational response must be measured; furthermore, instrumentation and equipment is not readily available for this type of experimentation. However, measurements of rotational frequency response has been successfully completed and utilised by Ewins and Silva[14] in which they have designed an exciting block to apply moments to the test structure whilst monitoring two adjacent accelerometers provided the means to determine the rotational response.

In this investigation the Technique utilised raw experimental data; raw data being the measured inertance, magnitude and phase, at each frequency increment. The utilisation of this raw data proved to be satisfactory since the quality of the predicted results were adequate for this demonstration exercise. However, slight errors were evident, in particular twin or split peaks occured at some predicted resonances. This was due to the non-rationalised raw data where the measured resonances of the sub-systems were not exactly the same when changing the force input position. Rationalising the data by measuring[26], comparing and then optimising on all modal parameters in the sub-systems and estimating some of the frequency response elements[27,28] might be necessary for systems of higher complexity[14] but this procedure is lengthy, and is very much dependent on the skill and judgement of the analyst.

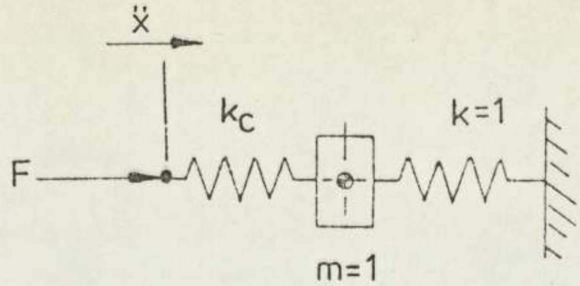

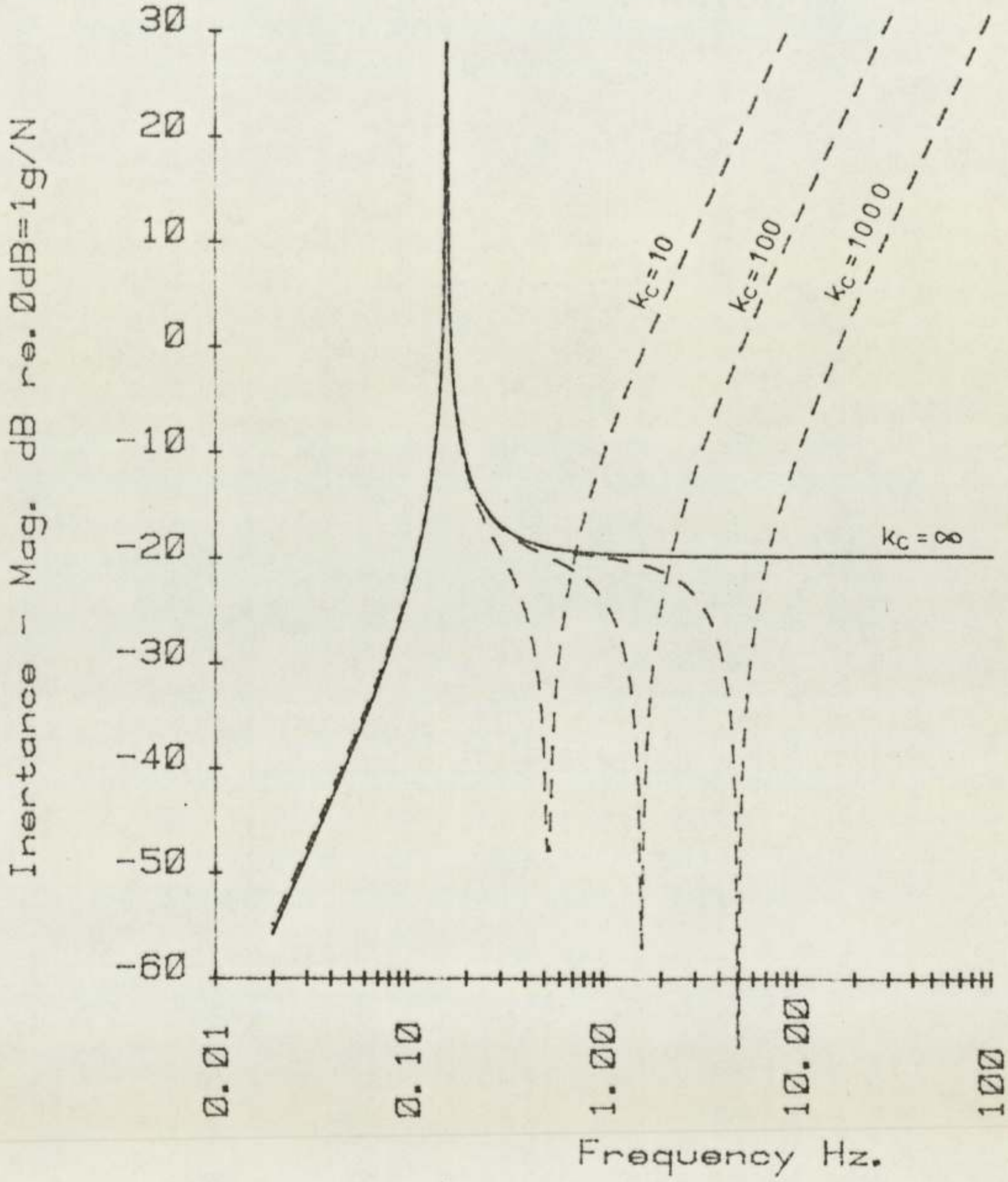

Fig. 6.1 EFFECT OF CONTACT STIFFNESS ON THE MEASURED FREQUENCY RESPONSE

CHAPTER SEVEN

CONCLUSIONS

CHAPTER SEVEN

CONCLUSIONS

An experimental model was successfully used to demonstrate the effect of varying the interface mechanism between two coupled complex structures on the overall system response. In this model the complex structures were represented by cantilevers and the interface consisted of simple connectors which allowed only axial forces to be transmitted from one cantilever to the other.

Experimental data was collected from frequency response tests on the un-coupled cantilevers and combined with theoretical connector data by the 'Impedance Coupling Technique' in order to predict the coupled system response. Throughout the investigation it was necessary to develop instrumentation and measuring techniques in order to obtain experimental data of an extremely high quality so that this raw data could be used directly in the 'Impedance Coupling Technique.' Considerable effort was expended in writing and developing software to enable a desk-top computer to be utilised as a controller in the experiments, data acquisition/manipulation system and to generate theoretical data.

It has been shown that the behaviour of complex coupled systems can be predicted to an acceptable degree of accuracy up to frequencies of about 500 Hz. Further, the results show quite clearly that in certain cases a considerable reduction in energy transmission between two coupled structures can be effected within a narrow frequency band by optimising on the dynamic characteristics of the interface mechanism. In particular, adjusting the stiffness of the interface was found to be very effective in this de-tuning process where relatively high coupling stiffness could be utilised without appreciably altering the overall dynamic response of the system and this might be an important factor if low frequency stability must be maintained.

REFERENCES

REFERENCES

1. C R WILLS — Cabin Noise Reduction Program Helicopter Tests, Vibration Transmission Paths, Preliminary Report. Westland Helicopters Ltd, internal note AA 1141, April 1976.

2. A L KLOSTERMAN, J R LEMON — Building Block Approach to Structural Dynamics. ASME paper 69-VIBR-30, 1969.

3. D J EWINS, M G SAINSBURY — Mobility Measurements for the Vibration Analysis of Connected Structures. S & VB (USA) No 42 Part 1, Jan 1972.

4. D R GAUKROGER — A Note on the Application of Impedance Techniques in Aeroelastic Problems. RAE Tech Memo Structures 848, Aug 1974.

5. C T MOLLOY — Notes on the Development of Mechanical Impedance. S & VB (USA) No 34 Part 3, 1964.

6. R E D BISHOP, D C JOHNSON — The Mechanics of Vibration. Cambridge University Press, 1960.

7. J P SALTER — Steady State Vibration. Mason, 1969.

8. C C KENNEDY, C D P PANCU — Use of Vectors in Vibration Measurement and Analysis. J Aero Sci, 14 (11), Nov 1947.

9. ASME — Proceedings of a Colloquium on Mechanical Impedance Methods held at the ASME Annual Meeting, New York, Dec 1958.

10. F SCHLOSS — Recent Advances in the Measurement of Structural Impedance. DTMB Report, 1584, Jan 1963.

11. F SCHLOSS — Recent Advances in Mechanical Impedance Instrumentation and Applications. DTMB Report 1960, Feb 1965.

12. G M REMMERS, R O BELSHEIM — Effects of Technique on Reliability of Mechanical Impedance Measurement. S & VB (USA) No 34 Part 3, 1964.

13. D J EWINS — A Classified Bibliography of Mechanical Impedance. Imperial College - Mechanical Engineering Department, 1975.

14. D J EWINS, J M M SILVA — Vibration Analysis of Helicopter External Store Carrier Structures. Imperial College - Mechanical Engineering Department, Report No 7805, 1978.

15. D J EWINS — Whys and Wherefores of Modal Testing. SEE Seminar, June 1978.

16. D J EWINS — Measurement and Applications of Mechanical Impedance Data. Parts 1,2 & 3. JSEE, Dec 1975, March 1976, June 1976.

17. R D COOK — Concepts and Applications of Finite Element Analysis. Wiley, 1974.

18. W C HURTY, M F RUBINSTEIN — Dynamics of Structures, Prentice Hall, 1964.

19. S A HOVANESSIAN, L A PIPES — Digital Computing Methods in Engineering. McGraw-Hill, 1969.

20. S P TIMOSHENKO, D H YOUNG, W WEAVER, Jr — Vibration Problems in Engineering - 4th Ed. Wiley, 1974.

21. D YOUNG
R P FELGAR, Jr
Tables of Characteristic Functions Representing Normal Modes of Vibration of a Beam. The University of Texas Publication No 4913, July 1949.

22. R P FELGAR, Jr
Formulas for Integrals Containing Characteristic Functions of a Vibrating Beam. The University of Texas Circular No 14, 1950.

23. J C SNOWDON
Vibration and Shock in Damped Mechanical Systems. Wiley, 1968.

24. D J EWINS
Some Whys and Wherefores of Impedance Testing. SEE Dynamic Testing Vol 1, 1971.

25. R L KERLIN
J C SNOWDON
Driving - Point Impedances of Cantilever Beams - Comparison of Measurement and Theory. JASA, Vol 47, No 1 Part 2, Jan 1970.

26. D R GAUKROGER
C W SKINGLE
K H HERON
Numerical Analysis of Vector Response Loci. JS & V, Vol 29 No 3, 1973.

27. A BERMAN
W G FLANNELLY
Theory of Incomplete Models of Dynamic Structures. AIAA Journal Vol 9, No 8, Aug 1971.

28. D J EWINS
On Predicting Point Mobility Plots from Measurements of other Mobility Parameters. Imperial College - Mechanical Engineering Department, Report No 79004, 1979.

29. R PREDMORE
J DAVIS
Complex Arithmetic Using the 9830 Matrix Option. Keyboard, A Hewlett-Packard Pub, 1978/3.

APPENDIX 1

AN EXAMPLE OF THE 'IMPEDANCE COUPLING TECHNIQUE'

USING SIMPLE STATIC DEFLECTIOM OF BEAM THEORY

APPENDIX 1

AN EXAMPLE OF THE 'IMPEDANCE COUPLING TECHNIQUE' USING SIMPLE STATIC DEFLECTION OF BEAM THEORY

INTRODUCTION

This example demonstrates the 'Impedance Coupling Technique' by using the stiffness influence coefficient method on a two cantilever system. The example is of interest since it shows how the rotations are accounted for by measuring only the translational elements in the flexibility matrix providing there are no externally applied moments to the coupled system.

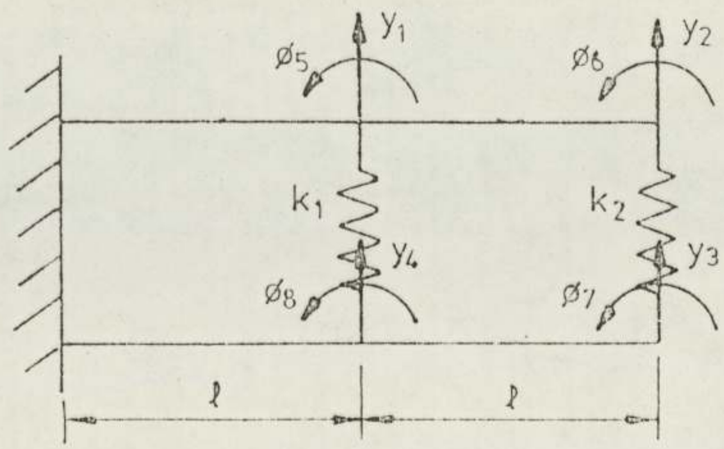

FIG A1.1 STATIC MODEL OF TWO CANTILEVER SYSTEM COUPLED AT TWO POSITIONS WITH PURE STIFFNESSES

The overall stiffness matrix equation of the system in Fig A1.1 is:-

$$\frac{EI}{\ell^3}\left[\begin{array}{cccc|cccc} 24+K & -12 & 0 & -K & 0 & 6\ell & 0 & 0 \\ -12 & 12+K & -K & 0 & 6\ell & -6\ell & 0 & 0 \\ 0 & -K & 12+K & -12 & 0 & 0 & -6\ell & -6\ell \\ -K & 0 & -12 & 24+K & 0 & 0 & 6\ell & 0 \\ \hline 0 & -6\ell & 0 & 0 & 8\ell^2 & 2\ell^2 & 0 & 0 \\ 6\ell & -6\ell & 0 & 0 & 2\ell^2 & 4\ell^2 & 0 & 0 \\ 0 & 0 & -6\ell & 6\ell & 0 & 0 & 4\ell^2 & 2\ell^2 \\ 0 & 0 & -6\ell & 0 & 0 & 0 & 2\ell^2 & 8\ell^2 \end{array}\right] \left[\begin{array}{c} y_1 \\ y_2 \\ y_3 \\ y_4 \\ \hline \phi_5 \\ \phi_6 \\ \phi_7 \\ \phi_8 \end{array}\right] = \left[\begin{array}{c} F_1 \\ F_2 \\ F_3 \\ F_4 \\ \hline \tau_5 \\ \tau_6 \\ \tau_7 \\ \tau_8 \end{array}\right] \quad \ldots \text{eq A1.1}$$

where $K = \dfrac{k\ell^3}{EI}$

but since the rotations are dependent on the deflections eq A1.1 can be reduced to a 4th order matrix by using equation 2.19, ie

$$[\bar{k}] = ([k_{11}] - [k_{12}]\,[k_{22}]^{-1}\,[k_{21}])$$

Therefore eq A1.1 becomes

$$\frac{EI}{7\ell^3}\begin{bmatrix} 96+K' & -30 & 0 & -K' \\ -30 & 12+K' & -K' & 0 \\ 0 & -K' & 12+K' & -30 \\ -K' & 0 & -30 & 96+K' \end{bmatrix} \begin{bmatrix} y_1 \\ y_2 \\ y_3 \\ y_4 \end{bmatrix} = \begin{bmatrix} F_1 \\ F_2 \\ F_3 \\ F_4 \end{bmatrix} \quad \ldots \text{eq A1.2}$$

where $K' = \dfrac{7k\ell^3}{EI}$

Since it is experimentally easier to obtain the flexibility matrix than the stiffness matrix, what happens if only the deflections are measured in the flexibility matrix?

Taking a simple cantilever,

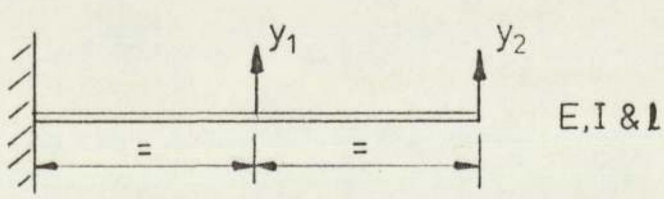

the flexibility matrix is measured as

$$\frac{\ell^3}{EI}\begin{bmatrix} 1/3 & 5/6 \\ 5/6 & 8/3 \end{bmatrix}\begin{bmatrix} F_1 \\ F_2 \end{bmatrix} = \begin{bmatrix} y_1 \\ y_2 \end{bmatrix} \qquad \text{. . . eq A1.3}$$

$$\text{where } \left[\bar{a}\right] = \frac{\ell^3}{EI}\begin{bmatrix} 1/3 & 5/6 \\ 5/6 & 8/3 \end{bmatrix} \qquad \text{. . . eq A1.4}$$

inverting eq A1.4 to give the stiffness matrix

$$\left[\bar{k}\right] = \frac{EI}{7\ell^3}\begin{bmatrix} 96 & -30 \\ -30 & 12 \end{bmatrix} \qquad \text{. . . eq A1.5}$$

If two cantilevers of the same dimensions are connected together as Fig A1.1 then the resulting stiffness matrix using the static equivalent of the 'Impedance Coupling Equation' 2.7 is the same as Eq A1.2. Therefore, the rotations, in this case, need not be measured.

APPENDIX 2

CALIBRATION OF TRANSDUCERS

APPENDIX 2

CALIBRATION OF TRANSDUCERS

INTRODUCTION

The force transducer and accelerometers used in the experimental work were checked for calibration and their respective charge amplifiers were adjusted such that their outputs represented voltage sensitivities of 100 mV/N and 100 mV/g.

EQUIPMENT

A B & K standard accelerometer set was used as the acceleration measuring reference. This set comprised a B & K standard accelerometer type 8305 serial number 397055 and conditioning amplifier type 2626; the output being set at 100 mV/g. The standard accelerometer was fixed to a Derritron electro-dynamic vibrator, type VP5, together with the transducers as shown in Fig A2.1.

Signal generation and output signal analysis was provided by the Solartron Frequency Response Analyser, type 1170, and the Hewlett Packard 9825A desk-top computing system used in the frequency response experiments as shown in Fig 3.3.

PROCEDURE

The outputs of the charge amplifiers from the standard accelerometer and the transducer to be calibrated were connected to FRA channels X and Y respectively. The FRA was set to manual operation at 200 Hz and continuous measurement was selected. The gain of the transducer amplifier was adjusted until the correct ratio appeared on the measurement display to give the necessary voltage sensitivities. A computer controlled sweep was then initiated to sweep between 30-500 Hz with a 1 Hz frequency step value thus giving the frequency response characteristics of the transducer and charge amplifier combination.

RESULTS

Accelerometers

Two D J Birchall Ltd Accelerometers, type A/04, serial numbers 139 and 140 were calibrated together with Environmental Equipments Ltd charge amplifiers, model CA_1. The amplifier gains were adjusted to give a FRA ratio of 1.000 thereby giving 100 mV/g. The sweep test results are shown in Fig A2.2.

Force Transducer

One B & K force transducer, type 8200, serial number 403132 was calibrated together with a charge amplifier, model CA_1.

The FRA ratio necessary to set the output sensitivity to 100 mV/N was obtained from the following analysis.

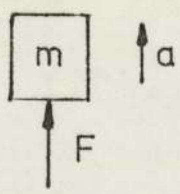

F is the force measured by the transducer whilst m is the total mass above the measuring point, including the transducer diaphragm (3 grams) and the mass of the standard accelerometer which measures the acceleration of this mass.

Therefore F = ma . . . eq A2.1

The total mass was measured as 139 grams.

$$a = \frac{\text{Std.Acc.O/P Volts}}{0.1\ \text{V/g}} \left[\frac{9.81\ \text{m/s}^2}{1\ \text{g}}\right] \quad \text{. . . eq A2.2}$$

$$F = \frac{\text{Force Trans.O/P Volts}}{0.1\ \text{V/N}} \quad \ldots \quad \text{eq A2.3}$$

Substituting eq A2.2 and A2.3 into eq A2.1 gives

$$\text{Ratio, } R = \frac{\text{Force Trans.O/P Volts}}{\text{Std.Acc.OP/ Volts}}$$

$$R = 1.36$$

The sweep test results are shown in Fig A2.3.

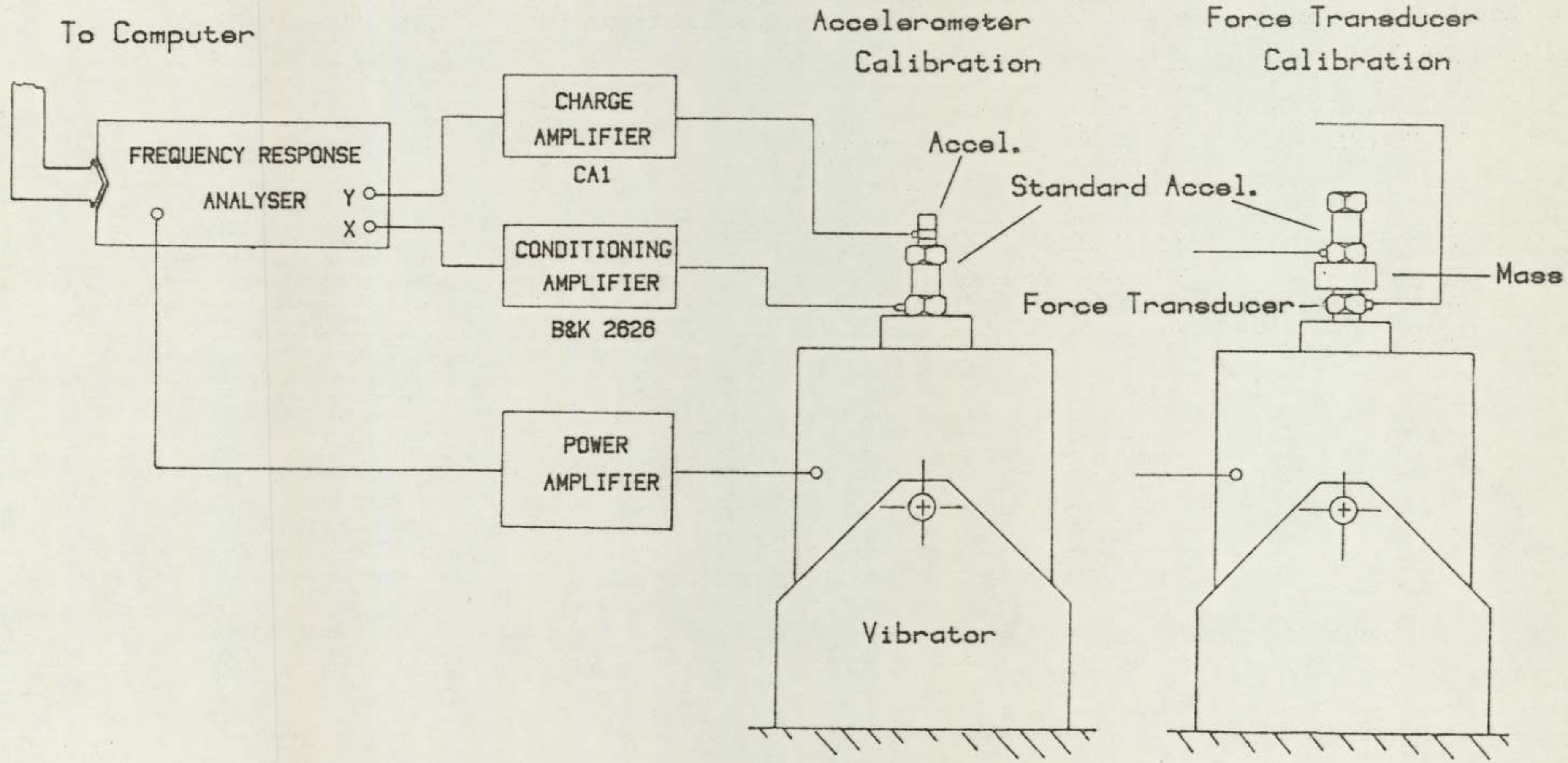

Fig. A2.1 SET-UP FOR CALIBRATION OF TRANSDUCERS

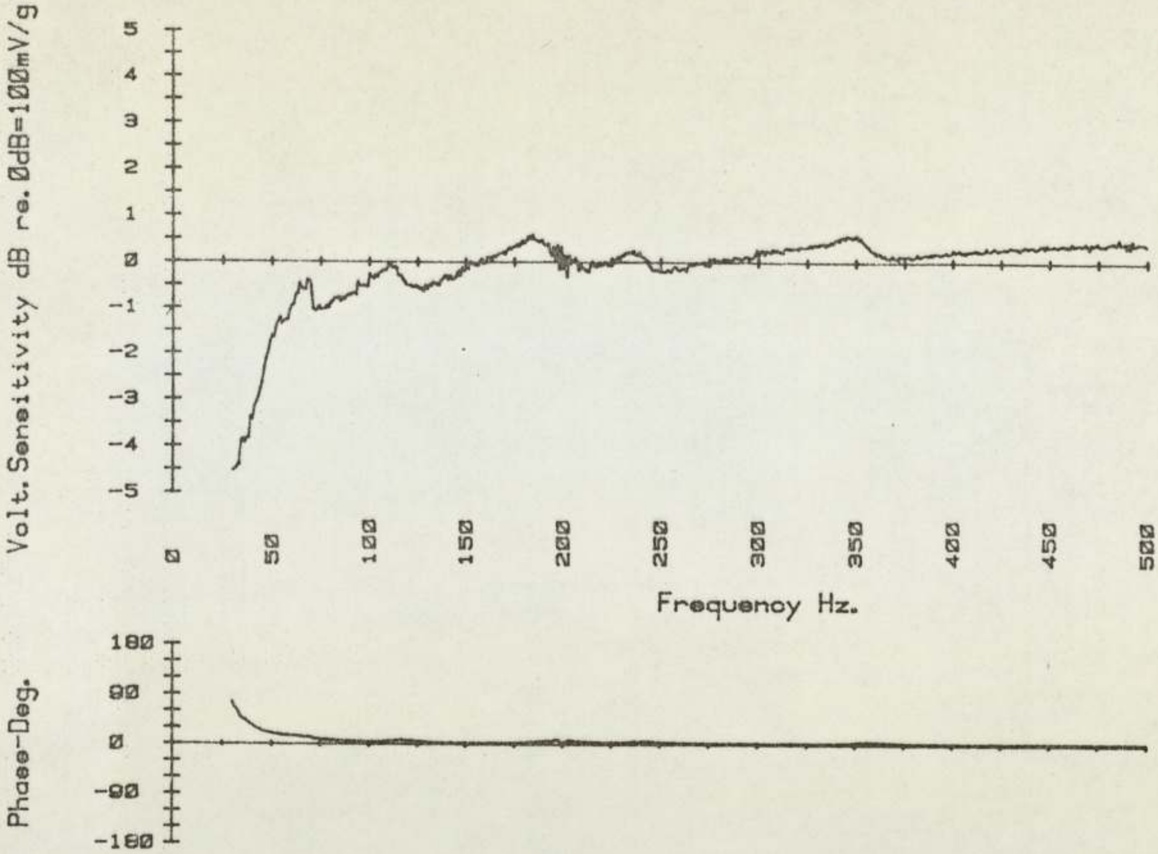

Fig. A2.2 CALIBRATION OF ACCELEROMETER DJB 139

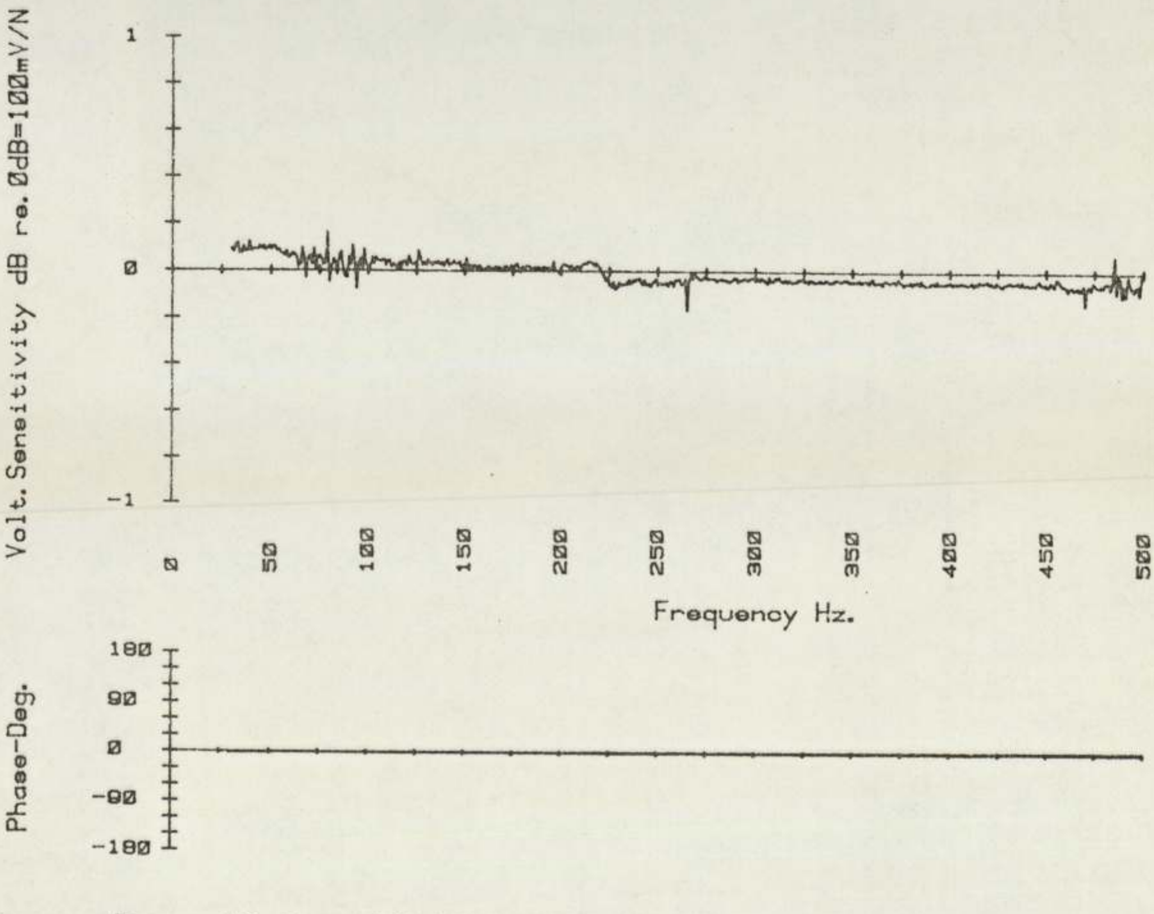

Fig. A2.3 CALIBRATION OF FORCE TRANSDUCER B&K 403132

APPENDIX 3

DETAILS OF COMPUTING SOFTWARE

APPENDIX 3

DETAILS OF COMPUTING SOFTWARE

INTRODUCTION

Various computer programs were written and developed during the investigation in order that a Hewlett Packard desk-top computer be used as a controller in the frequency response experiments, to acquire and store the data, to manipulate the frequency response data in the 'Impedance Coupling Technique' to generate theoretical frequency response data. The following programs were written.

SWFRA: To control a sweep test with the Frequency Response Analyser.

IMPC: To generate theoretical frequency responses of the connectors

CMOBB: To combine the experimental/theoretical frequency response data by the 'Impedance Coupling Technique'.

PMOB: A plotting program.

DET: A program similar to 'CMOBB' but takes one frequency at a time and calculates the effect of varying the interface stiffness on system inertance.

TCMOB: To generate theoretical cantilever frequency response functions.

These programs were written in HPL, an interpreter language similar to BASIC, for use on the HP9825A. Two of these programs are listed and explained in this Appendix, ie SWFRA and CMOBB.

SWFRA

This program illustrates some of the HPL statements required to allow the HP9825A computer to control the Solartron Frequency

Response Analyser (FRA). The two instruments are connected via a General Purpose Interface Bus (GPIB) system. A more detailed explanation of the system and some of the subroutines used may be found in the Solartron Operating Manual (1183-C; GPIB Interface).

The FRA outputs a program controlled analogue signal to drive the system under test and two transducer signals may be measured by the FRA to obtain their magnitude ratio and phase difference. The sweep generator, analyser and other functions may be programmed remotely by the computer and data can be sent from the FRA store to the computer. The program listing shown below uses the interrupt facility on the GPIB which allows the computer to carry on executing other tasks until the FRA sends a service request. The computer will then interrupt its present task in order to receive data from the FRA and also to reset the interrupt facility for the next measurement.

The listing of SWFRA is shown at the end of this Appendix and a line by line explanation follows.

LINE NUMBER

- 0: Label at beginning of 'SWFRA' program.
- 1: Dimension statement to allocate a string variable for the data file name.
- 2: Sends a selective device clear command to the FRA. This initialises the FRA.
- 3: Instructs the FRA to enter remote control state.
- 4: A program control variable is set to zero.
- 5-7: Operator is required to enter frequency limits and step value.
- 8-12: A file code is entered and space is allocated on the floppy disc.

13-16: The operator selects measurement mode and integration time and this is validated.

17: Calls subroutine 'analyser', ie lines 29-37 which sets the FRA analyser section to the required parameters via write statements. The parameter 718 is the device code for the FRA.

18: Calls subroutine 'generator', ie lines 39-52 which sets the FRA signal generator section to the required parameters.

19: Calls subroutine 'sweep', ie lines 54-63 which sets the sweep parameters.

20: The operator is required to start the test by entering 1.

21: All the setting up parameters are stored in the test file.

22: Defines the interrupt subroutine. When an interrupt is detected by the computer it will execute the subroutine 'results'.

23: Enables the computer to accept an interrupt from the FRA.

24: Sends coded message, decoded thus

S111 Enables and arms the measurement suspend and interrupt facility of the FRA.

;2 Instruct FRA to take a single measurement.

25: This line is necessary to prevent the computer finishing the program before all the interrupts have been received.

26: Loads the plotting program into the memory of the computer.

Subroutine 'results'

83: Label at beginning of subroutine 'results'. Once the interrupt has been received the computer executes this subroutine. The subroutine transfers the current measurement data from the FRA to the floppy disc test file.

84/5: Reads status byte. This should be 64 (decimal) when the measurement is completed.

86: Prints frequency response data in a + jb form to the test file. The a and b is transferred and decoded by the subroutines 'a', 'b' and 'Vans'. Subroutine 'fout' is also available to read the current frequency from the FRA.

87-89: Reads the sweep control settings. If the sweep has been completed Z is set to 1 and control is passed to main program.

90: If sweep has not ended the FRA is re-armed for the next measurement.

CMOBB

This program combines the two cantilevers with the coupling data to predict the coupled system response by the use of eq 2.7. The data for the sub-systems and couplings are retrieved from the data files and loaded into the matrices one frequency at a time. The matrices representing the cantilevers are inverted to give their apparent mass matrices. The resulting system apparent mass matrix is inverted to give the inertance matrix. All these matrices are complex, therefore, since the computer is unable to perform complex matrix arithmetic, the program uses method 2 in Appendix 4 to formulate real matrices.

Each data file represents a frequency response element and is divided into blocks (records) of 32 numbers. The first eight numbers in the file are the sweep test parameters and are compared for compatability. Each subsequent pair of numbers is the real and imaginary parts of the frequency response at a frequency determined by its position in the file.

LINE NUMBER

21-70: 'I' loop. The data is loaded into 32 element vectors block by block by the use of subroutines 'Red D' and 'Red Z'. The sweep parameters are checked in the first block by the subroutine 'ChData' and any mismatch causes the program to terminate.

40-68: 'K' loop. Processes data frequency by frequency.

41-46: The inertance data for the sub-systems, is loaded into real matrices by the use of subroutine 'MAT' and are inverted to give the apparent mass matrices.

47-62: The apparent mass data of the sub-system and couplings is combined and loaded into a real matrix [R], this being the system apparent mass matrix.

63-67: Matrix [R] is then inverted to give the system inertance matrix and the required elements are stored in data files.

```
0: "SWFRA":
1: dim N$[6]
2: clr 718
3: rem 718
4: 0→Z
5: ent "Fmin?",A
6: ent "Fmax?",B
7: ent "FREQ.STEP VALUE",C
8: ent "Enter test asgn.code",N$
9: asgn N$,1,0,X
10: if X#1;dsp "File in Existance";stp ;kill N$
11: int(((B-A)/C*2*8+64)/256)+1→r1
12: open N$,r1;asgn N$,1
13: ent "Measurement Mode 0=X,1=Y,2=Y/X",E
14: if E#0;if E#1;if E#2;jmp -1
15: ent "INT.TIME 1=MIN,10=X10,100=X100,1000=X1000",F
16: if F#1;if F#10;if F#100;if F#100;jmp -1
17: cll 'analyser'(718,0,E,F,0)
18: cll 'generator'(718,.2,0,1,A)
19: cll 'sweep'(718,0,0,A,B,0,C,.1)
20: ent "ENTER 1 TO START SWEEP",H;if H#1;jmp 0
21: sprt 1,A,B,C,D,E,F,"ens"
22: oni 7,"results"
23: eir 7
24: wrt 718,"S1112;2"
25: if Z=0;jmp 0
26: get "PMOB"
27: end
28: "--------------------------------------------":
29: "analyser":if p0<3;gto "anl"
30: int(abs(p2))→p2;if p2=0;7→p2
31: fmt 1,"T29",fz1.0;wrt p1+.1,p2+1
32: fmt 1,"T2<",fz1.0;wrt p1+.1,abs(p3+1)
33: fmt 1,"T2?",fz1.0;wrt p1+.1,int(log(abs(p4+1)))
34: wrt p1,"T42";red p1,p6
35: fmt 1,"T22",fz1.0;wrt p1+.1,ior(p6,2*p5)
36: wrt p1,"T42";red p1,p6
37: "anl":ret
38: "--------------------------------------------":
39: "generator":
40: fmt 1,"T1G0",fz3.0,"000",fz1.0
41: p2*tn↑(2-int(log(p2+.0001)))→p6
42: wrt p1+.1,p6,int(log(p2+.0001))+3
43: fmt 1,"T13",fz4.0,"0000";wrt p1+.1,drnd(p6*10,3)
44: fmt 1,"T1C0",fz3.0,"00",fz1.0,"0"
45: abs(p3*tn↑(2-int(log(abs(p3+.0001)))))→p7
46: wrt p1+.1,p7,sgn(p3)=-1
47: wrt p1,"T42";red p1,p6;band(p6,2)→p6
48: if abs(p3)>=.01;ior(p6,1)→p6
49: fmt 1,"T22",fz1.0;wrt p1+.1,p6
50: fmt 1,"T24",fz1.0;wrt p1+.1,abs(p4)
51: cll 'freq'(p1,22,p5);cll 'freq'(p1,23,p5)
52: "gel":ret
53: "--------------------------------------------":
```

```
53: "--------------------------------------------------------":
54: "sweep":if p0<2;stp
55: jmp 9-p0
56: fmt 1,"T2>",fz1.0;wrt p1+.1,int(log(1+10*abs(p8)))
57: cll 'freq'(p1,30,p7)
58: fmt 1,"T1?",fz4.0;wrt p1+.1,p6*100
59: cll 'freq'(p1,6,p5)
60: cll 'freq'(p1,14,p4)
61: fmt 1,"T2;0T280T28",fz1.0;wrt p1+.1,p3+2
62: fmt 1,"T27",fz1.0;wrt p1+.1,4*abs(p2)
63: "swl":ret
64: "--------------------------------------------------------":
65: "freq":fmt 1,"T1",c1,fz4.0,"000",fz1.0
66: int(p3*10↑(3-int(log(p3+.0001))))→p4
67: wrt p1+.1,char(p2),p4,int(log(p3+.0001))+4
68: ret
69: "--------------------------------------------------------":
70: "Vans":wrt 718,"T3"&char(p2);red 718,p3,p4
71: (p3*100+int(p4/100))*10↑(frc(p4/10)*10-9)→p3
72: ret p3*(-1)↑bit(0,int(p4/10))
73: "--------------------------------------------------------":
74: "a":wrt 718,"T4<";red 718,p2
75: ret 'Vans'(p1,p2*8+1)
76: "--------------------------------------------------------":
77: "b":wrt 718,"T4<";red 718,p2
78: ret 'Vans'(p1,p2*8+5)
79: "--------------------------------------------------------":
80: "fout":wrt p1,"T37";red p1,p2,p3
81: ret p2*tn↑(10*frc(p3/10)-7)
82: "--------------------------------------------------------":
83: "results":
84: rds(718)→X
85: if X#64;prt "error",X;jmp -1
86: sprt 1,'a','b',"end"
87: wrt 718,"T48"
88: red 718,X
89: if X=0;1→Z;gto "swpend"
90: wrt 718,"T2;0S1112;2"
91: eir 7
92: "swpend":iret
93: "--------------------------------------------------------":
```

```
0: "CMOBB":
1: dim A[4,4],B[4,4],T[4,4],U[4,4],V[4,4],S[8,8],R[8,8],Z[8,8]
2: dim C[32],D[32],E[32],F[32],G[32],H[32],I[32],J[32]
3: dim K[32],L[32],M[32],N[32],O[32],P[32],Q[32],W[32],X[32]
4: dim T$[3],B$[3],S$[3],C$[3],L$[3],N$[6]
5: ent "Top Cant Code 3ch",T$
6: ent "Bottom Cant.Code 3ch",B$
7: ent "Theoretical Coupling Imp.Code",C$
8: ent "Cal.Sys.Mob.Code 3ch",S$
9: T$&"M11"→N$;asgn N$,1;sread 1,A,B,C
10: fxd 2;wrt 6,"Fmin=",A;wrt 6,"Fmax=",B;wrt 6,"Fstep=",C
11: wrt 6,""
12: (B-A)/C+2→r2;int((2r2+9)*8/256)+1→r1
13: S$&"M13"→N$;asgn N$,5,0,X;if X#1;gsb "KILL"
14: open N$,r1;asgn N$,5
15: S$&"M14"→N$;asgn N$,6,0,X;if X#1;gsb "KILL"
16: open N$,r1;asgn N$,6
17: S$&"M23"→N$;asgn N$,7,0,X;if X#1;gsb "KILL"
18: open N$,r1;asgn N$,7
19: S$&"M24"→N$;asgn N$,8,0,X;if X#1;gsb "KILL"
20: open N$,r1;asgn N$,8
21: for I=1 to r1
22: 1→S;32→N
23: if I=r1;gsb "REDIM"
24: T$→L$;gsb "RedD"
25: ara C→G
26: ara D→I
27: ara E→J
28: ara F→K
29: B$→L$;gsb "RedD"
30: ara C→L
31: ara D→M
32: ara E→N
33: ara F→O
34: C$→L$;gsb "Red2"
35: ara C→P
36: ara D→Q
37: ara E→W
38: ara F→X
39: if I=1;gsb "PD"
40: for K=S to N-1 by 2
41: cll 'MAT'(G[K],G[K+1],I[K],I[K+1],J[K],J[K+1],K[K],K[K+1])
42: ara A→T
43: cll 'MAT'(L[K],L[K+1],M[K],M[K+1],N[K],N[K+1],O[K],O[K+1])
44: ara A→B
45: inv T→U
46: inv B→V
47: ina R;ina Z;ina S
48: for R=1 to 4
49: for C=1 to 4
50: U[R,C]→R[R,C]
51: V[R,C]→R[R+4,C+4]
52: next C
53: next R
```

```
53: next R
54: P[K]→Z[1,1]→Z[2,2]→Z[3,3]→Z[4,4]
55: P[K+1]→Z[1,2]→Z[3,4];-P[K+1]→Z[2,1]→Z[4,3]
56: Q[K]→Z[1,5]→Z[2,6]→Z[3,7]→Z[4,8]
57: Q[K+1]→Z[1,6]→Z[3,8];-Q[K+1]→Z[2,5]→Z[4,7]
58: W[K]→Z[5,1]→Z[6,2]→Z[7,3]→Z[8,4]
59: W[K+1]→Z[5,2]→Z[7,4];-W[K+1]→Z[6,1]→Z[8,3]
60: X[K]→Z[5,5]→Z[6,6]→Z[7,7]→Z[8,8]
61: X[K+1]→Z[5,6]→Z[7,8];-X[K+1]→Z[6,5]→Z[8,7]
62: ara R+Z→R
63: inv R→S
64: sprt 5,S[1,5],S[1,6],"ens"
65: sprt 6,S[1,7],S[1,8],"ens"
66: sprt 7,S[3,5],S[3,6],"ens"
67: sprt 8,S[3,7],S[3,8],"ens"
68: next K
69: dsp "Record No",I
70: next I
71: for I=5 to 8
72: sprt I,F,"end"
73: next I
74: stp
75: end
76: "-------------------------------------------":
77: "RedD":
78: "F":L$&"M22"→N$;asgn N$,4;on end 4,"E";rread 4,I;sread 4,F[*]
79: "E":L$&"M21"→N$;asgn N$,3;on end 3,"D";rread 3,I;sread 3,E[*]
80: "D":L$&"M12"→N$;asgn N$,2;on end 2,"C";rread 2,I;sread 2,D[*]
81: "C":L$&"M11"→N$;asgn N$,1;on end 1,"B";rread 1,I;sread 1,C[*]
82: "B":if I=1;gsb "ChData"
83: if I=r1;gsb "EFch"
84: "RedDend":ret
85: "-------------------------------------------":
86: "RedZ":
87: "G":L$&"Z11"→N$;asgn N$,1;on end 1,"H";rread 1,I;sread 1,C[*]
88: "H":L$&"Z13"→N$;asgn N$,2;on end 2,"I";rread 2,I;sread 2,D[*]
89: "I":L$&"Z31"→N$;asgn N$,3;on end 3,"J";rread 3,I;sread 3,E[*]
90: "J":L$&"Z33"→N$;asgn N$,4;on end 4,"K";rread 4,I;sread 4,F[*]
91: "K":if I=1;gsb "ChData"
92: if I=r1;gsb "EFch"
93: "RedZend":ret
94: "-------------------------------------------":
95: "ChData":
96: if L$=T$;ara C→H
97: for J=1 to 8
98: if H[J]#C[J];gto "PDM"
99: if H[J]#D[J];gto "PDM"
100: if H[J]#E[J];gto "PDM"
101: if H[J]#F[J];gto "PDM"
102: jmp 2
103: "PDM":prt J,L$;dsp "DATA MISSMATCH";stp
104: next J
105: "ChDend":ret
106: "-------------------------------------------":
```

```
106: "-----------------------------------------":
107: "MAT":
108: p1→A[1,1]→A[2,2]
109: p2→A[1,2];-p2→A[2,1]
110: p3→A[1,3]→A[2,4]
111: p4→A[1,4];-p4→A[2,3]
112: p5→A[3,1]→A[4,2]
113: p6→A[3,2];-p6→A[4,1]
114: p7→A[3,3]→A[4,4]
115: p8→A[3,4];-p8→A[4,3]
116: "MATend":ret
117: "-----------------------------------------":
118: "KILL":
119: dsp N$,"File Exists";stp ;kill N$
120: "KILLend":ret
121: "-----------------------------------------":
122: "PD":for D=1 to 8
123: sprt 5,H[D],"ens"
124: sprt 6,H[D],"ens"
125: sprt 7,H[D],"ens"
126: sprt 8,H[D],"ens"
127: next D
128: 9→S
129: "PDend":ret
130: "-----------------------------------------":
131: "REDIN":
132: 2r2+9-32*(r1-1)→N
133: rdm C[N],D[N],E[N],F[N],G[N],I[N],J[N],K[N]
134: rdm L[N],M[N],N[N],O[N],P[N],Q[N],W[N],X[N]
135: "RDNend":ret
136: "-----------------------------------------":
137: "EFch":
138: if L$=T$;C[N]→F;prt "Fend=",F
139: if F#C[N];gto "PFM"
140: if F#D[N];gto "PFM"
141: if F#E[N];gto "PFM"
142: if F#F[N];gto "PFM"
143: jmp 2
144: "PFM":prt L$;dsp "End Freq.MISSMATCH";stp
145: "EFchend":ret
```

APPENDIX 4

INVERSION OF A COMPLEX MATRIX USING REAL MATRIX ALGEBRA

APPENDIX 4

INVERSION OF A COMPLEX MATRIX USING REAL MATRIX ALGEBRA

INTRODUCTION

The 'Impedance Coupling Technique' involves complex matrix manipulations including matrix inversion. The HP9825A was not able to perform this type of arithmetic since it could only manipulate real matrices. Therefore, a method was required to invert the complex matrix using real matrix algebra. Two methods were investigated, one using conventional matrix algebra and substitution whilst the second requires the formulation of a specially coded real matrix. The latter method was taken from a paper by Predmore and Davis[29].

Take, as an example, a simple 2nd order complex matrix.

$$\begin{bmatrix} a_{11} + jb_{11} & a_{12} + jb_{12} \\ a_{21} + jb_{21} & a_{22} + jb_{22} \end{bmatrix}$$

METHOD 1

This complex matrix can be rewritten as:

$$\begin{bmatrix} a_{11} & a_{12} \\ a_{21} & a_{22} \end{bmatrix} + j \begin{bmatrix} b_{11} & b_{12} \\ b_{21} & b_{22} \end{bmatrix}$$

or $[A] + j[B]$

If the inverse of this matrix be

$$[C] + j[D]$$

such that

$$([C] + j[D])^{-1} = [A] + j[B] \qquad \text{. . . eq A4.1}$$

then $$([A] + j[B])\,([C] + j[D]) = [I] \qquad \text{. . . eq A4.2}$$

where $[I]$ is the identity matrix.

After some matrix algebra eq A4.2 yields the following equations:

$$[C] = - [B]^{-1} [A] [D] \qquad \ldots \text{ eq A4.3}$$

$$[D] = - ([A] [B]^{-1} [A] + [B])^{-1} \qquad \ldots \text{ eq A4.4}$$

Therefore, two inversions, four multiplications and one matrix addition are required to invert this 2nd order complex matrix.

METHOD 2

This method utilises a coded real matrix which is twice the order of the complex matrix. The matrix is divided into sub-matrices which are always 2 × 2 and contain the complex element; the real part being repeated on the two diagonals and the imaginary part on the off diagonals, there being a change of sign on the lower off diagonal. The coded real matrix for the 2nd order complex matrix is shown below.

$$\left[\begin{array}{cc|cc} a_{11} & b_{11} & a_{12} & b_{12} \\ -b_{11} & a_{11} & -b_{12} & a_{12} \\ \hline a_{21} & b_{21} & a_{22} & b_{22} \\ -b_{21} & a_{21} & -b_{22} & a_{22} \end{array}\right]$$

This matrix may be manipulated as a real matrix so matrix addition, multiplication and inversion is possible. The resulting matrix is decoded to give the complex matrix in exactly the same way since the position of the elements is not effected by these manipulations.